T-3936

DESICCATION-INDUCED EFFECTS ON HYDRAULIC CONDUCTIVITY AND COMPRESSIBILITY RELATIONS IN A NATURAL CLAY

by

Dixie L. Shear

ProQuest LLC.
789 East Eisenhower Parkway
P.O. Box 1346
Ann Arbor, MI 48106 – 1346

T-3936

A thesis submitted to the Faculty and the Board of Trustees of the Colorado School of Mines in partial fulfillment of the requirements for the degree of Master of Science (Applied Mechanics).

Golden, Colorado
Date 11/6/91

Signed: _____
Dixie L. Shear

Approved: _____
Dr. Karl R. Nelson
Thesis Advisor

Approved: _____
Dr. Harold W. Olsen
Thesis Co-Advisor

Golden, Colorado
Date 11/6/91

_____
Dr. Joan P. Gosink
Professor and Head,
Engineering Department

ABSTRACT

Four undisturbed and five reconstituted specimens of a soft gray marine clay were subjected to various degrees of desiccation, resaturated, and then tested to determine the hydraulic conductivity (k), void ratio (e), and effective stress (σ') relationships. The geotechnical properties of the clay were directly measured with a volume-controlled testing apparatus that allowed one-dimensional consolidation and simultaneous hydraulic conductivity measurements. The desiccation-induced effects on the clay were interpreted from the measured data trends and the cluster model of soil fabric.

Results showed that desiccation did not create cracks or fissures in the specimens, but did cause anisotropic shrinkage and void ratio reductions. Hydraulic conductivity and void ratio increased as desiccation increased in all of the clay specimens. The specimens also developed log k-e relationships with pronounced curvature in the direction of decreasing rates of change in log k with decreasing void ratio. The log k-e curves were characterized by an initial steep slope at high void ratios and a much flatter slope at lower void ratios. Specific storage was measured to decrease as desiccation increased for all specimens. The

undisturbed specimens exhibited a greater range of specific storage and compressibility than the reconstituted specimens. All specimens developed an increased resistance to compressibility as desiccation increased. Undisturbed materials were determined to be more compressible than the reconstituted specimens.

These findings are interpreted in terms of the cluster model and pore size distribution studies. Two levels of pore sizes were inferred from the log k-e curves, relating to the inter-cluster pore spaces and intra-cluster pore spaces. Desiccation caused shrinkage of the pore spaces both within and between the clusters. The technique used to prepare the reconstituted specimens did not break down the clusters to individual clay particles, but did rearrange the clusters. The undisturbed specimens were interpreted to have a porous structure, while the reconstituted specimens were characterized by a dense and more compact structure. Because the reconstituted specimens were prepared from air-dried materials, the primary effects of desiccation were considered to have taken place prior to sample testing.

TABLE OF CONTENTS

LIST OF FIGURES

Figure **Page**

Figure **Page**

Figure **Page**

LIST OF TABLES

LIST OF SYMBOLS

English Symbol	Explanation
a_v	Coefficient of Compressibility
A	Cross sectional area
ASTM	American Society for Testing and Materials
BP	Back Pressure
cc	Cubic centimeters
cm	Centimeter
C_c	Compression Index
CH	Highly plastic clay
CL	Low plastic clay
CRD	Constant Rate of Deformation
d	Pore diameter
D	Diameter of sample
D_o	Initial diameter of sample
D_f	Final diameter of sample
e	Void ratio
e_o	Initial void ratio
e_f	Final void ratio
EE	Edge-to-edge particle association
EF	Edge-to-face particle association
ft	Feet
°F	Degrees Fahrenheit

English Symbol	Explanation
FF	Face-to-face particle association
G_s	Specific gravity of soil
h	Pressure head
H	Sample height
H_o	Initial sample height
H_f	Final sample height
H_s	Height of solids
i	Hydraulic gradient
i.d.	Inner diameter
in	Inch
k	Hydraulic conductivity
k_o	Shape factor
K-C	Kozeny-Carmen equation
l.v.d.t.	Linear variable differential transducer
LL	Liquid Limit
m	meter
mm	Millimeter
ML	Low plastic silty clay
N/A	Not applicable
OH	Highly plastic organic material
OL	Low plastic organic material
psi	Pounds per square inch
P	Pressure

English Symbol	Explanation
PI	Plasticity Index
PL	Plasticity Limit
Q	Volumetric flow rate
Q_c	Constant volumetric flow rate
Q_e	External volumetric flow rate
R	Reconstituted specimen
s	Second
S	Compliance
S_o	Specific surface area per unit volume of particles
S_s	Specific storage
u	Pore pressure
u_b	Base pore pressure
U	Undisturbed specimen
USCS	Unified Soil Classification System
V_s	Volume of solids
V_t	Total volume
V_v	Volume of voids
w %	Water content
w_o %	Initial water content
w_f %	Final water content

Greek Symbol	Explanation
γ	Specific weight; density of pore fluid; surface tension of fluid
Δ	Delta
μ	Micro
σ'	Effective vertical stress
ϕ	Contact angle

ACKNOWLEDGEMENTS

The author wishes to thank Dr. Harold W. Olsen of the U.S. Geologic Survey for his excellent guidance in the research and writing of this thesis. The quality teaching and advice of Dr. Karl R. Nelson of the Engineering Department, Colorado School of Mines, is also greatly appreciated. Professors Jerry D. Higgins and Kenneth E. Kolm are duly noted for their interest and comments. Mr. George Erickson is thanked for his assistance in some of the index tests. Finally, the author wishes to thank her parents, Richard and Irene Shear, for their unending confidence and support of this academic endeavor.

Chapter 1

INTRODUCTION

The macroscopic effects of desiccation on fine-grained soils are well known. In nature, near-surface materials are often over-consolidated, and very fine-grained clays such as smectite develop large cracks and fissures in response to desiccation.

The microscopic effects of soil fabric from desiccation are less well known due to the limitations of conventional methods for direct observation. Existing data show that remolded materials undergo greater shrinkage than undisturbed materials during desiccation, because pore sizes are smaller in the remolded materials (Mitchell 1976). Pore size distribution studies with mercury intrusion porosimetry show that oven drying has large effects on both the size of macropores surrounding soil aggregates and the size of micropores within aggregates (Diamond 1970; Delage and Lefebvre 1984).

The purpose of this study was to investigate the effects of air drying on selected geotechnical properties of a natural clay. The scope of this investigation included direct measurements of the hydraulic conductivity (k), void ratio (e), and effective stress (σ') relationships in the desiccated materials. Results of the data trends were then

used to interpret the desiccation-induced fabric changes in the clay.

Natural clays are often used as impermeable barriers to fluid flow and are subject to the effects of desiccation. The results of this study may present information applicable to large scale projects that have restrictions to hydraulic conductivity and other measurable geotechnical properties.

This study used a soft gray Pleistocene clay acquired from a marine deposit in Carroll Island, Maryland. Clay specimens were prepared in both the undisturbed and reconstituted states and permitted to air dry to various degrees of desiccation from the natural water content prior to testing. The geotechnical properties of the clay were directly measured with a recently-developed volume-controlled testing apparatus that allows continuous one-dimensional consolidation and simultaneous hydraulic conductivity measurements.

A conceptual fabric model describing the behavior of clays was developed from known fabric characteristics and the results of pore size distribution studies of argillaceous materials. Fabric changes in the clay induced by desiccation were explained by this conceptual model.

A literature review identifies the early concepts, later advances, and the present state of knowledge of clay microstructure. The conceptual fabric model was formulated

from the principal features of clay fabric that have been observed and reported. The investigative approach, the experimental system and the testing program are explained in detail. Experimental results are summarized and divided into two categories for discussion: 1) observed desiccation-induced physical properties and 2) consolidation-induced relationships measured during testing. The interpretations made of the fabric changes are based on the experimental results and the conceptual model. Conclusions are discussed and recommendations are made for future fabric studies and improvements to the testing system. The appendices contain a series of plots which illustrate data trends and geotechnical properties measured in each of the undisturbed and reconstituted clay specimens.

Chapter 2

REVIEW OF SOIL FABRIC

2.1 Soil-Water Relations

The material properties of interest in this study are compressibility and hydraulic conductivity. Compressibility is indicated through one-dimensional compression of the clay skeleton. The coefficient of compressibility (a_v) is defined as the negative of the first derivative of the void ratio-effective stress relationship, presented in Equation 2.1 (Spangler and Handy 1982):

$$a_v = - \frac{de}{d\sigma'} \qquad (2.1)$$

Where:

a_v = Coefficient of compressibility

de = Void ratio increment

$d\sigma'$ = Effective stress increment

Figure 2.1 presents an ideal e-σ' curve where the slope defines a_v. The figure shows that changes in void ratio and effective stress result in varying values of a_v. These changes also indicate variations in the pore structure of the clay.

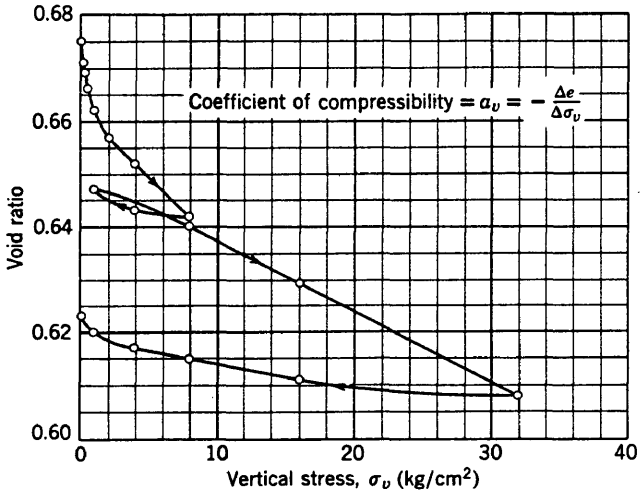

Figure 2.1 Void Ratio-Effective Stress Diagram. (Lambe and Whitman 1969)

Darcy's law states that the flow rate through a porous medium, due to an applied hydraulic gradient, is represented by a proportionality constant for hydraulic conductivity.

$$Q = k\, i\, A \qquad (2.2)$$

Where:

Q = Volumetric flow rate

k = Hydraulic conductivity

i = Hydraulic gradient

A = Cross sectional area

Typically, reductions in void ratio (and therefore porosity) caused by increases in effective stress result in lower values of hydraulic conductivity. Assuming all other factors are constant except the void ratio, the variations of hydraulic conductivity with void ratio can be predicted by the Kozeny-Carmen equation:

$$k = \left(\frac{\gamma}{\mu}\right) \left(\frac{1}{k_o T^2 S_o^2}\right) \left(\frac{e^3}{1 + e}\right) \qquad (2.3)$$

Where:

k = Hydraulic conductivity

γ = Density of pore fluid

μ = Viscosity of pore fluid

k_o = Shape factor

T = Tortuosity of pore space

S_o = Specific surface area per unit volume of particles

e = Void ratio

Equation 2.3 develops a theoretical log k-e relationship for soils using a capillary tube model that assumes all pore spaces have a uniform diameter. This single particle model of soil fabric has been used to identify the log k-e relationship as a straight line, illustrated by Figure 2.2.

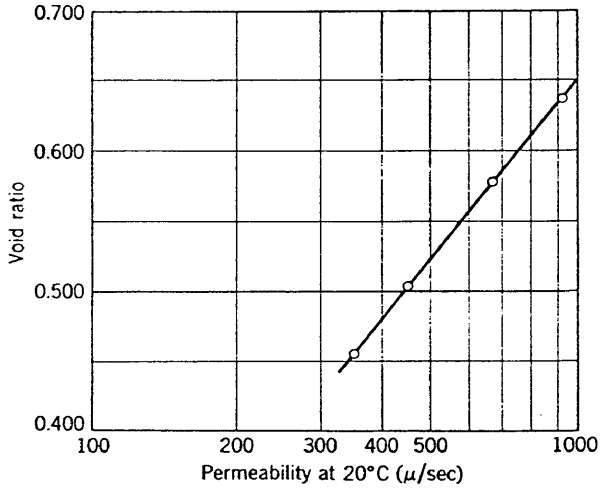

Figure 2.2 Void Ratio-Permeability Diagram. (Lambe and Whitman 1969)

In nature, clays are comprised of variably sized and interconnected fine-grained particles. The porous structure of a clay is affected by the particle characteristics of high surface area and electrical charge concentration (Iwata and Tabuchi 1988). Combinations of these characteristics influence the material properties of a soil.

Fine-grained soils are characterized by high values of specific surface. The soil particle will undergo greater exposure of its surface, edges and corners to the electrical influences of the surrounding fluid. The very nature of clay minerals is electrical. Since clay particles are

considered to have a thin, flat, rod-like shape, the crystal structure itself yields a net negative particle surface charge and positive edge charge. The amount of excess charge is dependent on the clay mineral type. Variable charge intensity and particle electrical instability require that a state of equilibrium occur. Electrical neutrality is achieved through particle bonding with cations naturally occurring in the soil moisture and with surrounding dipolar water molecules. The Gouy-Chapman theory of the diffuse double layer explains the formation of adsorbed water to the clay particle and defines the limits of attractive and/or repulsive forces. Dipolar properties of the adsorbed water also contribute to the plasticity characteristics of clayey soils (McCarthy 1982).

2.2 Early Concepts of Soil Fabric

Sorby (1908) was among the first to realize the importance of soil water in determining the structural properties of a clay mass. The first proposal of fabric for clay sediments was presented by Ehrenberg in 1918 (reproduced by Bennett and Hulbert 1986) and was based on the use of an ultramicroscope to estimate the formation of a "web" structure in an electrolytic clay suspension. This concept was later adapted to an engineering perspective to describe both the honeycomb structure and single-grain

structure (Terzaghi 1925, in Bennett and Hulbert 1986; Casagrande 1932). The honeycomb structure represented the end result of particle deposition in the presence of a strong electrolyte, while the single-grain structure indicated deposition in a weak or non-electrolyte solution. Figure 2.3 illustrates how the honeycomb structure was thought to be composed of variably sized and randomly oriented granular particles.

The influences of adsorbed water and the diffuse double layer theory were not widely accepted by the community of colloid chemists at the time. Instead, an assumption was made that a water layer with an unknown gelatinous salt surrounds and bonds the clay particles together to render the clay mass plastic.

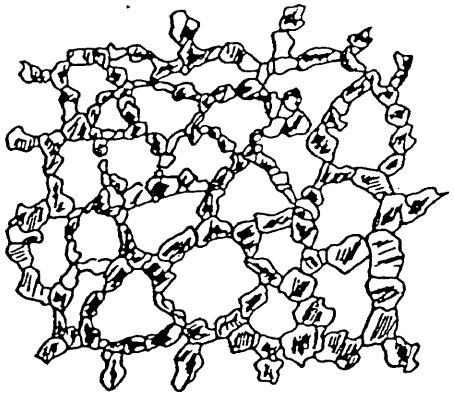

Figure 2.3 Honeycomb Structure. (Redrawn from Terzaghi 1925 and Casagrande 1932, in Bennett and Hulbert 1986)

The study of clay microstructure was left in a state of "almost hopeless empiricism" (Marshall 1949) by disputes of the fundamental properties of physico-chemical behavior. Eventually a greater understanding of the electrical charges critical to clay particle interactions was made possible by advances in the determination of clay crystal structures (Pauling 1930). These advances renewed interest in the study of clay microstructure.

The Gouy-Chapman theory was used to more fully develop schematics of the total potential energy versus interparticle distance relationships. Figure 2.4 illustrates the general energy relationship between two particles in a clay suspension of uniform electrolyte concentration. Double layer repulsive forces between like charges are shown to decrease exponentially with increasing distance and are indicated as a positive potential energy. Attractive van der Waals forces between the planar clay platelets are inversely proportional to the square of the separation distance, and are indicated as negative potential energies in Figure 2.4. The net energy distribution with regard to interparticle distance is characterized by a maximum that serves to regulate the input energy level required to cause attraction between the two clay platelets. Less energy input would permit the two particles to spontaneously separate. When the required energy is

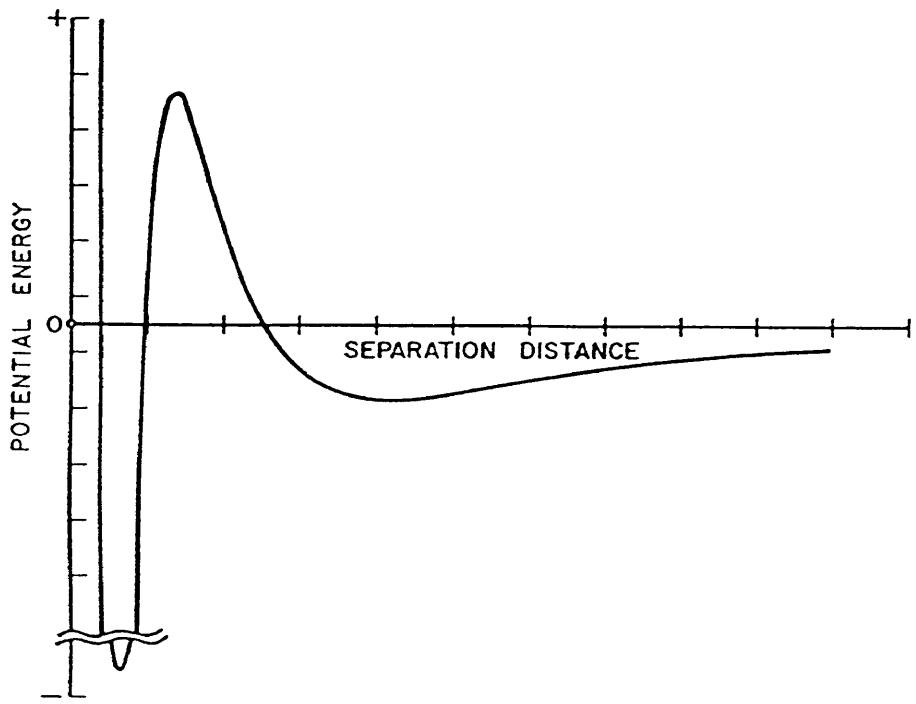

Figure 2.4 Potential Energy versus Particle Distance. (Bennett and Hulbert 1986)

provided to the system to bring the particles closer than the distance corresponding to the energy maximum, the particles continue to approach each other until the separation distance corresponding with the energy minimum is reached. In order to separate the two clay particles, an energy equal to the difference between the net energy minimum and maximum must be applied. This behavior is exhibited in natural clay systems in that particle

aggregation occurs more readily than particle separation. With regard to the Gouy-Chapman theory, the colloidal stability of a clay suspension is also controlled by the following factors (Lambe 1958):

1) Electrolyte concentration
2) Dielectric constant
3) Temperature
4) Size of hydrated ion
5) pH
6) Anion adsorption

2.3 Later Advances in Soil Fabric

Grim (1940) considered the mineral type, amount, and particle size distribution as factors necessary to evaluate the physical properties of clayey soils. The quantity and type of exchangeable cations were also included in this evaluation. These factors play a significant role in the initial deposition and structure of a clay. The electrolyte concentration of the clay suspension further affects the particle settling velocity through the total potential energy-particle separation distance relationship. In this relationship, the electrolyte concentration represents the energy barrier to be applied to the system for particle aggregation to occur. This phenomena was the basis for

interpretations made of the original honeycomb and single-grain structures (Lambe 1953). Figure 2.5 depicts the proposed honeycomb structure associated with a marine (salt-flocculated) environment. The salt-flocculated deposit is characterized by an open, high-volume structure resulting from the fast mode of deposition. Figure 2.6 presents the single-grain deposit in a freshwater (dispersed) environment. The dispersed deposit was considered to have a very dense, compacted structure achieved through slow particle settling velocities. After particle settlement, post-depositional stresses were thought to reorient the deposited particles to a minimum energy position. It was further proposed that the most preferred particle arrangement is the fabric associated with a remolded clayey material, illustrated by Figure 2.7. The remolded structure has a definite compact and horizontal particle arrangement with very little pore space between individual particles.

Mitchell used photomicrographs to identify other structural relationships between flocculated and dispersed clays (1956). These relationships are summarized as follows:

1) Under a given stress, the weight of clay in a flocculated structure comprises a greater volume than that of a dispersed structure.

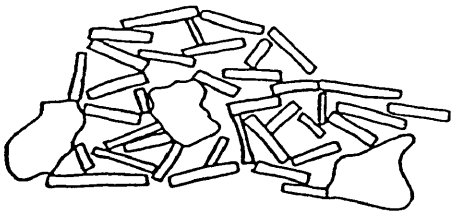

Figure 2.5 Undisturbed Saltwater Deposit. (Lambe 1953)

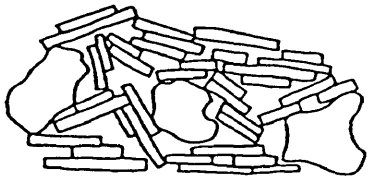

Figure 2.6 Undisturbed Freshwater Deposit. (Lambe 1953)

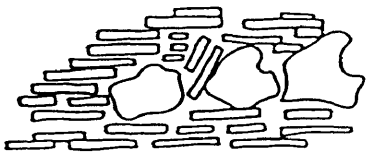

Figure 2.7 Remolded Structure. (Lambe 1953)

2) Flocculated clays have a less uniform particle distribution than do dispersed clays.

3) A given stress increment imposes a greater degree of particle reorientation for a flocculated structure than for a dispersed structure.

This same study noted that silts were not interconnected throughout the fabric. Rather, silt particles seemed to "float" randomly within the clay matrix. Dramatic increases in particle reorientation toward parallelism were also observed in this study at pressures greater than the preconsolidation stress. Later investigations (Quigley and Thompson 1966; Bowles 1968; Crawford 1968) have affirmed both of these findings.

The earlier proposals for flocculated and dispersed clay structures were later revised in regard to the electrolytic influences to the clay suspension (Lambe 1958). General groupings of clay-only particle-to-particle contacts were considered to form the salt-flocculated structure, depicted by Figure 2.8. A similar clay-only fabric for a dispersed structure indicated particle orientation as more compact and horizontal, shown by Figure 2.9. This structure was almost identical to the earlier remolded structure. Figure 2.10 illustrates the non-salt flocculated (cardhouse) structure that was also proposed. This particular structure was comprised of definite particle edge-to-face contacts.

Van Olphen described several particle arrangements due to the electrolytic influences on sedimentation and identified three modes of flocculation as 1) face-to-face (FF), 2) edge-to-face (EF), and 3) edge-to-edge (1963).

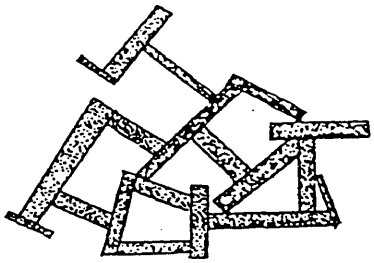

Figure 2.8 Saltwater Flocculation. (Lambe 1958)

Figure 2.9 Dispersed Structure. (Lambe 1958)

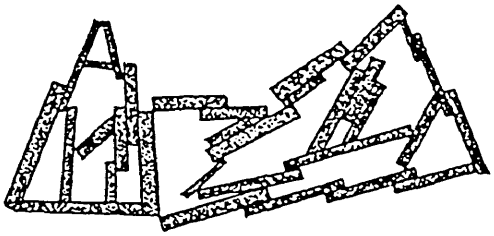

Figure 2.10 Non-Salt Flocculation. (Lambe 1958)

Variations of these modes in both the dispersed and aggregated states are presented in Figure 2.11.

Ideas of particle-to-particle contacts were challenged when water and nitrogen isotherms revealed a series of parallel crystals in a clay and identified a turbostratic structure (Aylmore and Quirk 1960). This structure was clarified by electron micrographs of the fractured sample

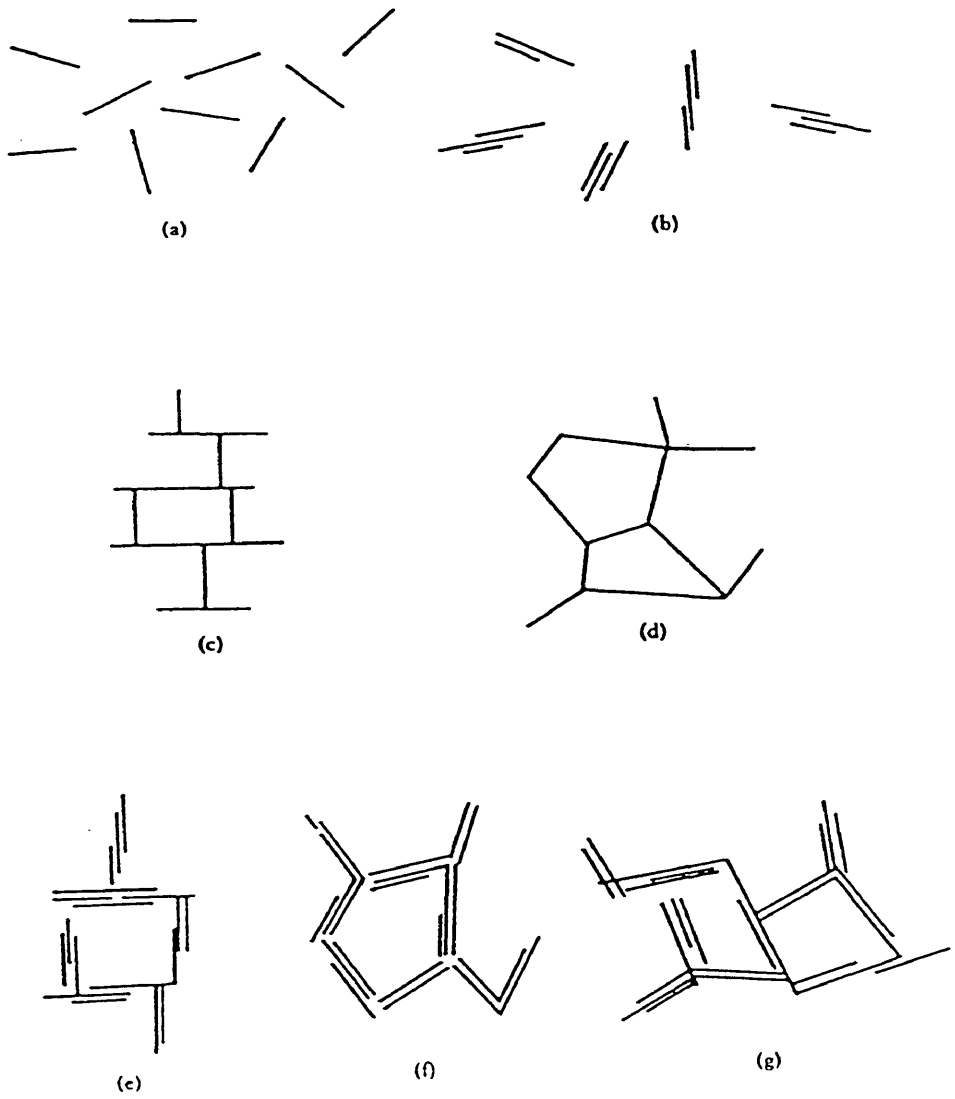

Figure 2.11 Particle Association Modes. (van Olphen 1963): (a) dispersed and deflocculated, (b) aggregated but deflocculated, (c) EF flocculated but dispersed, (d) EE flocculated but dispersed, (e) EF and FF flocculated and aggregated, (f) EE flocculated and aggregated, (g) EF and EE flocculated and aggregated.

surface, redrawn in Figure 2.12, in which definite groupings of parallel particles can be observed.

The Kozeny-Carmen equation was used by Olsen (1962) to estimate the structural effects on hydraulic conductivity and led to development of the cluster model of clay fabric. The cluster model presented a unique analysis of clay fabric interpretation in which two levels of pore sizes are presumed. Figure 2.13 illustrates how the model is composed of uniformly sized and porous particle clusters to create unequal pore sizes. Since flow is known to be proportional to the fourth power of the pore radii, flow rates through the cluster pores were considered negligible. Only flow around and between the clusters was thought to be significant. Compressive forces would therefore reorient the clusters to initially reduce the macropore spaces and leave the micropores unaffected. While individual particle alignment may remain unchanged, the overall hydraulic conductivity and void ratio would be reduced.

2.4 Present State of Knowledge of Soil Fabric

The present concept of soil fabric has advanced beyond the scope of the original single-grain clay particle arrangement. The ideas of a turbostratic structure proposed earlier (Aylmore and Quirk 1959) have since been accepted and subdivided into "tactoid", "packet", "stack", or

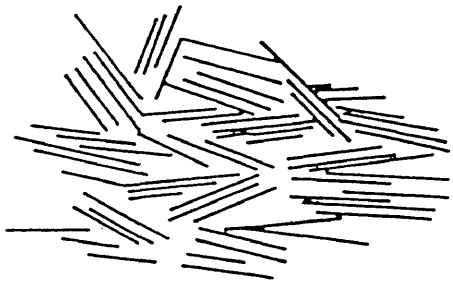

Figure 2.12 Turbostratic Structure. (Redrawn from Aylmore and Quirk 1960, in Bennett and Hulbert 1986)

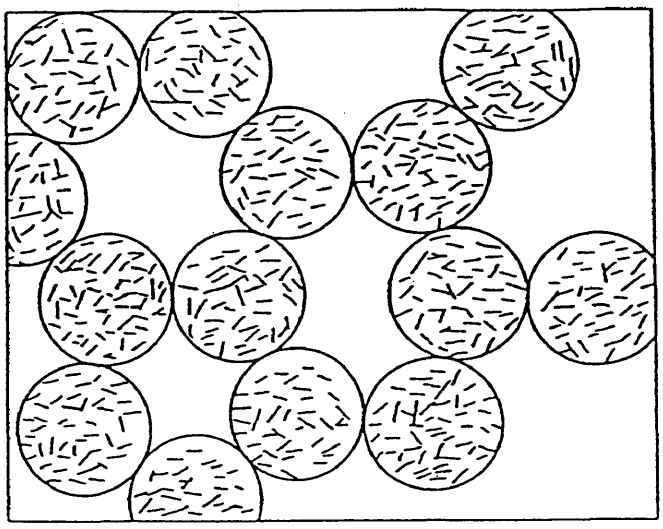

Figure 2.13 Cluster Model. (Olsen 1962)

"bookhouse" fabric types (Sloane and Kell 1966; Sides and Barden 1971).

The idealized modes of single particle association presented by van Olphen are considered unlikely to occur in

natural sediments (Moon 1972). Electron microscopy techniques have shown that undisturbed sediments (Bennett, et al. 1981) and consolidated sediments (Bowles and Bryant 1969) may be more accurately represented by domain or aggregate arrangements of clay particles. These results are similar to Ingles'(1968) concept of particle reorientation from a cardhouse structure to a domain grouping during consolidation. Figure 2.14 graphically describes this shifting of particles and reduction of void ratio during one-dimensional consolidation.

During the last two decades, the results of mercury intrusion porosimetry and electron microscopy studies have confirmed that hydraulic conductivity of clays is governed by the pore size distributions (Garcia-Bengochea et al. 1979). These studies have also shown that clay pores are distributed among 1) macropores surrounding assemblages of particles, 2) minipores within aggregations of particle groups, and 3) micropores between adjacent particles. The fabric model derived from electron microscopy studies by Collins and McGown is redrawn (Griffiths and Joshi 1990) in Figure 2.15 to illustrate these three fabric levels. The particle assemblages of this model correspond to the clusters in Olsen's model. In Collins and McGown's model, the first fabric level describes the macropores governing hydraulic conductivity to exist between particle

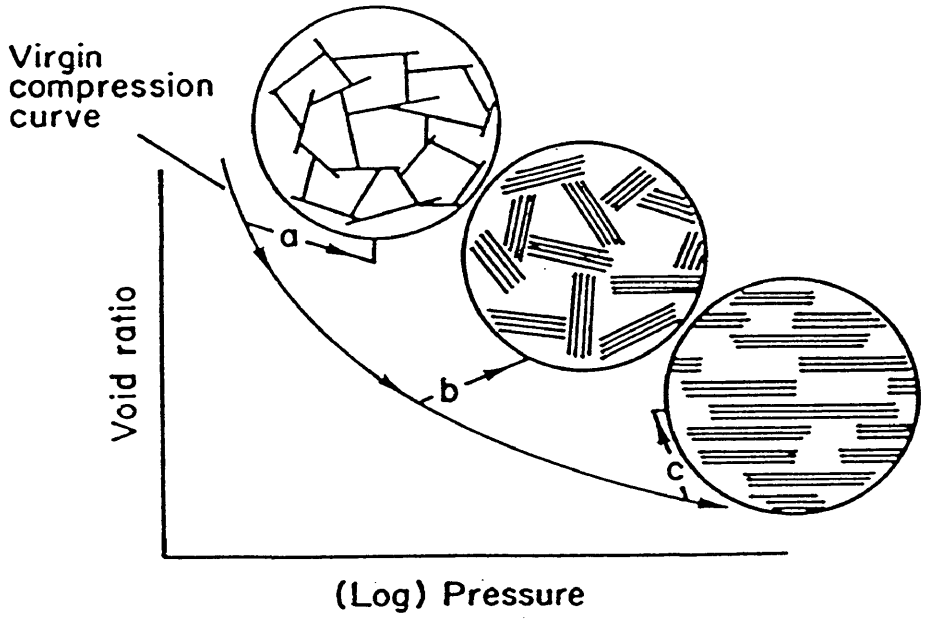

Figure 2.14 Fabric Changes During Consolidation. (Redrawn from Ingles 1968)

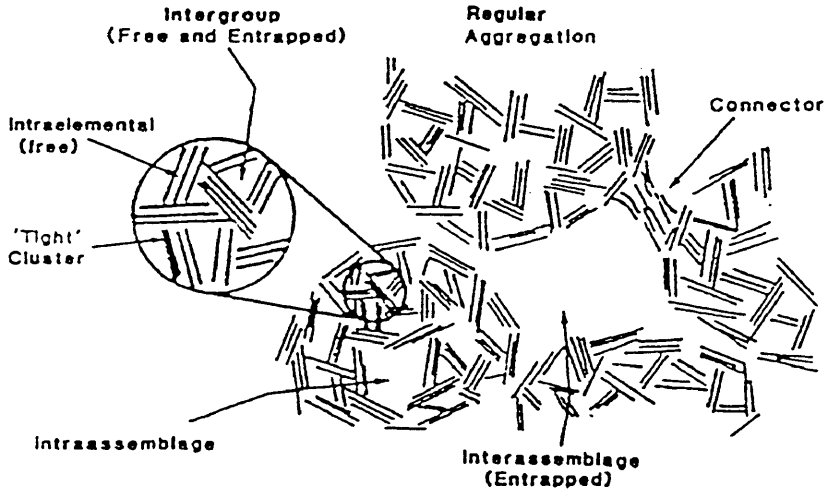

Figure 2.15 Fabric Elements and Pore Types. (Interpreted from Collins and McGown (1974) by Griffiths and Joshi (1990)

assemblages, which is comparable to the inter-cluster pores in Olsen's model. Collins and McGown's model identifies much smaller pore spaces within the assemblages. These include second level minipores between particle groups and third level micropores between individual particles. The smaller micropores and minipores within the clusters are combined in Olsen's model and referred to as intra-cluster pores.

More recent electron microscopy and mercury intrusion porosimetry investigations support Olsen's assumption that the intra-cluster void ratio remains constant during compression at high void ratios. These studies show that the volume decrease during consolidation of soft clays is due to changes in the volume of the largest existing pores; only minor to negligible changes in the micropores have been observed (Delage and Lefebvre 1984; Delage 1987; Griffiths and Joshi 1989, 1990, and Nagaraj et al. 1990).

Studies of compaction effects on hydraulic conductivity address the formation of "clods" of clay (Benson and Daniel 1990) and "interclod" pore size relationships through dye-stained seepage pathways (Elsbury, et al. 1990). In these studies, clods were used to describe the large aggregations of clay particles visible to the naked eye. The results strengthen the assumption made by the cluster model that flow through the micropores of the intra-cluster arrangement

is negligible in comparison to flow paths around the clusters.

2.5 Desiccation Influences

The evaporation of pore water in a clayey soil results in tensile forces within the capillary menisci. Minute tensile forces are thought to act equally in all directions (Spangler and Handy, 1982) and reorient the clay particle groupings. The greatest capillary stresses occur in the more dispersed fabric structures with smaller pore sizes. The parallel particle orientation of a dispersed fabric should allow greater ease of particle group movement and thereby permit the most shrinkage.

Remolded clays may be expected to undergo greater shrinkage and volume reduction than undisturbed materials, as indicated by lower dry void ratios (Mitchell 1976). Further, anisotropic soil structures reflect the corresponding processes of anisotropic shrinkage. Remolded clay samples have been observed to exhibit greater vertical shrinkage than lateral shrinkage (Warentkin and Bozozuk 1961).

Desiccation also contributes to a rigid soil skeleton that is more resistant to compression; this is similar to an overconsolidated soil (Lambe and Whitman 1969). Studies of air- and oven-dried clays indicate extreme distortion of the

original fabric (Naymik 1974, in Bennett and Hulbert 1986), almost like that of a "cornflake structure" in some clays (Yong 1972). Upon rewetting, it can be assumed that a different fabric exists than the fabric prior to desiccation.

2.6 Conceptual Model of Soil Fabric

A conceptual fabric model is necessary to aid in the interpretation of desiccation-induced fabric changes that are reflected through the directly measured k-e relationships. Characteristics of the cluster model and results of pore size distribution studies of argillaceous materials have been combined to develop such a model.

A baseline of understanding must first be established by defining the terms "structure" and "fabric". **Structure** is defined herein as the complex framework of solid particles held together by both plastic and rigid bonds. **Fabric** refers to the size, shape, and geometric arrangement of soil particles, groups of particles, and the pore spaces between the particles.

Prior to compression, individual uniformly-sized clusters of clay particles, each consisting of several domains, are oriented in a fashion respective to the undisturbed or remolded fabric. Both fabric types

are characterized by unequal pore sizes, through which flow around and between the clusters is most significant.

Compressive stresses applied to a clay will reorient the clusters and reduce only the inter-cluster pore spaces; the intra-cluster pores will remain unaltered. Hydraulic conductivity and void ratio will be reduced due to the smaller inter-cluster pore spaces. Additional compression will continue to reorient the clusters and reduce the inter-cluster pores until there is no longer a significant effect on hydraulic conductivity and void ratio relationships. At this point in the compressive phase, reductions in the intra-cluster pores will become significant as the particle domains are reoriented to the least energy position. The hydraulic conductivity and void ratio relationships will continue to decrease.

The effects of progressive desiccation on the clay mass prior to desiccation will also act to reduce the initial cluster size. A reduction in cluster size will physically reduce the intra-cluster pore spaces, thereby enlarging the inter-cluster pore spaces. Void ratio and hydraulic conductivity of the clay mass will increase. The measurable effects of desiccation-induced cluster size reduction are anticipated to be two-fold:

1) Higher values of hydraulic conductivity are expected to be measured in desiccated clays than that measured in undesiccated clays.
2) The clay structure is expected to be strengthened from the tensile stresses within the capillary menisci and therefore develop a greater resistance to compression.

Chapter 3

INVESTIGATIVE APPROACH

3.1 Introduction

Fabric determination in fine-grained soils may be accomplished by either a direct or indirect approach. Observation techniques, such as scanning electron microscopy (SEM) and pore size distribution, offer the advantage of direct measurement of specific fabric features.

Indirect fabric characterizations can be made from directly measured physical properties (Mitchell 1976). The physical properties of compressibility and hydraulic conductivity depend strongly on the nature of the soil structure and are fundamental to the study of soil phase relationships.

The following sections provide a review of three selected techniques for fabric measurement. SEM and pore size distribution were selected as two direct fabric observation techniques, while the measurement of physical properties was chosen as an indirect method of fabric interpretation. The practical and technical advantages of the physical properties method are compared with those of the direct fabric observation techniques. Lastly, the experimental system used in this investigation is described in detail.

3.2 Review of Fabric Observation Techniques

Many fabric observation techniques are available for laboratory use. Data needs and experimental objectives must first be evaluated prior to the selection of a specific technique. The prospective investigator is aided by Mitchell's comparison (1976) of commonly used direct and indirect methods of fabric study. This investigation considers the following physical properties affected by fabric:

1) Extreme range of clay mineral type, amount and particle sizes encountered in naturally occurring clays.
2) Variability of pore size.
3) Interrelation of soil structure with physical properties.

3.2.1 Scanning Electron Microscopy

The scanning electron microscopy technique directly reveals individual clay particle orientations, particle group arrangements, and pore spaces over a wide range of view (up to 20,000 X) (Barden and Sides 1970). A fine beam of electrons reflected across the specimen surface allow clay features (such as fabric and texture) to be seen and interpreted. This technique is limited to very small samples (approximate volume of 0.5 in^3) and is better suited

to certain clay minerals than others (Bohor and Hughes 1971). Pore fluid removal of the specimen is necessary, which eliminates the direct study of wet soils. The drying process also introduces the possibility of alteration of the microstructure (Diamond 1971). Clays characterized by a high swell potential, high water content, or high void ratio are expected to be significantly affected by drying. Sample preparation may be difficult, and the replication of the undisturbed sample surface by ultrathin sections can be questioned.

3.2.2 Pore Size Distribution

The size and distribution of pore spaces between groups of particles reveal important elements of clay fabric. Direct measurement of pore sizes indicates the hydraulic conductivity and compressibility relationships of a clay.

Forced intrusion of a non-wetting fluid (usually mercury) allows measurement of pore sizes ranging from 0.01 μm to several tens of micrometers. Pores are assumed to be cylindrical in shape and filled under pressure by the following relationship (Washburn 1921):

$$P = - \frac{4 \gamma \cos\phi}{d} \qquad (3.1)$$

Where:

P = Pressure applied

γ = Surface tension of fluid

ϕ = Contact angle (assumed)

d = Pore diameter

Limitations to the mercury pore size distribution method have been identified as (Diamond 1970):

1) Pores must initially be dry.
2) Isolated pores cannot be measured from the sample exterior.
3) Measurement of larger pores accessed by smaller pores is not allowed until the smallest pore is first intruded.
4) Instrument pressure capacity may not be sufficient to intrude the smallest pores.

As in the SEM technique, specimen shrinkage is possible due to the required emptying of pores by drying. Drying significantly decreases the total sample porosity and makes replication of in-situ properties questionable.

3.2.3 Physical Properties

As stated in Section 2.1, the physical properties of concern in this investigation are compressibility and hydraulic conductvitity. A clay structure and its related pore size distribution are dependent upon these material properties. The size and distribution of pore spaces are a function of the clay particle orientation and arrangement. Therefore, data trends observed in the directly measured physical properties can be utilized to indirectly characterize the clay fabric state.

Soil compressibility is indicated through the consolidation process. One-dimensional consolidation is a commonly used technique that allows measurement of undisturbed, variably sized wet soils, which are considered to better reflect in-situ conditions. Hydraulic conductivity measurements support deductions of fabric alteration caused by collapse of the clay skeleton. The conceptual fabric model presented in Section 2.4 allows an interpretation of the measured hydraulic conductivity and compressibility relationships.

3.3 Advantages of Physical Properties Approach

Each method previously discussed has substantial merits and disadvantages. Advantages of the physical properties approach to fabric interpretation are summarized as follows:

Practical Advantages:

1) Testing equipment is common and easily obtainable.
2) Comparable expenses of laboratory facilities for testing are much less, allowing for a greater quantity of samples to be analyzed.

Technical Advantages:

1) Sample preparation is straightforward and simple.
2) In-situ conditions are better reflected by testing soils maintained at the natural water content.
3) Larger sample sizes contribute to the assumption of in-situ conditions.
4) Use of wet soils reduces the possibility of unwanted desiccation-induced fabric alteration prior to loading.
5) Measurement of either multi- or single mineral sample compositions is allowed.
6) Fabric changes occurring throughout the range of induced stresses in a test are reflected by a single sample.
7) Fewer restrictive assumptions of the sample are made, such as cylindrical pore shapes, interconnecting pores, and single contact angles.

3.4 Experimental System

The constant head or falling head methods are typically used to measure hydraulic conductivity. Development of the constant flow (flow pump) method (Olsen 1966) provides another direct measurement technique with greater advantages over traditional approaches (Olsen, et al 1985).

Methods of one-dimensional consolidation have traditionally used stress-controlled, incremental loading as a means of measuring compressibility. Continuous loading approaches have been developed by others that control 1) the rate of strain (Crawford 1964; Smith and Wahls 1969; Wissa et al. 1971), 2) the hydraulic gradient (Lowe et al. 1969), or 3) the pore pressure-load ratio (Janbu et al. 1981).

Recent advances incorporate both principles of direct measurement to formulate a volume-controlled, continuous loading technique with periodic, constant flow hydraulic conductivity tests (Gill 1989). The quantity and quality of data obtained with this particular experimental system far exceeds the information gained with conventional consolidation equipment.

This study used the same system developed Gill (1989). The system has been slightly modified to allow the application of a vacuum on the specimen prior to saturation in order to avoid entrapment of air bubbles. Section 4.4.4. explains the test system modifications in further detail.

In general terms, the apparatus used for this thesis consists of a one-dimensional back pressure consolidometer that has been configured for continuous loading. A flow pump provides a constant rate of volume change (a constant rate of sample deformation). A second flow pump permits intermittent hydraulic conductivity measurements by superimposing a constant external flow across the sample base. Transducers continuously monitor the effective stress, the base pore pressure, and the sample deformation rate.

3.4.1 Boundary Conditions

The boundary conditions described by Gill (1989) for this system remain the same, and are presented as follows:

1) All flows and stresses are considered one-dimensional.
2) At any selected point in time, the void ratio distribution across the specimen is considered to be constant.
3) A fixed ring apparatus allows fluid flow to or from the top of the sample. Excess, undrained pore water pressure at the base of the sample is continuously monitored.
4) A constant flow rate (Q_c) imposed at the top of the sample and the corresponding base pore pressure (u_b)

are synonymous with a constant rate of deformation (CRD) test.

5) An assumed linear head loss through the sample is caused by an external constant flow rate (Q_c) periodically imposed across the sample.

Figure 3.1 illustrates the vertical distribution of pore pressure through the sample, reflective of most CRD one-dimensional consolidation tests. Figures 3.2 and 3.3 illustrate the profile of steady state boundary conditions for flows superimposed upward and downward through the sample, respectively. The sum of the parabolic and linear profiles of base pore pressure are used to calculate hydraulic conductivity using Darcy's law.

3.4 System Description

Figure 3.4 presents a schematic of the experimental system. A sample (n) is situated in a Teflon lined fixed ring, between an upper and lower porous stone. Fluid pressure in the back pressure chamber (m) is controlled by the absolute pressure regulator (b) and the back pressure bellofram (c). The chosen back pressure is transmitted to the confined sample by way of the top porous stone.

Loading is conducted by either one of two methods. The first method is a stress-controlled system that utilizes the

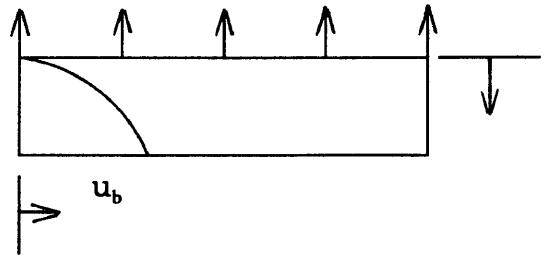

Figure 3.1 Boundary Conditions for a CRD Test.

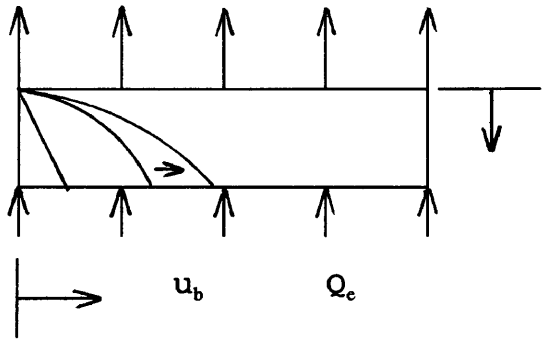

Figure 3.2 Boundary Conditions for Upward Flow.

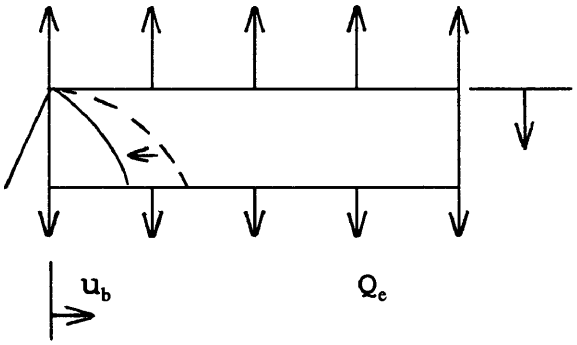

Figure 3.3 Boundary Conditions for Downward Flow.

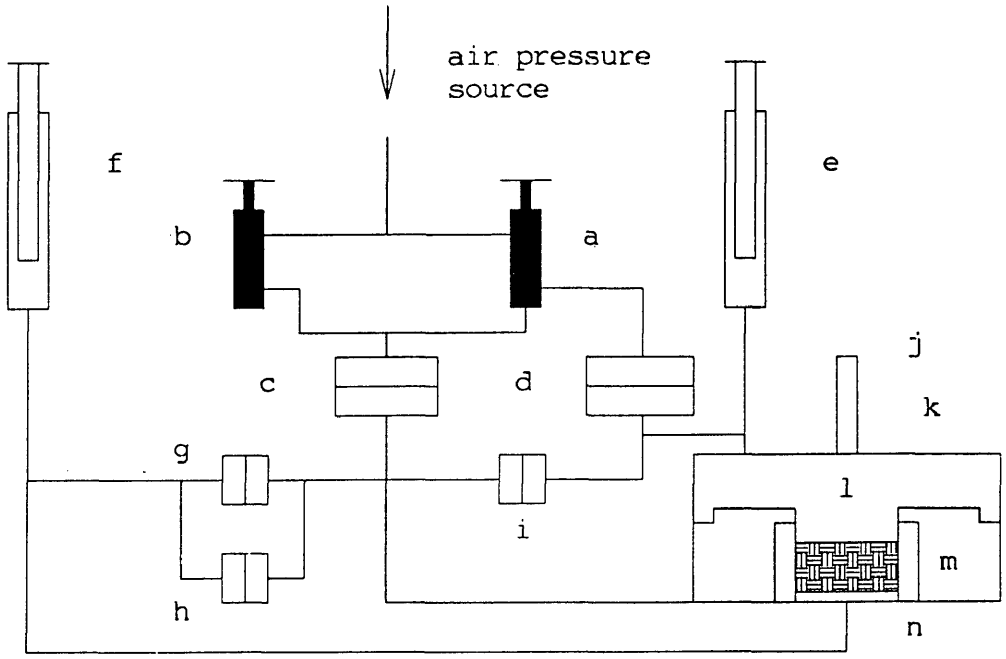

Figure 3.4 Schematic of Experimental System. (Redrawn from Gill 1989)

a) Differential pressure regulator
b) Absolute pressure regulator
c) Back pressure bellofram
d) Air-water interface
e) Deformation flow pump
f) Hydraulic conductivity flow pump
g) Differential pore pressure transducer (high range)
h) Differential pore pressure transducer (low range)
i) Differential load pressure transducer
j) Linear variable differential transducer (l.v.d.t.)
k) Back pressure consolidometer
l) Load chamber
m) Back pressure chamber
n) Sample

differential pressure regulator (a) and air-water interface (d). Typically, a small, constant seating load is applied in this fashion through the load chamber (l) while the sample is saturated for a specified period. The second method allowed is the volume-controlled approach, which uses the deformation flow pump (e) to continuously load the sample.

Periodic hydraulic conductivity tests are conducted with the hydraulic conductivity flow pump (f). The external flow across the sample base induces a small hydraulic gradient, reflected as an increase or decrease in base pore pressure.

The total vertical stress, being the effective stress at the top of the sample, is measured by the differential load pressure transducer (i). Pore pressure at the sample base is measured by the high or low range differential pore pressure transducer (g or h). Sample deformation is measured by the linear variable differential transducer (l.v.d.t.) (j).

An analog strip chart recorder (not shown) continuously monitors the effective stress, base pore pressure, and sample deformation. System equipment and the respective capabilities are presented in Table 3.1.

Table 3.1 System Equipment and Capability

ITEM	EA	MANUFACTURER	MODEL	RANGE	ACCURACY
Back Pressure Consolidometer	1	Anteus Corp.	A-1	N/A	N/A
Flow Pumps:					
7/8" i.d.	1	Harvard Apparatus	901	0.411225 to 8.22e-5 cc/s	N/A
3/8" i.d.	1	Harvard Apparatus	906	0.075531 to 1.511e-5 cc/s	N/A
Pressure Measurement:					
Panel meter	1	Validyne Engineering	MCI-10	N/A	N/A
Differential transducers	3	Validyne Engineering	P300-D P300-D P300-D	±500 psi ± 50 psi ± 5 psi	±0.5 full scale ±0.5 full scale ±0.5 full scale
Deformation Voltmeter (l.v.d.t.)	1	Shaevitz	500 HR-DC	±0.5 in.	±0.5 full scale
Power Supply	1	Hewlett-Packard	6215-A	N/A	N/A
Digital Multimeter	1	Kiethley	178	N/A	N/A
Analog Strip Chart Recorder	1	Soltec	1243	Output resolution	σ': 0.1 psi u_b: 0.002 psi

Table 3.1 continued

ITEM	EA	MANUFACTURER	MODEL	RANGE	ACCURACY
Pressure regulators	2	Anteus Corp. (original equip.)	N/A	N/A	N/A
Belloframs	2	Bellofram, Inc.	Type D, Size 4	N/A	N/A
1/8" Stainless Steel Tubing			N/A	N/A	N/A
Fittings		Swagelock	N/A	N/A	N/A
Valves	65	Whitey	N/A	N/A	N/A

3.4.3 System Compliance and Head Loss

Compliance refers to the variation of liquid volume contained within the system in response to a head change, also within the system (Olsen, et al. 1988):

$$S = \frac{dv}{dh} \qquad (3.2)$$

Where:

S = Compliance

dv = Liquid volume increment

dh = Head change

The permeant system compliance has not been significantly affected by the modifications of the original testing apparatus. The accuracy of the hydraulic conductivity flow pump remains very much the same, indicated by Figure 3.5.

The permeant system head loss from only the stainless steel tubing, porous stones, and filter paper arrangement is presented in Figure 3.6. As in the original system, no head loss corrections are needed, since flow rates less than 3.7766×10^{-4} cc/s do not reflect any head loss effects. The flow rates for hydraulic conductivity testing used in this investigation are less than this measurable value.

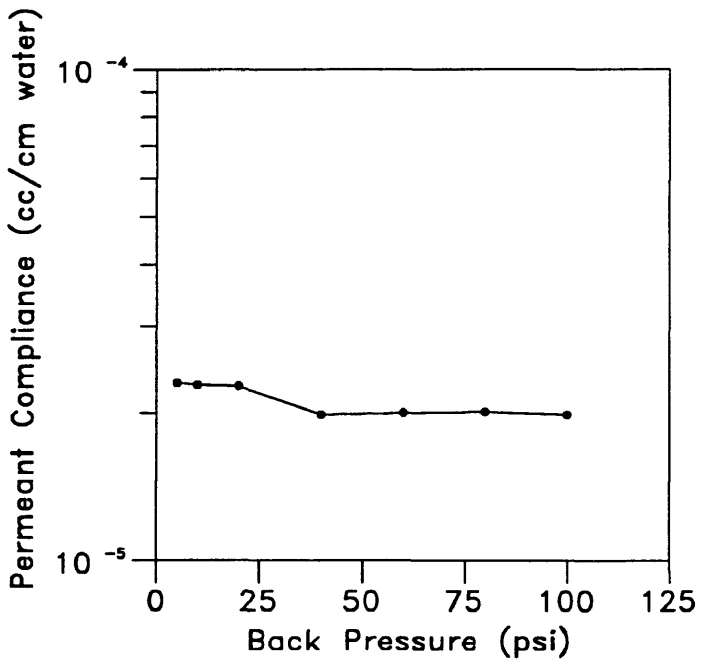

Figure 3.5 Permeant Compliance as a Function of Back Pressure.

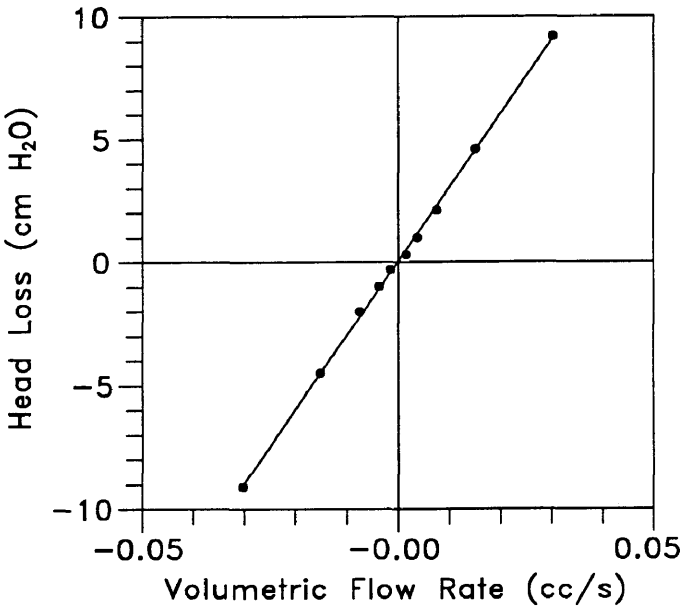

Figure 3.6 Permeant System Head Loss (without sample).

The loading system compliance has been improved through tighter fittings in the load pressure chamber and the loading bell. Figure 3.7 presents a comparison of the original and revised loading system compliance curves. It is important to note that the revised compliance curve was measured with a smaller loading flow rate and at a lower system back pressure than the original, yet revealed almost an 80 percent improvement in system compliance. The improvement is illustrated by the increased slope and linearity of the revised compliance curve. The overall results are 1) better volume control, 2) reduced testing time, and 3) more accurate sample deformation. A small curvature still remains during the initial pressure build-up, which is assumed to reflect the compressibility of the neoprene bellofram membrane used in the load pressure chamber.

As in the original system, stainless steel tubing has been included to reduce the effects of expansion under pressure. It is known that elevated back pressures force small air bubbles to dissolve in the water. The duration of time the system is maintained at a constant back pressure is also thought to improve loading compliance. Figures 3.8 and 3.9 compare separate loading system compliance tests at selected back pressures 1) immediately after elevating the back pressure (immediate loading), and 2) after allowing the

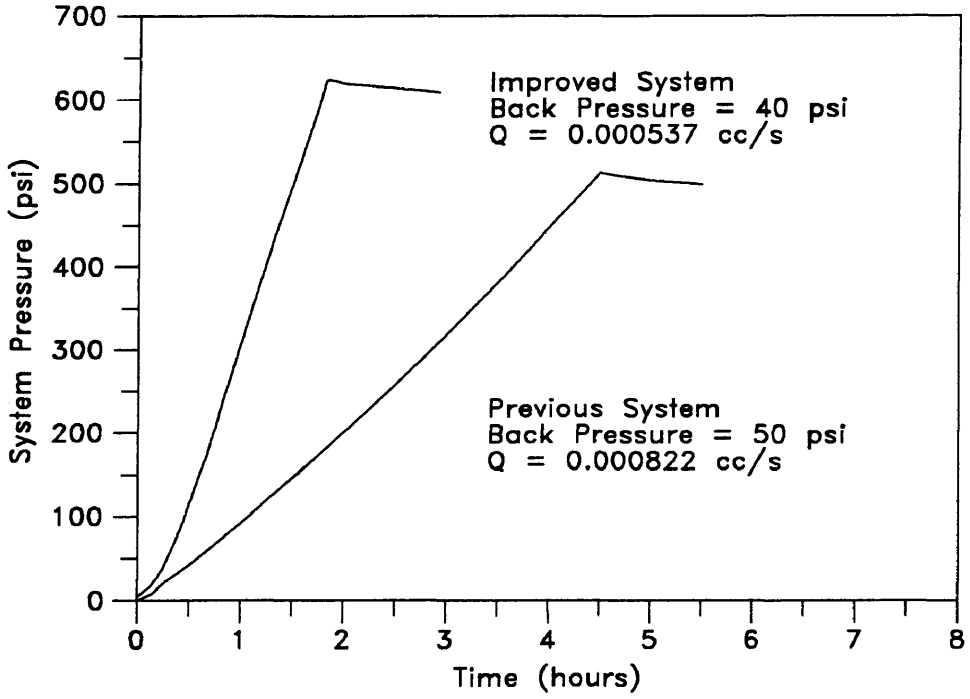

Figure 3.7 Improved and Original Loading System Compliance.

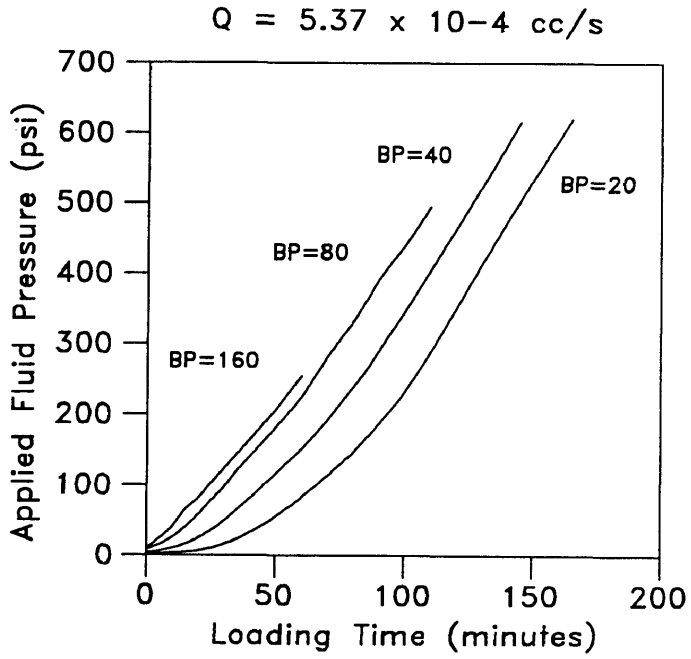

Figure 3.8 Immediate System Compliance Test Curves.

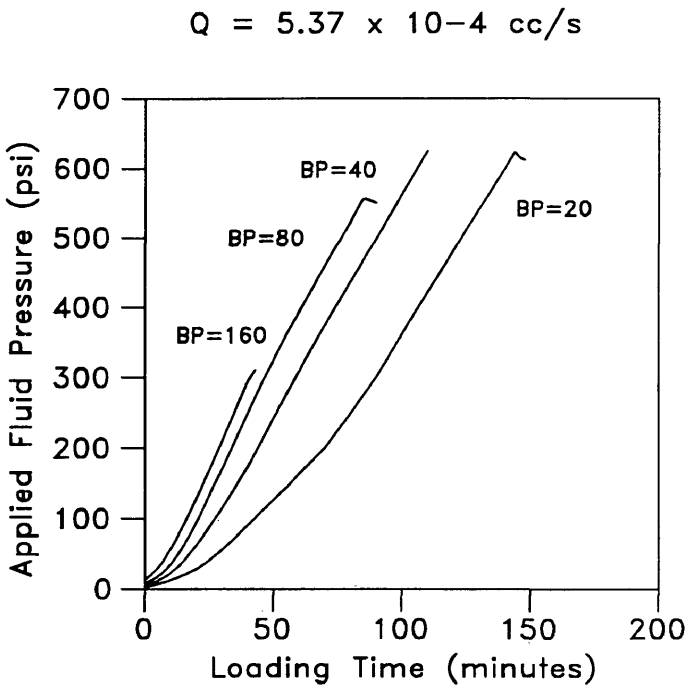

Figure 3.9 Delayed System Compliance Test Curves.

system to stabilize under back pressure for at least twenty-four hours (delayed loading). The average slope of the delayed loading family of curves is greater than that of the immediate loading family of curves. This increase in slope is interpreted as a transient means to improve loading system compliance.

Based on the information from Figures 3.8 and 3.9, a minimum saturation period of 24 hours under a back pressure of 60 psi was selected for the testing program. The back pressure was chosen because of the decreasing shift of the

delayed loading system compliance curve. A separate loading system compliance curve was generated under a back pressure of 60 psi and was used in the final data reduction and analysis.

Chapter 4

TESTING PROGRAM

4.1 Sample Receipt and Storage

The natural clay tested in this investigation was obtained in thin-walled Shelby tubes and was therefore considered to represent an undisturbed soil (ASTM 1990). Upon arrival to the laboratory, the clay was extruded from the Shelby tubes, wrapped tightly in plastic, and stored in a humid room to prevent moisture loss.

4.2 Undisturbed Sample Preparation

A small portion of clay is first cut from the main sample and vertically trimmed to a diameter of two and one-half inches with a stainless steel cutter. The trimmed clay is extruded into a Teflon lined stainless steel ring, which will serve as the fixed ring apparatus during the consolidation testing program. The clay is then trimmed from the ends of the ring to an approximate height of one-half inch using a stainless steel extruder and soil saw. Desiccation of the trimmed sample is monitored after it is pushed out of the ring onto a porous stone and placed in a ceramic dish. The initial sample height, diameter, and water content (indicated by the trimmings) are recorded. The dish is then tightly wrapped in plastic and a small

puncture is made in the center. It is assumed that the small hole will allow slow, uniform air drying of the sample.

When the sample has dried to a preselected water content, testing may begin. Sample height, diameter, and water content are again recorded prior to testing to estimate the desiccation-induced changes in the undisturbed soil fabric.

4.3 Reconstituted Sample Preparation

Trimmings collected during preparation of the undisturbed specimens are allowed to fully air dry, are broken down to a grain size passing through a #40 standard sieve, and are then rewetted and mixed with deionized water to form a viscous slurry. The slurry is placed under a vacuum to reduce excessive air voids and then carefully poured into a Teflon lined stainless steel ring. Upper and lower porous stones and filter paper confine the slurry solids in the ring, but allow excess pore water to drain freely. Agitation of the slurry is avoided because of the possibility of particle segregation. The slurry is uniaxially compressed at a constant rate to a precalculated height and water content that reflect an initial void ratio similar to that of the undisturbed, natural clay.

When the initial, remolded state is achieved, the sample is trimmed, extruded onto a porous stone, and allowed to air dry in the same manner previously described for the undisturbed material. Again, the reconstituted sample height, diameter, and water content are recorded after a preselected desiccation state has been achieved.

4.4 Sample Testing

After the undisturbed and reconstituted specimens are prepared and permitted to desiccate to the appropriate stage, consolidation testing is begun. Several compressibility and hydraulic conductivity measurements are made over a range of consolidation states in the adapted oedometer apparatus. The testing program for each sample consists of the following activities:

- Calibration of the transducers.
- Filling the system.
- Loading the sample.
- Filling the test cell and saturating the sample.
- Performing the test.
- Removing the sample.

4.4.1 Calibration of Transducers

The low range (± 5 psi) pore pressure transducer is calibrated with an equivalent standing head of water. Regulated air pressure serves as the basis for the high range pore pressure transducer (± 50 psi) and the effective stress transducer (± 500 psi) calibration.

The l.v.d.t. has been built into the top of the test cell, making conventional calibration impossible because of the confined shaft and surrounding fluid. Instead, a series of machined gage blocks are selectively placed inside the test cell under the loading bell for calibration under atmospheric conditions. The l.v.d.t. voltage readings are plotted as a function of the gage block heights. The resulting linear relationship is used to calculate sample displacement and void ratio due to compression. The l.v.d.t. calibration curve used for this investigation is presented in Figure 4.1.

The applicability of an indirect method for estimating sample displacement by volumetric measurements of the pore water has also been investigated. This method and the results are further explained in Section 6.4.

4.4.2 Filling the System

The air-water interface is manually filled with deaired, deionized water at atmospheric pressure. An

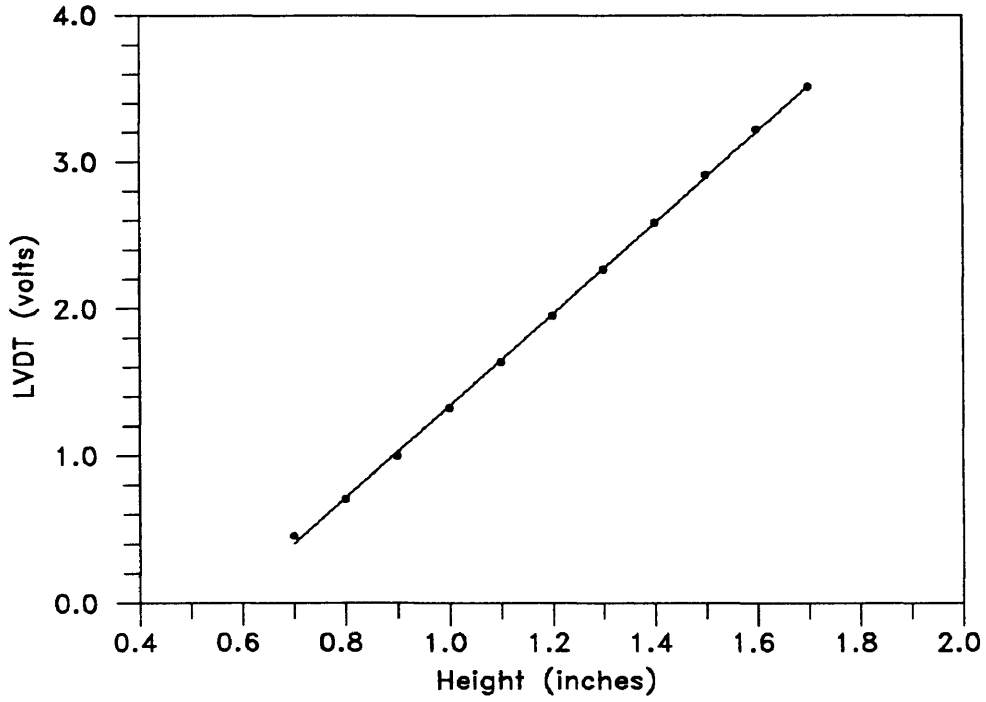

Figure 4.1 l.v.d.t. Calibration Curve.

overhead reservoir of deaired, deionized water, normally kept under a vacuum of 24 inches of mercury, is brought to atmospheric pressure. The back pressure bellofram is isolated from the rest of the system, under atmospheric pressure, and filled under gravity flow from the reservoir. The reservoir is disconnected from the bellofram, which is then brought back into the system and placed under a regulated air pressure.

The flow pumps are cycled back and forth several times, each time drawing pressurized fluid from the back pressure bellofram and purging air bubbles into an Erlenmeyer flask.

The flow pumps are then isolated under pressure from the remainder of the system.

The bleed ports of the pressure transducers are opened and allowed to flow to the atmosphere until no more air bubbles are observed. It is important to sequentially purge air from the lowest to the highest placed transducer in order to assure that isolated air bubbles are successfully forced upward and out of the bleed ports.

The load pressure chamber line is purged of air bubbles by way of the deformation flow pump, back pressure bellofram, and air-water interface. The back pressure line and base pore pressure line are each purged of air using the back pressure bellofram and hydraulic conductivity flow pump, respectively.

The pore pressure subsystem is isolated from the remainder of the system to allow a final calibration of the low range pressure transducer.

The load pressure chamber, illustrated by Figure 4.2, is filled separately from the system. Deaired, deionized water is manually transmitted through the load pressure port into the load pressure chamber. Air is purged from the chamber by way of the l.v.d.t. core assembly as the loading bell is pushed upward. It is important that fluid (free of air bubbles) flow continuously from the hollow core assembly as the bleed screw is simultaneously replaced.

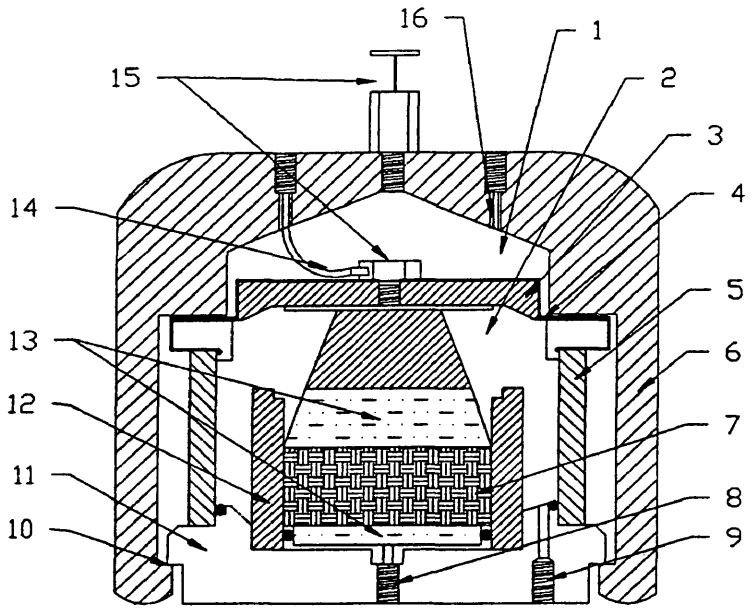

Figure 4.2 Load Pressure Chamber. (Redrawn from Gill 1989)

1) Load pressure chamber
2) Back pressure chamber
3) Loading disk
4) Rolling diaphragm
5) Lucite chamber wall
6) External wall
7) Specimen
8) Pore pressure port
9) Back pressure port
10) Bayonet type lock
11) Base
12) Consolidation ring
13) Porous stones
14) Back pressure chamber bleed port
15) Deformation measurement system
16) Load pressure port

4.4.3 Loading the Sample

The water reservoir, test cell, and its respective lines connecting it to the back pressure bellofram and the reservoir, all are kept at atmospheric pressure. The remainder of the system is isolated and maintained under pressure. The lucite chamber wall is removed. A saturated base porous stone is covered with a trimmed piece of wetted filter paper and connected to the cell base. A slight amount of water is allowed to drain from the reservoir through the base porous stone to maintain saturation of the stone and filter paper.

The partially air-dried sample is placed atop the base porous stone and filter paper. The confining ring is lowered onto the base porous stone and sample assembly, and pushed downward to complete the O-ring seal between the stone and ring wall. A slight gap may remain between the sample and ring wall, depending on the extent of desiccation-induced volume reduction and fabric state. This gap must be eliminated prior to conducting the test.

The lucite chamber wall is replaced and the saturated top porous stone and filter paper assembly is placed in the ring and on top of the sample. The load pressure chamber is locked into place with the bayonet connection and brought on line with the remainder of the system, all at atmospheric pressure.

The l.v.d.t. is placed on the core assembly and allowed to stabilize at room temperature. The laboratory is maintained at a temperature of 70 °F, ± 1 °F, which reduces system compliance effects caused by thermal expansion and contraction. A plexiglass housing contains the entire system so that output voltage fluctuations of the l.v.d.t., initially caused by temperature maintaining wind currents in the laboratory, are reduced.

The back pressure chamber bleed port is connected to a vacuum line, in series with the reservoir. A small seating load is applied to the sample by the differential pressure regulator. The pressure source is then disconnected at the air-water interface, so that a constant seating load is maintained in the load pressure chamber and monitored by the effective stress transducer.

4.4.4 Filling the Test Cell and Saturating the Sample

To avoid the possibility of entrapment of air bubbles at the sample base, a vacuum of twenty-four inches of mercury is applied to the system and reservoir. Figure 4.3 describes the changes in pressure as air is removed and the test cell is filled with fluid.

The test cell and load pressure chamber are initially free of fluid and at atmospheric pressure. A slight pressure increment is added to the loading pressure chamber,

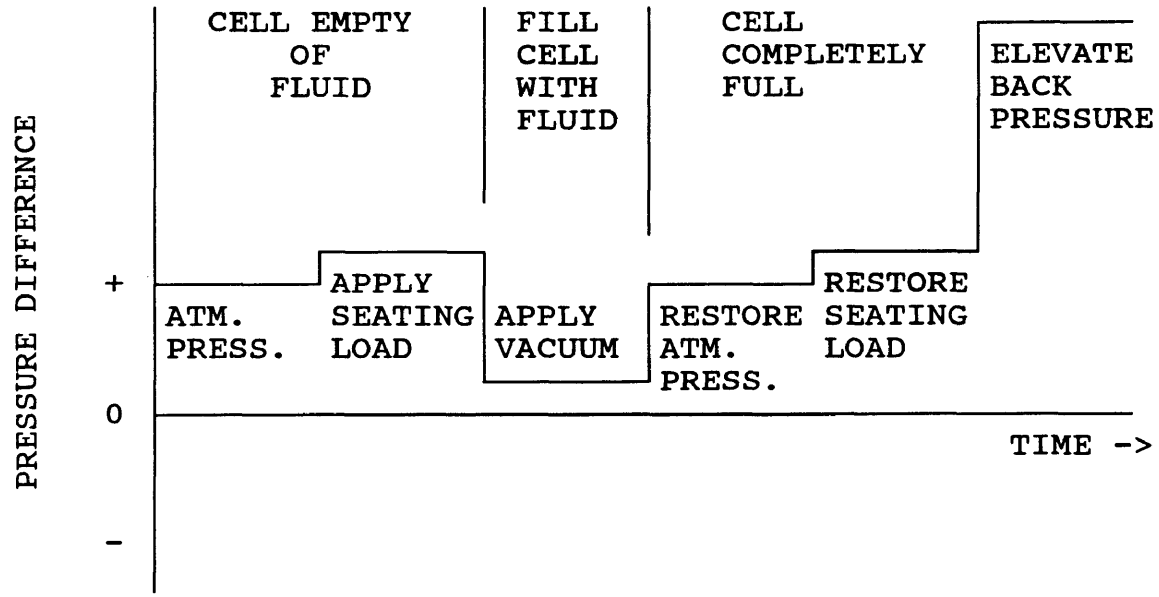

Figure 4.3 Pressure Changes During Test Cell Filling.

causing a small seating load to be placed on the sample. The vacuum is then applied, and the pressure difference across the sample is reduced as air is removed. A second Erlenmeyer flask on line with the back pressure chamber and reservoir serves as a vacuum trap. Air is considered to be completely purged from the test cell when very few bubbles are observed in the flask and after the reduced effective stress has stabilized under the vacuum.

While the vacuum is still applied, the reservoir is connected to the system and the test cell is filled by gravity drainage. Air entrapment within the sidewall gaps and sample-base porous stone interface is significantly

reduced by the vacuum application. As the test cell is slowly filled with fluid, any possible sample swelling is continuously monitored by the l.v.d.t. Water under vacuum can be observed rising above the system through the back pressure chamber bleed port, indicating that the test cell is completely filled.

The system is then isolated from the vacuum and reservoir and brought back to atmospheric. The original seating load is restored by connecting the air-water interface; the back pressure is elevated. Sample saturation is allowed for at least twenty-four hours which will further force any remaining air bubbles into solution.

4.4.5 Performing the Test

The stages of sample testing can be itemized as follows:

Stress Controlled:

- Initial hydraulic conductivity testing under a constant seating load.

Volume Controlled Deformation:

- Continuous loading causing sample deformation.
- Intermittent hydraulic conductivity tests during deformation.

Relaxation:

- System and sample relaxation at maximum vertical effective stress.

Volume Controlled Rebound:

- Continuous unloading allowing sample rebound.
- Intermittent hydraulic conductivity tests during rebound.

Figure 4.4 illustrates a typical time history plot for a test. The variations in total stress, base pore pressure, and void ratio are plotted separately. During the stress controlled stage, the total stress and void ratio remain constant under application of a seating load, while initial hydraulic conductivity tests, designated as "k-tests" are performed. The volume controlled deformation stage induces continuous compression of the sample, causing a constant rate of void ratio decrease and buildup of base pore pressure, indicated as "compression baseline". Intermittent k-tests performed throughout the entire test are recorded as small vertical spikes on the compression baseline. The relaxation stage begins after the maximum stress is achieved and the loading flow pump is turned off. Stresses are redistributed throughout the system and the sample stresses decay slightly. Void ratio remains constant and base pore pressure decays to approximately zero. The final volume

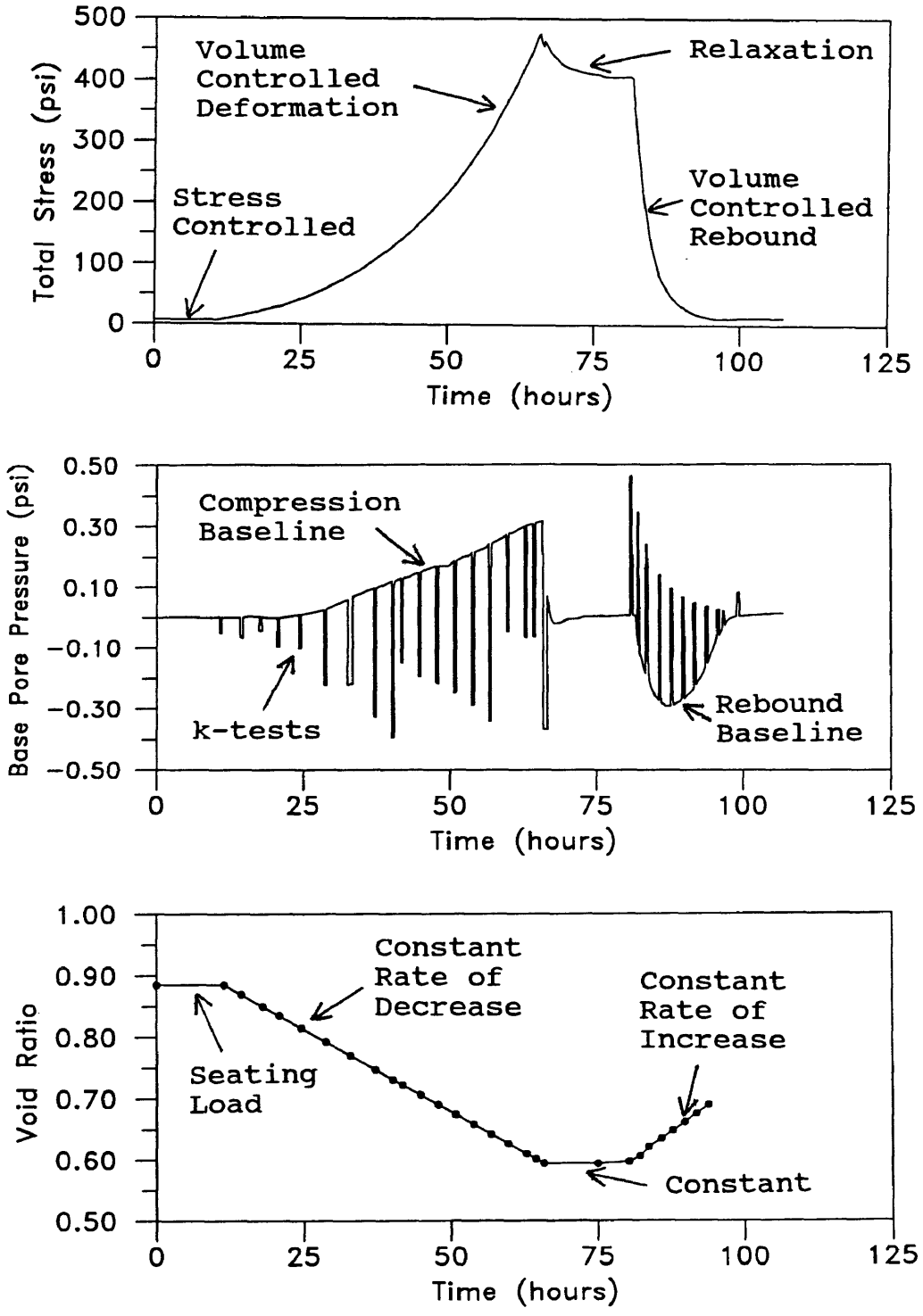

Figure 4.4 Time History Plots of Total Stress, Base Pore Pressure, and Void Ratio.

controlled rebound stage permits a constant rate of void ratio increase and decay of the "rebound baseline". The individual stages are outlined and described below in further detail.

Stress Controlled Stage

A constant seating load is applied via the differential pressure regulator and air-water interface during sample saturation. Initial hydraulic conductivity tests are conducted to determine when sidewall leakage has been eliminated. The regulated back pressure is isolated from the pore pressure subsystem, which allows measurement of the difference between the base pore pressure and the back pressure at the top of the sample. The hydraulic conductivity flow pump is placed on the "withdraw" setting and turned on a low gear speed. A very small, external flow rate is induced across the sample base, which causes a low, but measurable hydraulic gradient. Steady state flow across the sample base at the low hydraulic gradient indicates that sidewall leakage has been eliminated.

Volume Controlled Deformation Stage

The sample is readied for continuous loading by isolating the regulated pressure at the air-water interface and connecting the deformation flow pump. The flow pump is

placed on the "infuse" setting at the slowest deformation rate possible and then turned on. The l.v.d.t. records sample height throughout the entire test.

After a small transient response, a compression baseline is developed and the base pore pressure increases. Intermittent hydraulic conductivity tests are performed simultaneous to sample loading, providing information of the k-e relationship for that stress increment. It is necessary that the hydraulic conductivity tests be periodically interrupted in order to maintain the compression baseline.

Relaxation Stage

The loading process continues until the maximum vertical effective stress is achieved. The flow pump is then shut off and the excess base pore pressure is allowed to decay. Void ratio is held constant as the system and sample stresses decrease due to relaxation.

Volume Controlled Rebound Stage

The deformation flow pump is placed on the "withdraw" setting and turned on. Another transient response occurs during unloading prior to establishment of a rebound baseline. Hydraulic conductivity tests are performed in the same manner as previously described, with the exception that the "infuse" setting is now used on the flow pump. Sample

unloading and hydraulic conductivity tests are continued until the vertical effective stress is reduced to approximately zero.

4.4.6 Removing the Sample

Upon completion of the test, the pore pressure subsystem is again isolated under back pressure from the remainder of the system. The test cell, back pressure bellofram, and load pressure chamber are brought to atmospheric pressure. The cell is drained by gravity flow and the load pressure chamber is removed. The sample is extruded from the confining ring and the final height and wet weight are recorded prior to oven drying.

4.5 Suite of Samples Tested

Undisturbed and reconstituted clay specimens were exposed to similar degrees of desiccation and tested in this investigation. Although both suites of samples have similar initial void ratios, the different fabric states are reflected by the measured properties of compressibility and hydraulic conductivity.

Table 4.1 presents the testing scheme for each specimen type and the degree of desiccation prior to testing.

4.6 Geological Setting and Depositional History

The material used in this testing program was obtained from a single borehole in Carroll Island, Maryland. The area is described (Bennett and Meyer 1952) as being comprised of Pleistocene deposits that overlie pre-Cambrian

Table 4.1 Suite of Samples Tested

Specimen Type:	Undisturbed, naturally deposited				
Sample:	U-1	U-2	U-3	U-4	
w (%):	31.1	25.2	10.6	7.2	
Specimen Type:	Disturbed, reconstituted				
Sample:	R-1	R-2	R-3	R-4	R-5
w (%):	33.5	21.0	17.9	9.4	6.4

rocks and Cretaceous formations. The Pleistocene deposits are of variable thickness and consist chiefly of sand, gravel, and clay. Two similar units, an upland and a lowland deposit make up the Pleistocene materials. The two units are distinguished primarily by the altitude of the alluvial terraces from which the deposits originate. Samples were taken from the Talbot formation of the lowland deposit, at a depth of 15 to 17 feet. The Talbot formation

is largely a coastal plain deposit that slopes gently into the sea in the southeastward direction. The soft gray clay was interpreted as being deposited in a marine environment atop an older fluvial deposit of coarse sand and gravel.

4.7 Geotechnical Properties

The natural clay tested for this thesis has a natural water content of approximately 30% and is a well-graded silty clay with a clay fraction (grain size less than 2 μm) of approximately 22%. The particle size distribution is shown by Figure 4.5. The material is slightly organic and of moderately low plasticity, indicated by Figure 4.6. Table 4.2 summarizes the average geotechnical properties of the natural clay. Data tables included in Chapter 5 present detail measurements of the physical properties of each specimen tested.

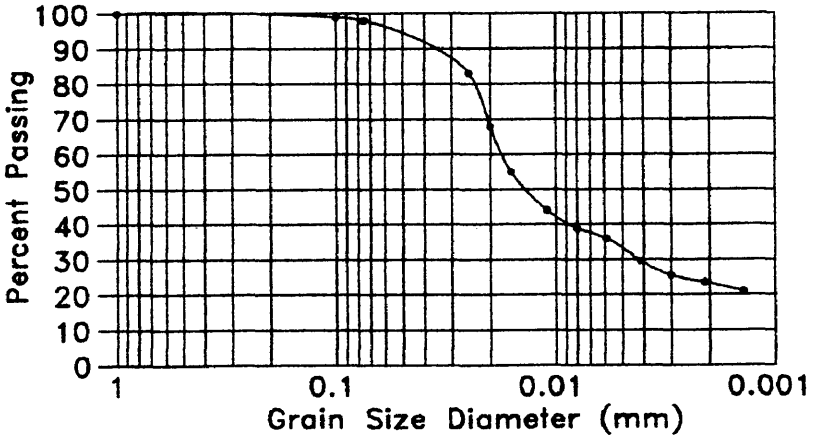

Figure 4.5 Particle Size Distribution. (ASTM D-422)

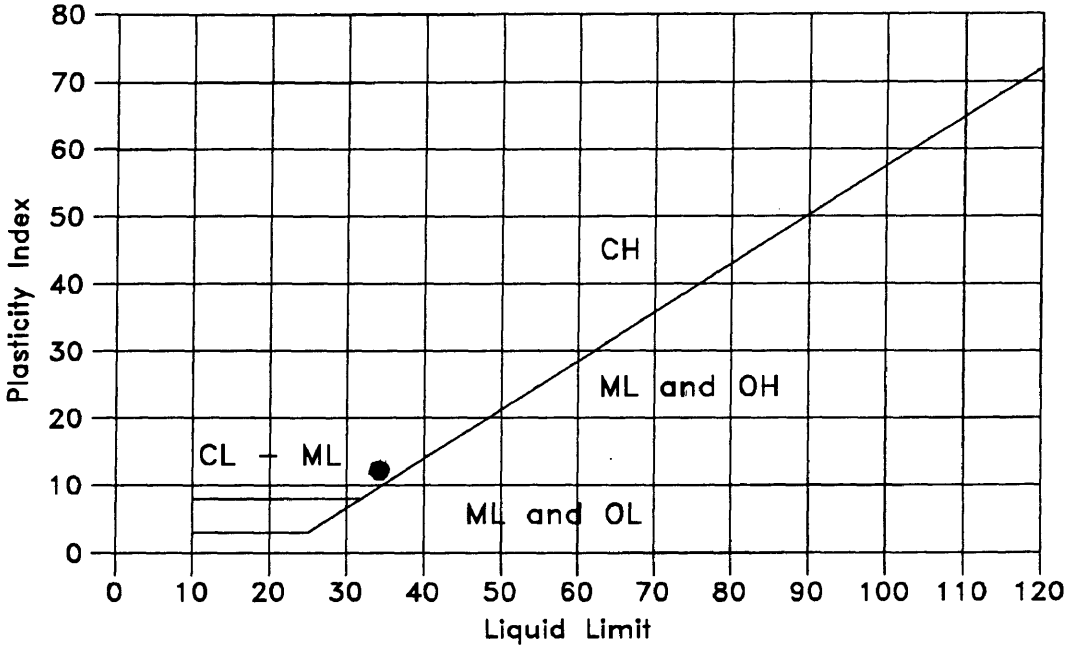

Figure 4.6 Plasticity Characteristics. (ASTM D-4318)

Table 4.2 Geotechnical Properties of Carroll Island Clay (Well I-28)

Depth	15-17 ft
Avg. e_o	0.86
Liquid Limit	34.8 %
Plastic Limit	24.0 %
Plasticity Index	10.8 %
Clay Fraction	22 %
Activity	49 %
G_s	2.73
USCS	CL

Chapter 5

EXPERIMENTAL RESULTS

5.1 Fabric Interpretation Data

The experimental results of this investigation have been separated into two sections. The first section presents desiccation-induced physical properties of the natural clay measured prior to air drying, after air drying, and at the end of consolidation testing. The physical properties include data of water content, void ratio, and sample deformation. Data is subdivided into two tables for the undisturbed and reconstituted materials to distinguish physical similarities and differences during desiccation.

The second category of results presents three types of plots respective to each specimen suite that summarize the consolidation-induced relationships. Plots of hydraulic conductivity-void ratio (log k-e), specific storage-effective stress (S_s-σ'), and void ratio-effective stress (e-σ') identify data trends for each specimen suite that are attributed to desiccation and followed during consolidation. Appendices A and B of Chapter 9 present individual plots and the respective data tables for each of the undisturbed and reconstituted clay specimens.

5.2 Desiccation-Induced Physical Properties

Four undisturbed and five reconstituted natural clay specimens were prepared and tested for this investigation. All specimens were permitted to desiccate from an average natural water content of approximately 30% to similar "as dried" water contents to represent specific desiccation states. Table 5.1 presents the desiccation-induced physical properties for the undisturbed clay specimens prior to air drying, after air drying, and at the end of consolidation testing. Data includes changes in water content, void ratio, vertical and lateral deformation, height of solids, and specific gravity. The data is obtained through back calculation of the final soil phase relationships, total deformation, and deformation rate. Void ratio estimates are expressed in terms of the l.v.d.t. measurements calculated with the calibration curve described in Chapter 4. The same type of data for the reconstituted specimens is presented in Table 5.2. The similarities and differences of data compared from both tables are summarized as follows:

1) No visible fractures were observed to result in any of the clay specimens during the air drying process.
2) Significant volumetric reductions in all of the specimens were measured after desiccation and after completion of consolidation testing.

Table 5.1 Desiccation-Induced Physical Properties of Undisturbed Clay Specimens

Property	U-1	U-2	U-3	U-4	Average
w initial, %	31.10	29.96	29.22	29.91	30.05
w′ dried, %	31.10	25.21	10.63	7.20	
w final, %	24.78	25.20	23.97	23.69	24.41
e initial	0.9524	0.8411	0.8527	0.8394	0.8813
e′ dried	0.9524	0.7846	0.7851	0.7684	
Δe dried	0.0000	0.0554	0.0676	0.0710	0.0674
e final	0.6900	0.6794	0.6592	0.6427	
Δe total	0.2624	0.1606	0.1935	0.1967	0.2033
H init, cm	1.326	1.352	1.345	1.326	1.337
H′ dried	1.326	1.345	1.334	1.320	1.331
ΔH dried	0.000	0.007	0.011	0.006	0.008
H final	1.148	1.234	1.189	1.184	
ΔH total	0.178	0.117	0.156	0.142	0.148
D init, cm	6.350	6.350	6.350	6.350	
D′ dried	6.350	6.270	6.240	6.241	6.275
ΔD dried	0.000	0.080	0.110	0.109	0.100
D final	6.350	6.350	6.350	6.350	
H solids, cm	0.6791	0.7348	0.7262	0.7208	0.7113
Gs	2.78	2.70	2.75	2.71	2.75

Table 5.2 Desiccation-Induced Physical Properties of Reconstituted Clay Specimens

Property	R-1	R-2	R-3	R-4	R-5	Average
w init, %	33.54	30.47	31.24	30.09	31.97	31.26
w'dried,%	33.54	21.03	17.91	9.42	6.41	
w final,%	22.20	22.82	21.14	22.23	21.44	21.97
e initial	0.8687	0.8113	0.8291	0.8758	0.8561	0.8482
e' dried	0.8687	0.7019	0.6822	0.7364	0.7067	
Δe dried	0.0000	0.1094	0.1469	0.1394	0.1494	0.1363
e final	0.6052	0.6071	0.5737	0.6151	0.5229	
Δe total	0.2635	0.2042	0.2554	0.2607	0.3332	0.2634
H init,cm	1.326	1.412	1.352	1.431	1.365	1.377
H' dried	1.326	1.409	1.350	1.426	1.361	1.374
ΔH dried	0.000	0.003	0.002	0.006	0.004	0.004
H final	1.139	1.253	1.164	1.232	1.167	
ΔH total	0.187	0.159	0.188	0.199	0.198	0.186
D init,cm	6.350	6.350	6.350	6.350	6.350	
D' dried	6.350	6.162	6.094	6.120	6.097	6.164
ΔD dried	0.000	0.188	0.256	0.230	0.253	0.232
D final	6.350	6.350	6.350	6.350		
H sol, cm	0.7096	0.7797	0.7392	0.7628	0.7354	0.7453
Gs	2.73	2.66	2.71	2.77	2.74	2.72

3) During desiccation of both specimen types, individual Δe values increased as the extent of desiccation increased. Values of Δe for the reconstituted specimens were more than double the desiccation-induced Δe values of the undisturbed specimens.

4) Total Δe (including consolidation testing) in both specimen types increased as desiccation increased.

5) The average vertical shrinkage of the reconstituted specimens, indicated by "ΔH dried", was half that of the undisturbed specimens.

6) The lateral shrinkage, designated as "ΔD dried", of the reconstituted specimens was more than twice the amount of the undisturbed specimens.

7) The average final water content after completion of consolidation testing was greater for the undisturbed specimens than for the reconstituted specimens.

8) As the degree of desiccation increased, consolidation-induced reductions of undisturbed specimen height lessened; the exception to this trend is the specimen desiccated to a water content of 25.21%. The reconstituted specimens did not develop such a trend.

9) The reconstituted specimens had a greater average height of solids than the undisturbed specimens.

5.3 Consolidation-Induced Relationships

The log k-e relationships of the four undisturbed clay specimens are summarized in Figure 5.1. Similarly, Figures 5.2 and 5.3 summarize the respective log S_s-σ' and the e-σ' relationships of the four undisturbed specimens. In each of these figures, the specimens are designated by the water content after desiccation. Consolidation-induced relationships for the five reconstituted clay specimens are respectively characterized by the same types of plots, illustrated by Figures 5.4, 5.5, and 5.6.

A line labelled "K-C Eqn" is illustrated in both of the log k-e plots for the undisturbed and reconstituted specimens. This line represents variations in hydraulic conductivity with void ratio predicted by the Kozeny-Carmen equation, described earlier in Section 2.1. All of the log k-e relationships measured during consolidation have a common shape that is characterized by a steep slope at high void ratios and a large divergence from the Kozeny-Carmen prediction. The measured log k-e slopes become much flatter at lower void ratios and have a smaller divergence from the Kozeny-Carmen prediction. Desiccation influences prior to consolidation, and reflected during consolidation, are seen from comparison of log k-e data trends in each specimen plot. It is evident that the position of the log k-e plots shifts toward increasing magnitudes of hydraulic

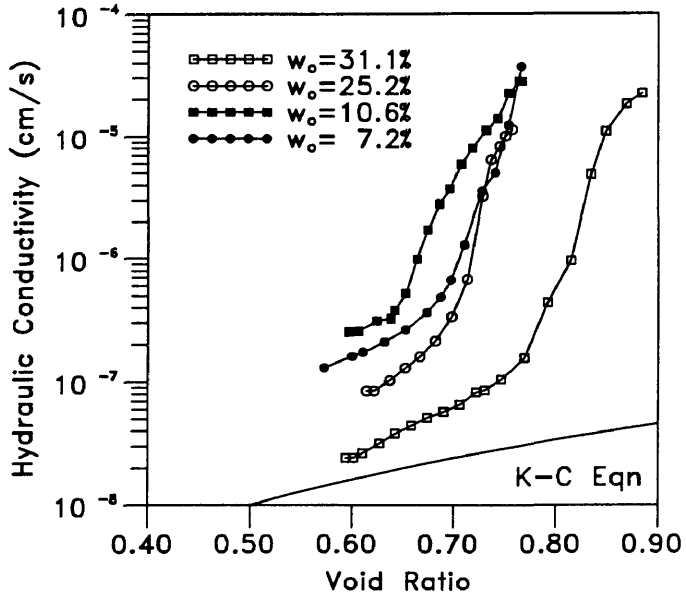

Figure 5.1 Log k-e Summary for Undisturbed Specimens.

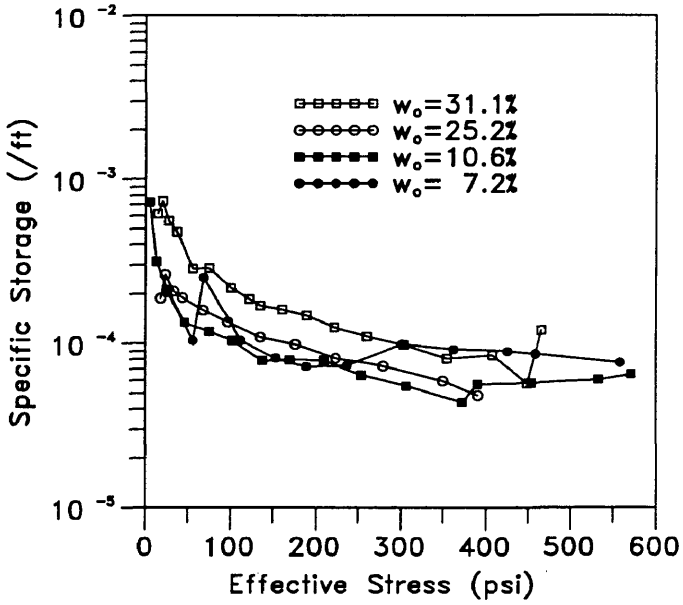

Figure 5.2 Specific Storage Summary for Undisturbed Specimens.

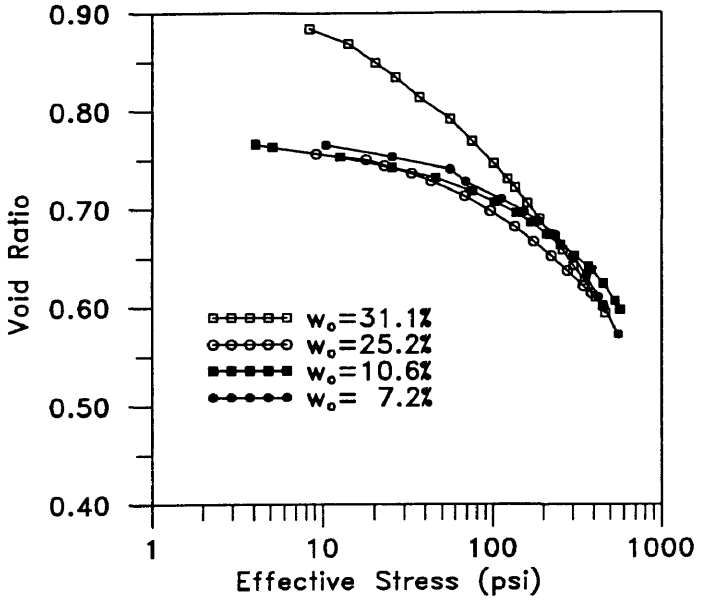

Figure 5.3 Compressibility Summary for Undisturbed Specimens.

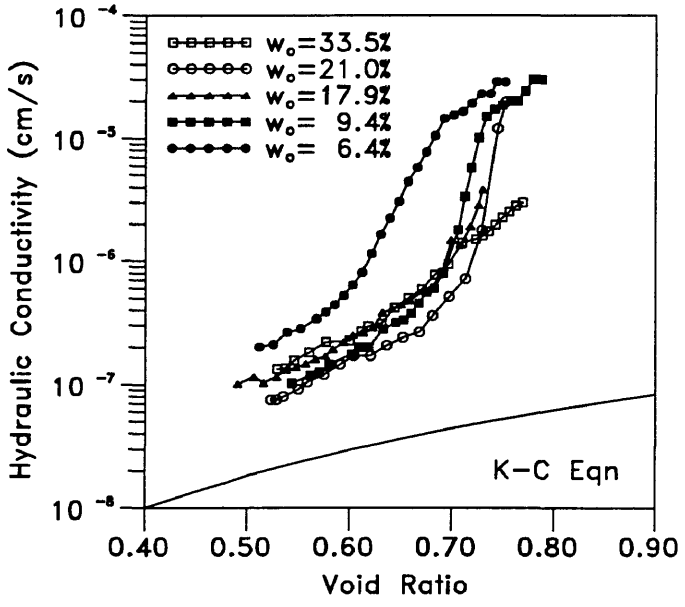

Figure 5.4 Log k-e Summary for Reconstituted Specimens.

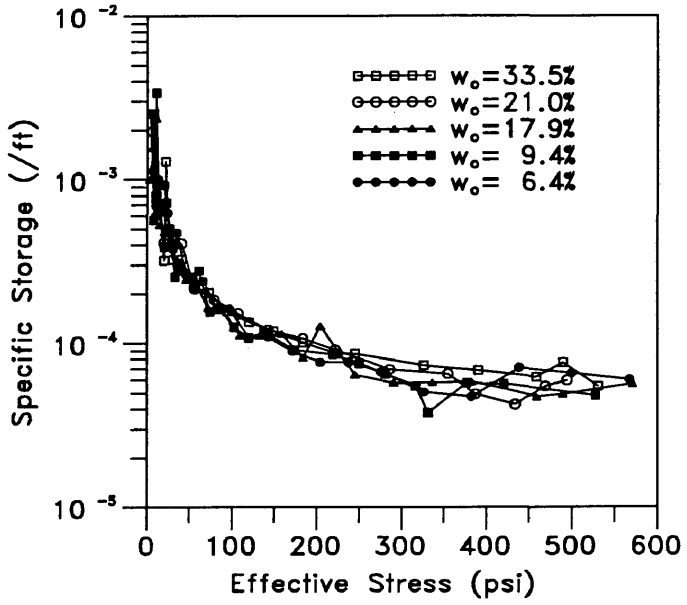

Figure 5.5 Specific Storage Summary for Reconstituted Specimens.

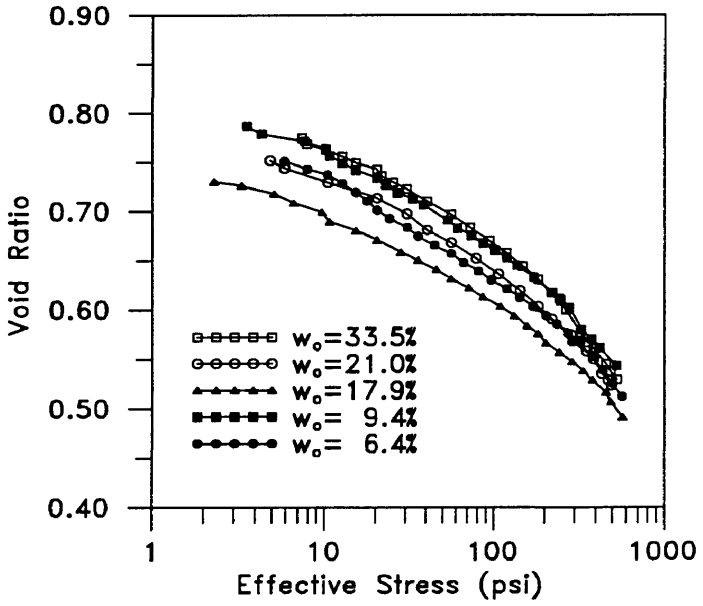

Figure 5.6 Compressibility Summary for Reconstituted Specimens.

conductivity with increasing desiccation state. The undisturbed specimen suite illustrates this point quite clearly in Figure 5.1, with one exception in the specimen air dried to a water content of 10.63%. Figure 5.4 shows that the reconstituted suite also follows this same general trend, but with exceptions in the specimen desiccated to 9.42% and the undesiccated specimen at a water content of 33.54%.

Specific storage in all of the specimens decreased with increasing stress. Each suite of specimens shows a general decrease of specific storage as desiccation state increases. Figure 5.2 indicates this trend well for the undisturbed materials. The reconstituted specimens in Figure 5.5 show less variability in this S_s relationship with desiccation, but do follow the trend nonetheless.

Figure 5.3 shows almost identical e-σ' relationships for each of the desiccated undisturbed specimens. This relationship developed in the desiccated specimens is unlike that for the undesiccated specimen at a water content of 31.10%. There is little variance in the compression index (C_c) for each of the air dried samples, regardless of the state of desiccation. Figure 5.6 also illustrates similar e-σ' plots for the reconstituted materials; however the plots shift toward decreasing void ratio as desiccation state increases. The variance of this shift in the

reconstituted materials is greater than that presented by the desiccated undisturbed specimens. Exceptions to the trend of decreasing void ratio with increasing desiccation are noted for specimens air dried to water contents of 9.42% and 6.41%. All of the reconstituted materials have approximately the same value for C_c as the desiccated undisturbed materials.

Chapter 6

DISCUSSION

6.1 Introduction

The geotechnical data measured in this investigation are used to distinguish both consistencies and deviations from earlier models of soil fabric. These results are related to the conceptual fabric model presented in Chapter 2. The conceptual model directs interpretations of the desiccation effects on the natural clay fabric to be of a qualitative nature. The experimental results described in the previous chapter are based on soil phase relationships, which permit the interpretations of some clay properties to overlap and support others. In addition, experimental considerations for the l.v.d.t. method of sample deformation measurement are presented.

6.2 Desiccation-Induced Physical Properties

During the desiccation process, no visible fractures were developed in the clay specimens. The small, round specimen shape was considered to be unaffected by tensile stresses normally affecting larger cross-sectional areas; however, measurable reductions in each of the total specimen volumes did occur. No macrofabric changes are assumed to have affected the physical character of the undisturbed and

reconstituted clays. Instead, it is assumed that fabric changes occurred at least at the minifabric level, and most likely at the microfabric level.

Previous studies of clay materials (Mitchell 1976) suggest that the dried void ratio will decrease as desiccation increases (Δe will increase as desiccation state increases). The results of desiccation effects on the undisturbed specimens agree with these earlier findings. The reconstituted materials reflected little change in void ratio reduction, since the amount of Δe for each specimen remained constant, regardless of the degree of desiccation.

Each specimen suite had similar initial water contents and void ratios. After air drying, the reconstituted samples experienced almost twice the amount of void ratio reduction as the undisturbed materials. Upon resaturation for consolidation testing, the available void space was filled with water. Because void ratio reduction of the undisturbed specimens during air drying was less than that of the reconstituted materials, the desiccated undisturbed specimens had more filled void space upon resaturation than the reconstituted specimens. Both specimen suites experienced the same amount of void ratio reduction during consolidation. After completion of consolidation, the final water content of the undisturbed clays always exceeded the final water content of the reconstituted clays, indicating

greater retention of pore water within the voids of the undisturbed fabric.

The observations of desiccation-induced void ratio changes and water content differences are used to interpret the structure of the specimen suites. The undisturbed specimens are characterized by a high volume, porous structure, indicated by the variability of void ratio reduction and greater final water content. The reconstituted materials may have a dense, more compact structure, based on the uniform void ratio reduction and lower final water content. This assumption of a dense structure is further supported by the greater average height of solids measured in the reconstituted samples.

Anisotropic fabric changes were observed in the clay specimens from the desiccation-induced vertical and lateral shrinkages. The vertical shrinkage in the reconstituted specimens was measured to be half that of the undisturbed specimens. Lateral shrinkage of the reconstituted specimens was far greater than that for the undisturbed specimens. These two measurements suggest that the structure of the reconstituted specimens was not the horizontally aligned, individual and dispersed particle arrangement advanced by Lambe (1953, 1958). Figure 6.1 illustrates how a dispersed structure should have experienced greater vertical shrinkage and less lateral shrinkage than its undisturbed counterpart.

(a) (b)

Figure 6.1 Dispersed Structure (a) Before Air Drying and (b) After Air Drying.

This is because the average pore sizes are smaller and allow greater capillary stresses, and because the parallel particle structure permits easier movement of the particle groups. Rather, the method of soil reconstitution used in this investigation seemed not to break down the clay clusters, but instead arranged the clusters so that a structure with increased resistance to vertical stresses resulted.

6.3 Consolidation-Induced Relationships

The overall magnitudes of the desiccation effects on the undisturbed and reconstituted specimens are presented in Figure 6.2 for the log k-e trends, Figure 6.3 for the S_s-σ' trends, and Figure 6.4 for the e-σ' trends. The width of the band between the upper and lower data boundaries are

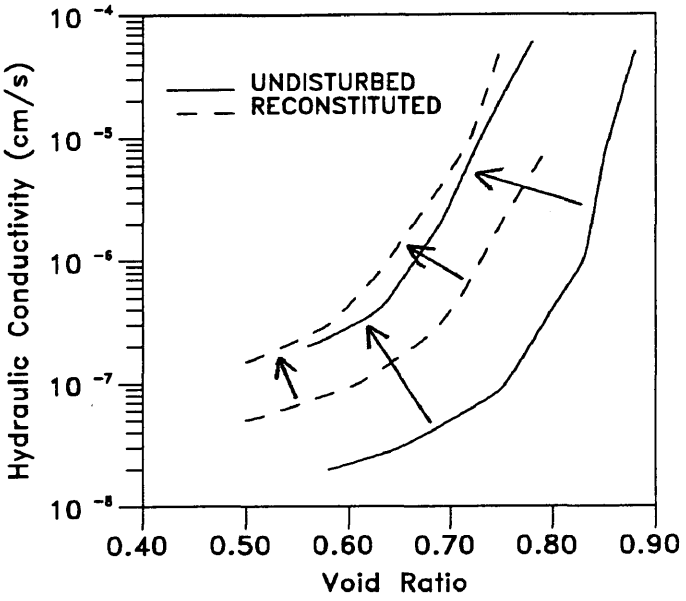

Figure 6.2 Data Ranges Between Upper and Lower Bounds of Log k-e Relationships for Undisturbed and Reconstituted Specimens.

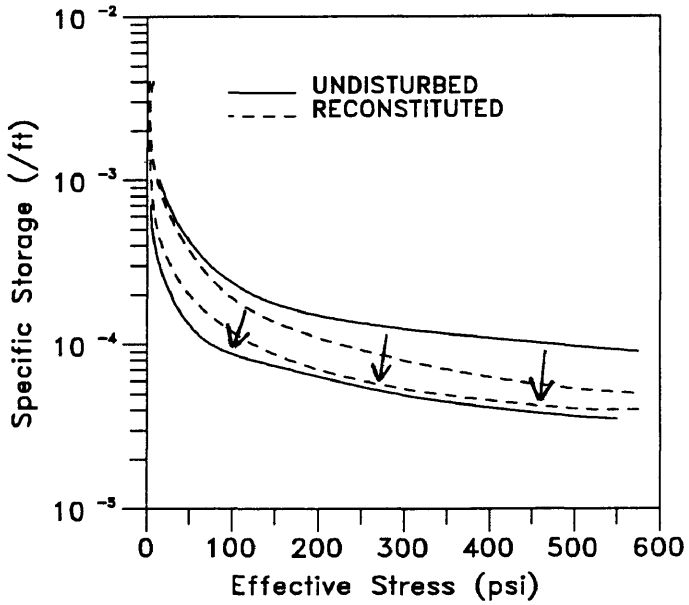

Figure 6.3 Data Ranges Between Upper and Lower Bounds of S_s-σ' Relationships for Undisturbed and Reconstituted Specimens.

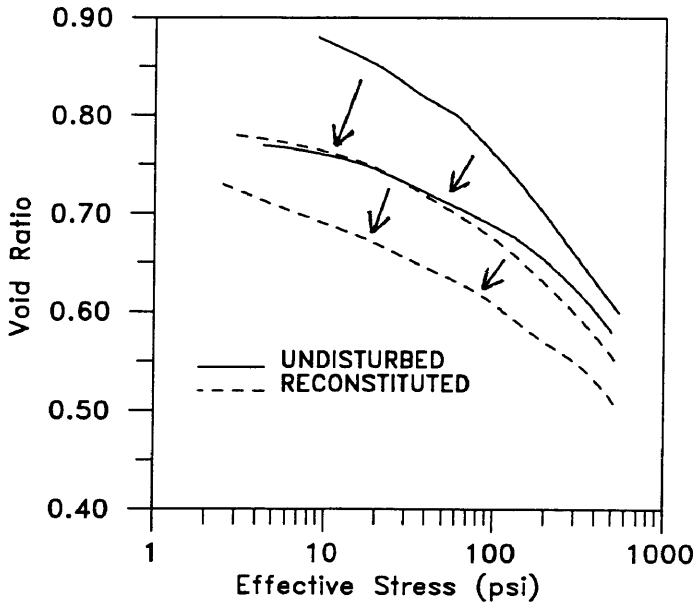

Figure 6.4 Data Ranges Between Upper and Lower Bounds of e-σ′ Relationships for Undisturbed and Reconstituted Specimens.

presented for each specimen suite. All of the figures include arrows that indicate general fabric changes caused by increasing degrees of desiccation.

6.3.1 Log k-e Relationships

The log k-e relationships indicate that both specimen types generally experienced increases in hydraulic conductivity as specimen desiccation increased. The influence of desiccation on the position of the log k-e relationships presented in Figures 5.1, 5.4, and 6.2 is indicated by the desiccation-induced capillary forces which

increase in magnitude as pore size decreases. In the cluster model, desiccation will cause shrinkage of the clusters, and increasing degrees of desiccation will cause decreasing magnitudes of cluster void ratios. When the log k-e curves in either Figure 5.1 or 5.4 are compared at the same total void ratio, the more desiccated specimens will have smaller cluster void ratios and larger inter-cluster void ratios. It is to be expected that the more desiccated specimens will have larger interparticle pore spaces and therefore higher hydraulic conductivities. The trend is clearly evident in Figure 5.1 and appears to a lesser extent in Figure 5.4. In Figure 6.2, the range in values, or bandwidth, is small for the reconstituted specimens. Because the specimens were prepared from air dried materials, the primary effects of desiccation took place before the specimens were tested. In contrast, the wide bandwidth for the undisturbed specimens reflects the full range of desiccation effects.

6.3.2 S_s-σ' Relationships

Specific storage defines the quantity of fluid expelled from storage during consolidation and is due primarily to the compressibility of the clay structure. Specific storage decreased as effective stress increased in all of the clay specimens. Individual S_s-σ' curves were also seen to

decrease as desiccation increased in both the undisturbed and reconstituted specimens. This is interpreted as decrease in specimen compressibility as the degree of desiccation increased. A greater range of the S_s-σ' relationships with regard to desiccation was observed in the undisturbed materials than the trend represented by the reconstituted specimens, meaning a greater range of compressibility existed in the undisturbed suite. The bandwidth shown in Figure 6.3 for the undisturbed specimens is almost twice that for the reconstituted samples. Like the log k-e bandwidths, the primary desiccation effects are presumed to have occurred in the reconstituted materials prior to formation of the specimens and consolidation testing.

6.3.3 e-σ' Relationships

Figure 5.3 presented void ratio-effective stress relationships of the desiccated undisturbed specimens that were almost identical, regardless of the desiccation state. The dramatic shift in all of these curves when compared to the undesiccated specimen at a water content of 31.10% indicates that the effects of desiccation on the clay were immediate and uniform. The reconstituted materials developed e-σ' curves with similar shapes to those of the undisturbed specimens, but the progressive effects of

desiccation were more evident. In Figure 6.4, the steep slope of the upper solid curve for the undesiccated undisturbed fabric state indicates it to be most compressible. The remaining bandwidths for the desiccated undisturbed specimens and all of the reconstituted specimens suggest more incompressible structures. It is assumed that the effects of desiccation took place immediately during the first stages of air drying in the undisturbed specimens. Since the reconstituted specimens were prepared from air dried materials, the primary effects of desiccation are thought to have occurred before the specimens were tested.

6.4 Sample Deformation Considerations

The l.v.d.t. system was used to directly obtain all sample deformation data used for this study. This data was compared with estimates for sample deformation based on the "volume-controlled" method of void ratio estimation. To summarize, the volume-controlled method is an indirect measurement of sample deformation based on system compliance. Compliance curves presented in Chapter 3 identified specific fluid volumes necessary to cause pressure head changes in the experimental system itself, and are represented as a linear relationship. Compressible soils are typified by nonlinear curves, since more fluid is required to cause the combined system and sample stresses.

Chapters 3 and 4 described how fluid is delivered to the loading chamber by the system flow pump and drives the loading bell downward to compress the soil sample. The volume of pore fluid expelled from the compressed soil is proportional to the volume of fluid in the loading chamber. This volume of pore fluid is equal to the change in volume of voids, ΔV_v. Fundamental soil mechanics dictates that the volume of specimen solids, ΔV_s, remain constant, and that changes in the total void ratio, V_t, be a function only of ΔV_v. Therefore, Δe may be estimated from the fluid volume-pressure differences in the system compliance plot and specimen time history plot.

Volume-controlled void ratio estimates were compared with the l.v.d.t. measurements and identified discrepancies with over 50% error. The primary cause of this deviation is attributed to the inability of the experimental system to exactly measure total fluid forced into the loading bellofram. First, the loading bellofram is made of compressible neoprene rubber, of which exact volume calculations are impossible to obtain, both at atmospheric and elevated pressures. Second, no flow meter of any type is on line between the loading flow pump and the upper chamber. It is possible that small air bubbles instead of water could be forced from the flow pump into the loading bellofram, thereby causing discrepancies in total fluid

volume. The inconsistencies in the direct l.v.d.t. measurements and volume-controlled estimates warrant further investigation.

Chapter 7

CONCLUSIONS AND RECOMMENDATIONS

7.1 Conclusions

This investigation was a pioneering attempt to use integrated hydraulic conductivity and consolidation data for interpreting microscopic characteristics of clay fabric. Undisturbed and reconstituted specimens of a soft gray Pleistocene clay were subjected to various degrees of desiccation, resaturated, and then tested to directly measure the hydraulic conductivity (k), void ratio (e), and effective stress (σ') relationships. The data trends observed in these geotechnical relationships were used with a conceptual model to interpret the effects of desiccation on the fabric of the clay specimens.

The results of this study showed that none of the specimens experienced cracking or fissuring during desiccation to cause macrofabric changes. Hydraulic conductivity and void ratio increased as desiccation increased in all of the clay specimens. Log k-e relationships for all specimens exhibited pronounced curvature in the direction of decreasing rates of change in log k with decreasing void ratios. The magnitude, and not the shape, of the log k-e curves was affected by desiccation.

Specific storage decreased as desiccation increased in all specimens. The range of specific storage in the undisturbed materials was greater than that exhibited in the reconstituted specimens. The undisturbed specimens were also observed to have a greater range of compressibility than the reconstituted specimens.

Compressibility of the specimens decreased as desiccation increased. The undisturbed materials were more compressible than the reconstituted materials, due to the effects of remolding. Void ratio-effective stress relationships for the reconstituted specimens were displaced in the direction of decreasing void ratio.

These experimental results are explained in terms of the cluster model of clay fabric and the findings of pore size distribution studies. As clusters shrink during desiccation, the intra-particle pore space decreases and the inter-particle pore spaces between clusters increases. Increases in the degree of desiccation also affect the tensile stresses within the clay structure and increase its resistance to compression. Consolidation at high void ratios reorients the clusters to reduce the inter-particle pore spaces, but does not affect the intra-particle pore space. Hydraulic conductivity is also decreased. At lower void ratios, pore size reduction within the clusters becomes increasingly important. A point is reached during

compression at which the no further reduction of the inter-particle pore space is possible. As compression continues, reduction of the intra-particle pores within the clusters then occurs and hydraulic conductivity is lowered.

It can be concluded that desiccation affected only the minifabric and microfabric of the clay specimens. The clay fabric consisted of clusters of particle aggregations that shrank in accordance with the extent of desiccation. The technique used to prepare the reconstituted specimens did not break down the clusters to individual clay particles, but did rearrange the clusters. The undisturbed specimens were interpreted to have a porous structure, while the reconstituted specimens were characterized by a dense and more compact structure. Two levels of fabric were observed in relation to the inter-particle pore spaces and intra-particle pore spaces. Because the reconstituted specimens were prepared from air dried materials, the primary effects of desiccation were considered to have taken place prior to sample testing.

7.2 Recommendations

It is suggested that integration of this indirect fabric study with other approaches, such as pore size distribution measurements and SEM, may clarify some common assumptions of clay fabric. Inconsistencies with the data

trends measured in this study may be due to variability of the natural clay materials or to fabric complexities not yet recognized by the cluster model. It is recommended that clay specimens of a single clay mineral type be tested to focus on a particular range of particle sizes and characteristics.

Secondly, improvements to the experimental system should be pursued. The fixed ring apparatus used for this study permitted simultaneous consolidation and hydraulic conductivity testing, but did not fully eliminate initial side-wall leakage of the desiccated specimens. An experimental system that utilizes a flexible membrane for hydraulic conductivity testing, and also allows one-dimensional sample compression would present a wider range of data with greater accuracy of the initial measurements.

Sample deformation estimates made with the volume-controlled method require further investigation in regard to exact fluid measurements. Several compliance tests of individual system components may lead to a greater understanding of the equipment flexibility under extreme pressures.

Complete system automation should be the ultimate goal of this experimental setup. Automation should include flow pump cycling, data collection and reduction, and automatic system shut-off at maximum stresses.

Finally, the effects of desiccation on minifabric and microfabric observed in this approach may prove useful in regard to large scale investigations. Interrelationships observed at the microscopic level could also affect the macroscopic features that control the behavior of compacted earth structures, such as clay liners.

REFERENCES CITED

ASTM. (1990). "Standard method for particle-size analysis of soils, D422-83." Annual Book of ASTM Standards, 4.08: Soil and Rock; Dimension Stone; Geosynthetics, Section 4 - Construction, 91-97.

_____. (1990). "Standard method for thin-walled tube sampling of soils, D-1587-83." Annual Book of ASTM Standards, 4.08: Soil and Rock; Dimension Stone; Geosynthetics, Section 4 - Construction, 233-235.

_____. (1990). "Standard method for liquid limit, plastic limit, and plasticity index of soils, D-4318-84." Annual Book of ASTM Standards, 4.08: Soil and Rock; Dimension Stone; Geosynthetics, Section 4 - Construction, 591-601.

Aylmore, L. A. G., and Quirk, J. P. (1959). "Swelling of clay-water systems." Nature, 183, 1752-1753.

_____. (1960). "Domain or turbostratic structure of clays." Nature, 187, 1046-1048.

Barden, L., Sides, G. R., and Karunaratne, J. P. (1970). "A microscopic examination of aspects of clay structure." Proceedings of the 2nd Southeast Asian Conference on Soil Engineering, Singapore, 67-72.

Bennett, R. R., and Meyer, R. R. (1952). "Geology and ground-water resources of the Baltimore area." Department of Geology, Mines, and Water Resources, Board of Natural Resources, State of Maryland, Bulletin No. 4, 24-72.

Bennett, R. H., Bryant, W. H., and Keller, G. H. (1981). "Clay fabric of selected submarine sediments: fundamental properties and models." Journal of Sedimentary Petrology, 51, 217-232.

Bennett, R. H., and Hulbert, M. H. (1986). Clay Microstructure. International Human Resources Development Corporation, Boston, 161 p.

Benson, C. H., and Daniel, D. E. (1990). "Influence of clods on hydraulic conductivity of compacted clay." Journal of Geotechnical Engineering, ASCE, 116(8), 1231-1248.

Bohor, B. F., and Hughes, R. E. (1970). "Scanning electron microscopy of clays and clay minerals." Clays and Clay Minerals, 19, 49-54.

Bowles, F. A. (1968). "Microstructure of sediments: Investigation with ultra-thin sections." Science, 159, 1236-1237.

Bowles, F. A., and Bryant, R. H. (1969). "Microstructure of unconsolidated and consolidated marine sediments." Journal of Sedimentary Petrology, 39, 1546-1551.

Casagrande, A. (1932). "The structure of clay and its importance in foundation engineering." Journal of the Boston Society of Civil Engineers, 168.

Collins, K., and McGown, A. M. (1974). "The form and function of microfabric features in a variety of natural soils." Geotechnique, 24, 223-254.

Crawford, C. B. (1964). "Interpretation of the consolidation test." Journal of the Soil Mechanics and Foundations Division, ASCE, 90(5), 87-102.

_____. (1968). "Quick clays of Eastern Canada." Engineering Geology, 2(4), 239-265.

Delage, P., and LeFebvre, G. (1984). "Study of the structure of a sensitive Champlain clay and its evolution during consolidation." Canadian Geotechnical Journal, 21, 21-35.

Delage, P. (1987). "Microstructure and compressibility of some Eastern Canadian sensitive soft clays." Proceedings of the International Symposium on Geotechnical Engineering of Soft Soils, Mexico City, Mexico, Vol. 1, 33-38.

Diamond, S. (1970). "Pore size distribution in clays." Clays and Clay Minerals, 18, 7-23.

_____. (1971). "Microstructure and pore structure of impact compacted clays." Clays and Clay Minerals, 19, 239-249.

Elsbury, B. R., Daniel, D. E., Sraders, G. A., and Anderson, D. C. (1990). "Lessons learned from compacted clay liner." Journal of Geotechnical Engineering, ASCE, 116(11), 1641-1660.

Garcia-Bengochea, I., Lovell, C. W., and Altschaeffl, A. G. (1979). "Pore distribution and permeability of silty clays." Journal of Geotechnical Engineering, ASCE, 105(7), 839-856.

Gill, J. D. (1989). "Simultaneous measurement of compressibility and hydraulic conductivity using volume controlled methods." Master of Science Thesis, Colorado School of Mines, Golden, Colorado, 184 p.

Griffiths, F. J., and Joshi, R. C. (1989). "Change in pore size distribution due to consolidation of clays." Geotechnique, 39(1), 159-167.

_____. (1990). "Change in pore size distribution due to consolidation of clays." Discussion by Nagaraj, T. S., Vatsala, A., Srinivasa Murthy, B. R., Geotechnique, 40(2), 303-309.

_____. (1990). "Clay fabric response to consolidation." Applied Clay Science, 5, 37-66.

Grim, R. E. (1940). Clay mineralogy. McGraw-Hill, New York, 384 p.

Ingles, O. G. (1968). "Soil chemistry relevant to the engineering behavior of soils." In Soil mechanics - Selected topics, I. K. Lee, ed., Elsevier, New York, 1-57.

Iwata, S., Tabuchi, T., and Warkentin, B. P. (1988). Soil-water interactions: Mechanisms and applications. Marcel Dekker, New York, 380 p.

Janbu, N., Tokheim, O., and Senneset, K. (1981). "Consolidation tests with continuous loading." Proceedings of the Tenth International Conference on Soil Mechanics and Foundation Engineering, Stockholm, Sweden, Vol. 1, 645-654.

Lambe, T. W. (1953). "The structure of inorganic soil." Proceedings of the American Society of Civil Engineers, 79, 1-49.

_____. (1958). "The structure of compacted clay." Journal of the Soil Mechanics and Foundations Division, ASCE, 84(2), 1-34.

Lambe, T. W., and Whitman, R. V. (1969). Soil mechanics. Wiley and Sons, New York, 553 p.

Lowe, J., III, Jonas, E. M., and Obrician, V. F. (1969). "Controlled gradient consolidation test." Journal of the Soil Mechanics and Foundations Division, ASCE, 95(1), 77-97.

McCarthy, D. F. (1982). Essentials of soil mechanics and foundations. Reston, Virginia, 601 p.

Marshall, C. E. (1949). The colloid chemistry of silicate minerals. Academic Press, New York, 195 p.

Mitchell, J. K. (1956). "The fabric of natural clays and its relation to engineering properties." Highway Research Board Proceedings, 35, 693-713.

Mitchell, J. K., Hooper, D. R., and Campanella, R. G. (1965). "Permeability of compacted clay." Journal of the Soil Mechanics and Foundations Division, ASCE, 91(4), 41-65.

Mitchell, J. K. (1976). Fundamentals of soil behavior. Wiley and Sons, New York, 450 p.

Moon, C. F. (1972). "The microstructure of clay sediments." Earth Sciences Review, 8, 303-321.

Olsen, H. W. (1962). "Hydraulic flow through saturated clays." Proceedings on the Ninth National Conference on Clays and Clay Minerals, Lafayette, Indiana, Vol. 9, 131-161.

_____. (1966). "Darcy's law in saturated kaolinite." Water Resources Research, 2(2), 287-295.

Olsen, H. W., Nichols, R. W., and Rice, T. L. (1985). "Low gradient permeability measurements in a triaxial system." Geotechnique, 35(2), 145-157.

Olsen, H. W., Morin, R. W., and Nichols, R. W. (1988). "Flow pump applications in triaxial testing." Proceedings of the ASTM Symposium on Advanced Triaxial Testing of Soil and Rock.

Pauling, L. (1930). "The structure of the micas and related materials." Proceedings of the National Academy of Sciences, 16, 123-129.

Quigley, R. M., and Thompson, C. D. (1966). "The fabric of anisotropically consolidated sensitive marine clay." Canadian Geotechnical Journal, 3, 61-73.

Sides, G., and Barden, L. (1971). "The microstructure of dispersed and flocculated samples of kaolinite, illite, and montmorillonite." Canadian Geotechnical Journal, 8, 391-399.

Sloane, R. L., and Kell, T. F. (1966). "The fabric of mechanically compacted kaolin." Clays and Clay Minerals, 14, 289-296.

Smith, R. E., and Wahls, H. E. (1969). "Consolidation under constant rates of strain." Journal of the Soil Mechanics and Foundations Division, ASCE, 95(2), 519-539.

Sorby, H. C. (1908). "On the application of quantitative methods to the study of the structure and history of rocks." Quarterly Journal of the Geological Society of London, 64, 171-233.

Spangler, M. G., and Handy, R. L. (1982). Soil engineering. Harper and Row, New York, 819 p.

Van Olphen, H. (1963). An introduction to clay colloid chemistry. Wiley and Sons, New York, 301 p.

Warkentin, B. P., and Bozozuk, M. (1961). "Shrinking and swelling properties of two Canadian clays." Proceedings of the Fifth International Conference on Soil Mechanics and Foundation Engineering, Paris, France, Vol. 3A, 851.

Washburn, E. W. (1921). "A note on a method of determining the distribution of pore sizes in a porous material." Proceedings of the National Academy of Sciences, 7, 115-116.

Wissa, A. E. Z., Christian, J. T., Davis, E. H., and Heiberg, A. M. (1971). "Consolidation at constant rate of strain." Journal of the Soil Mechanics and Foundations Division, ASCE, 97(10), 1393-1413.

Yong, R. N. (1972). "Soil technology and stabilization." Proceedings of the 4th Asian Regional Conference on Soil Mechanics and Foundation Engineering, Bangkok, Thailand, Vol. 2, 111-124.

Appendix A:

Geotechnical Properties of Undisturbed Specimens

The results of four undisturbed natural clay specimens are presented in this appendix. Three of the specimens were permitted to desiccate from an average initial water content of 30%. The undesiccated specimen water content was 31.1%, and the air dried specimens were desiccated to water contents of 25.2%, 10.6%, and 7.2%, respectively. All specimens were then resaturated, continuously consolidated, and simultaneously tested for hydraulic conductivity.

The sample total stress, base pore pressure, and void ratio were measured throughout the entire conduct of a test and are presented by the time history plots. Typically, each sample was fully loaded to over 500 psi and unloaded in less than 125 hours. Hydraulic conductivity, specific storage, and void ratio relationships with effective stress are also represented in both the linear and logarithmic format. Each specimen was tested in a single compression-rebound cycle. Two specimens, at desiccated water contents of 10.6% and 7.2%, were retested in a second cycle to yield additional compression-rebound data. The following legend identifies the testing cycles represented by each of the plots:

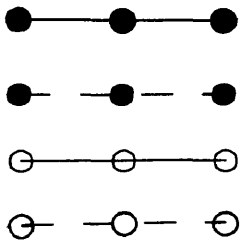

Initial Compression

Initial Rebound

Final Compression

Final Rebound

Data tables of the specimen geotechnical properties are included with each of the plots. All plots were developed with data of the final soil phase relationships, total sample deformation, and rate of deformation. These data were incorporated with the l.v.d.t. calibration curve to calculate the void ratio-time relationship with stresses applied during the test.

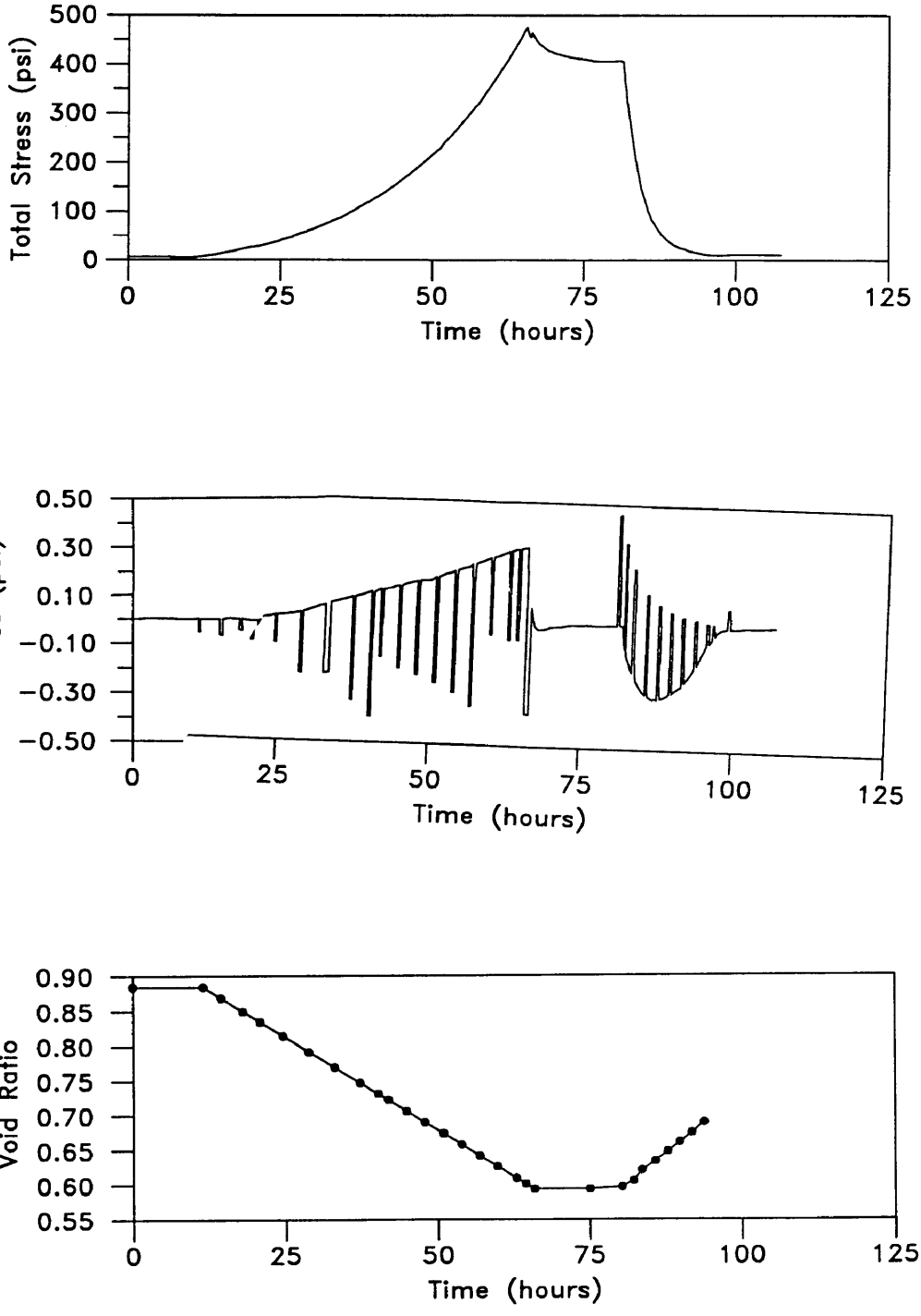

Figure A.1.1 Time History Plots, Undisturbed Specimen, w_o = 31.1%

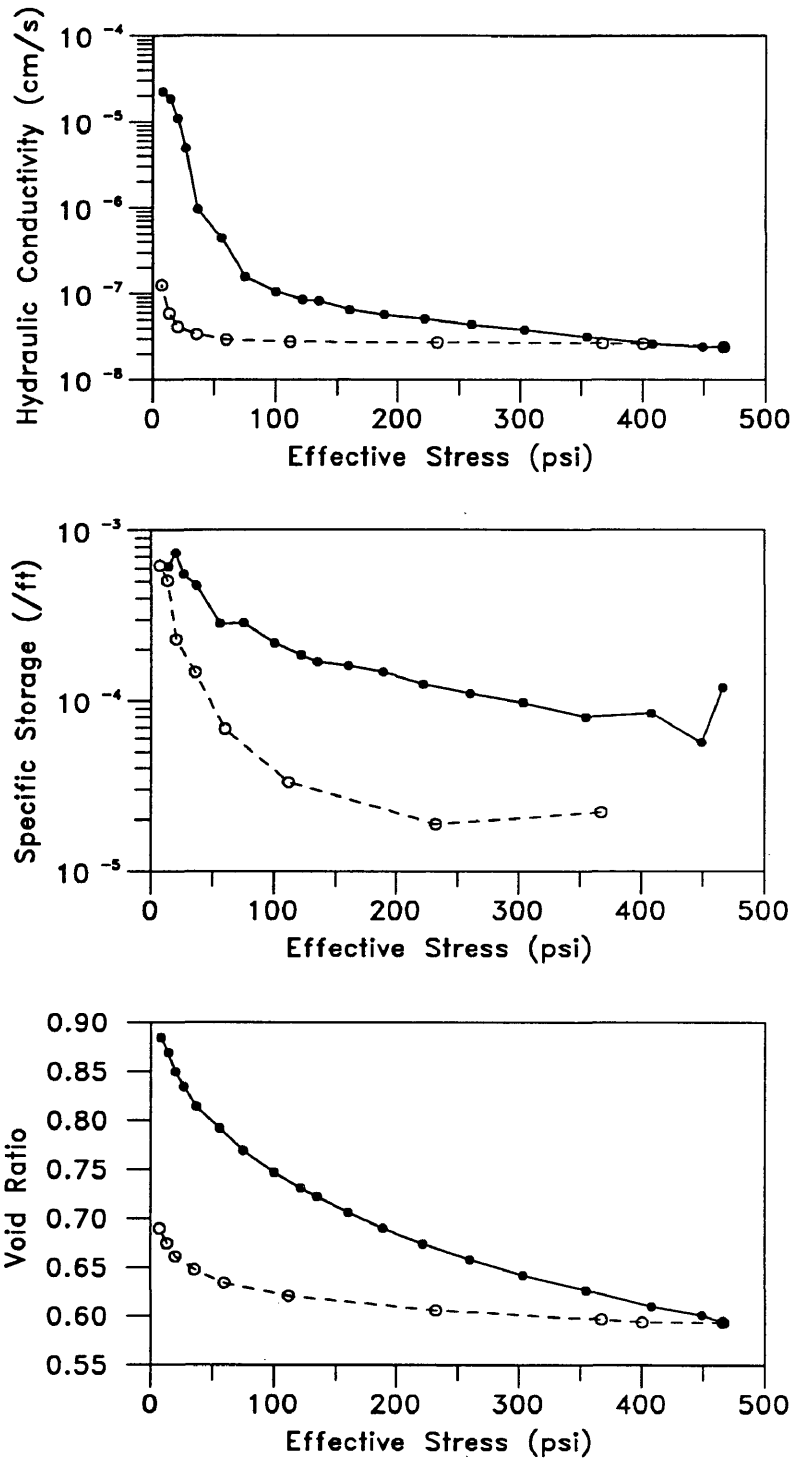

Figure A.1.2 k-σ', S_s-σ', and e-σ' Plots, Undisturbed Specimen, w_o = 31.1%

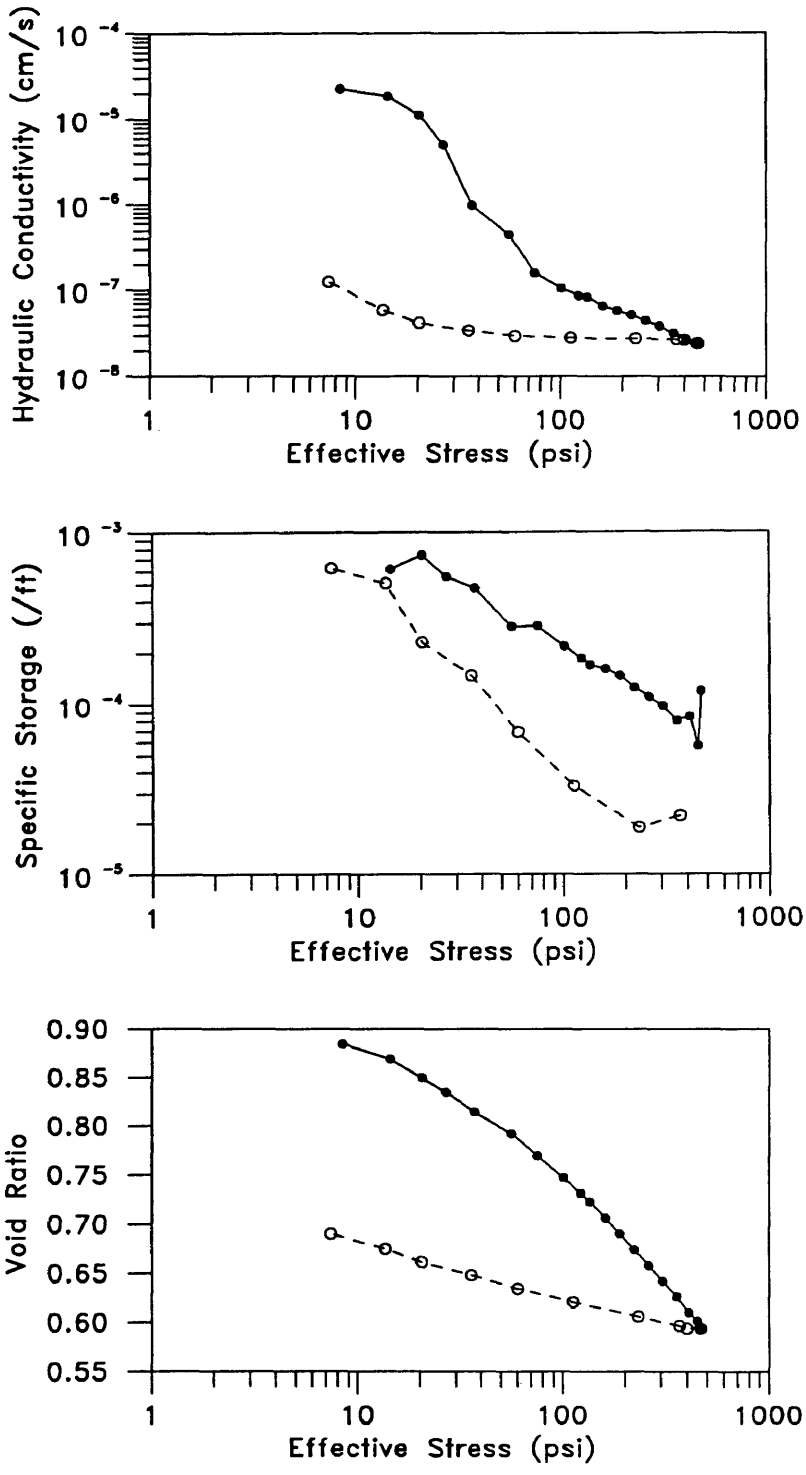

Figure A.1.3 k-σ', S_s-σ', and e-σ' Plots, Undisturbed Specimen, w_o = 31.1%

Table A.1 Geotechnical Properties, Undisturbed Specimen, w_o = 31.1%

σ' (psi)	u_b (psi)	Flowrate (cm^3/s)	k (cm/s)	Void Ratio e
8.41	0.010	3.7660E-04	2.2E-05	0.8846
14.28	0.012	3.7660E-04	1.9E-05	0.8691
20.40	0.020	3.7660E-04	1.1E-05	0.8498
26.77	0.045	3.7660E-04	5.0E-06	0.8348
36.97	0.115	1.8883E-04	9.8E-07	0.8145
56.10	0.250	1.8883E-04	4.5E-07	0.7920
75.22	0.280	7.5531E-05	1.6E-07	0.7695
100.72	0.420	7.5531E-05	1.1E-07	0.7470
122.40	0.515	7.5531E-05	8.7E-08	0.7310
135.15	0.270	3.7766E-05	8.3E-08	0.7224
160.65	0.340	3.7766E-05	6.6E-08	0.7063
188.69	0.385	3.7766E-05	5.8E-08	0.6903
221.84	0.430	3.7766E-05	5.2E-08	0.6742
260.09	0.500	3.7766E-05	4.5E-08	0.6581
303.44	0.580	3.7766E-05	3.9E-08	0.6421
354.44	0.350	1.8883E-05	3.2E-08	0.6267
407.99	0.420	1.8883E-05	2.7E-08	0.6100
448.79	0.460	1.8883E-05	2.4E-08	0.6014
465.87	0.460	1.8883E-05	2.4E-08	0.5939
400.34	0.420	1.8883E-05	2.7E-08	0.5939
367.19	0.420	1.8883E-05	2.7E-08	0.5966
232.04	0.410	1.8883E-05	2.7E-08	0.6061
112.20	0.405	1.8883E-05	2.8E-08	0.6210
59.92	0.380	1.8883E-05	3.0E-08	0.6345
35.70	0.330	1.8883E-05	3.4E-08	0.6480
20.40	0.270	1.8883E-05	4.2E-08	0.6616
13.51	0.190	1.8883E-05	5.9E-08	0.6751
7.39	0.090	1.8883E-05	1.2E-07	0.6900

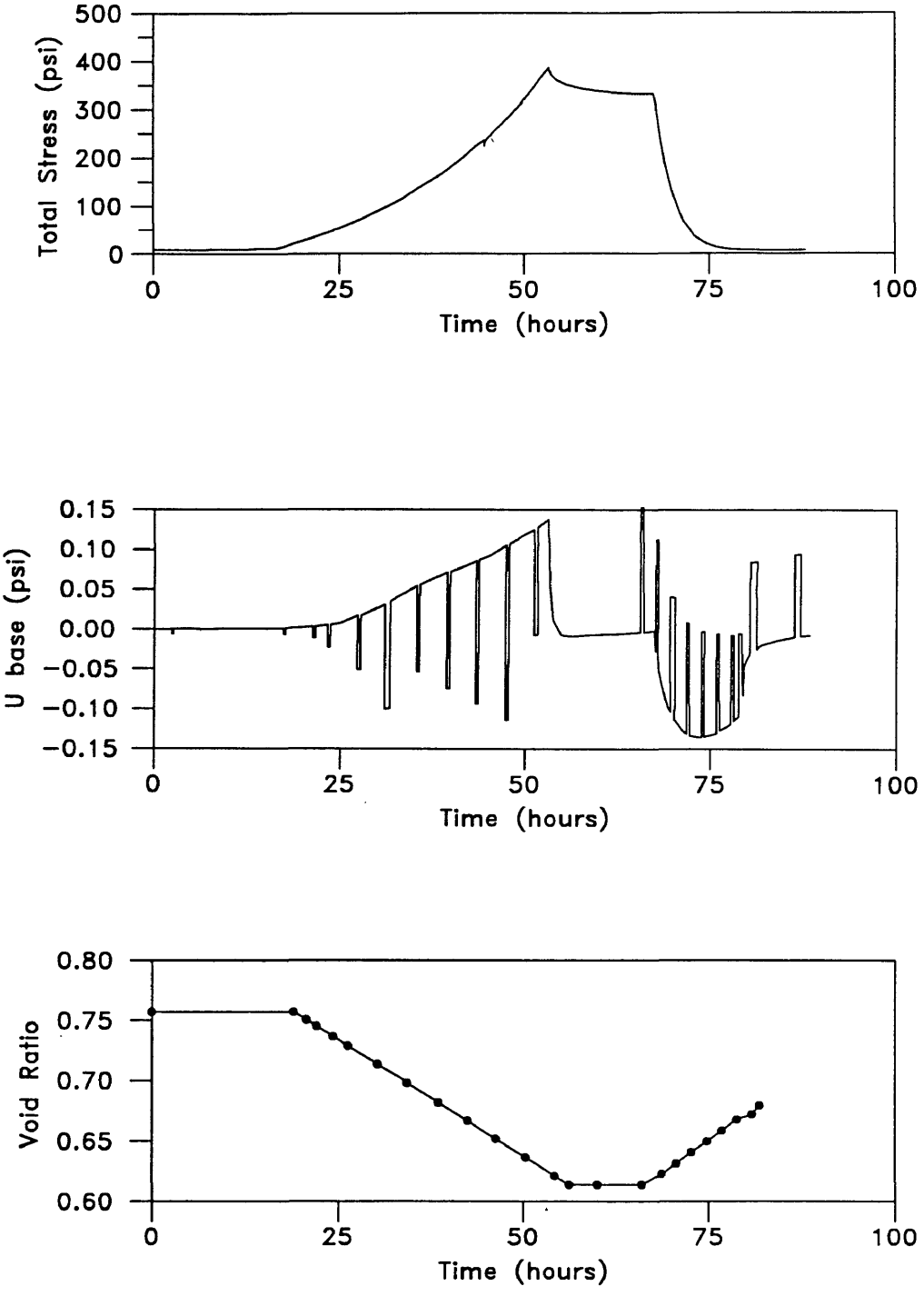

Figure A.2.1 Time History Plots, Undisturbed Specimen, w_o = 25.2%

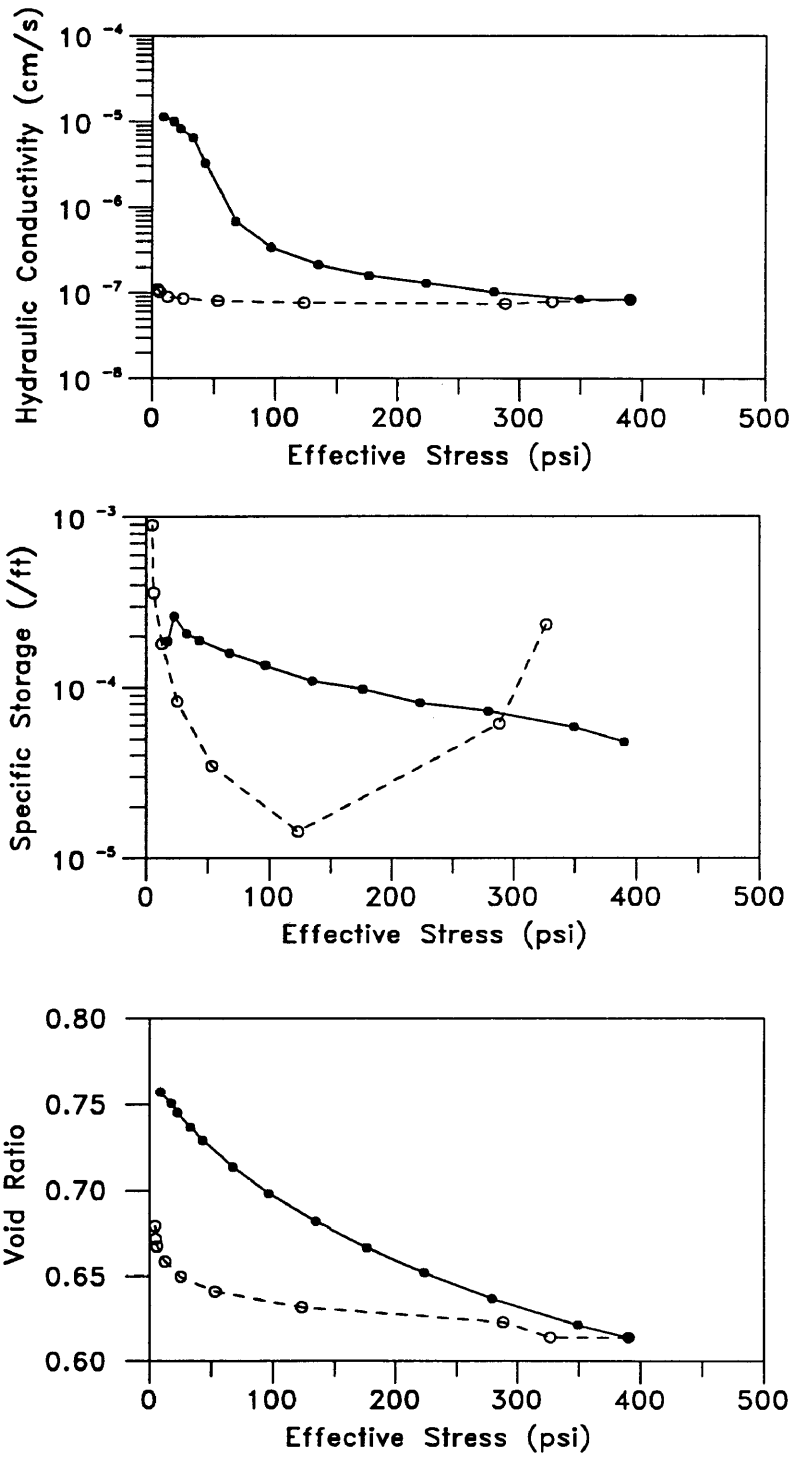

Figure A.2.2 k-σ', S_s-σ', and e-σ' Plots, Undisturbed Specimen, w_o = 25.2%

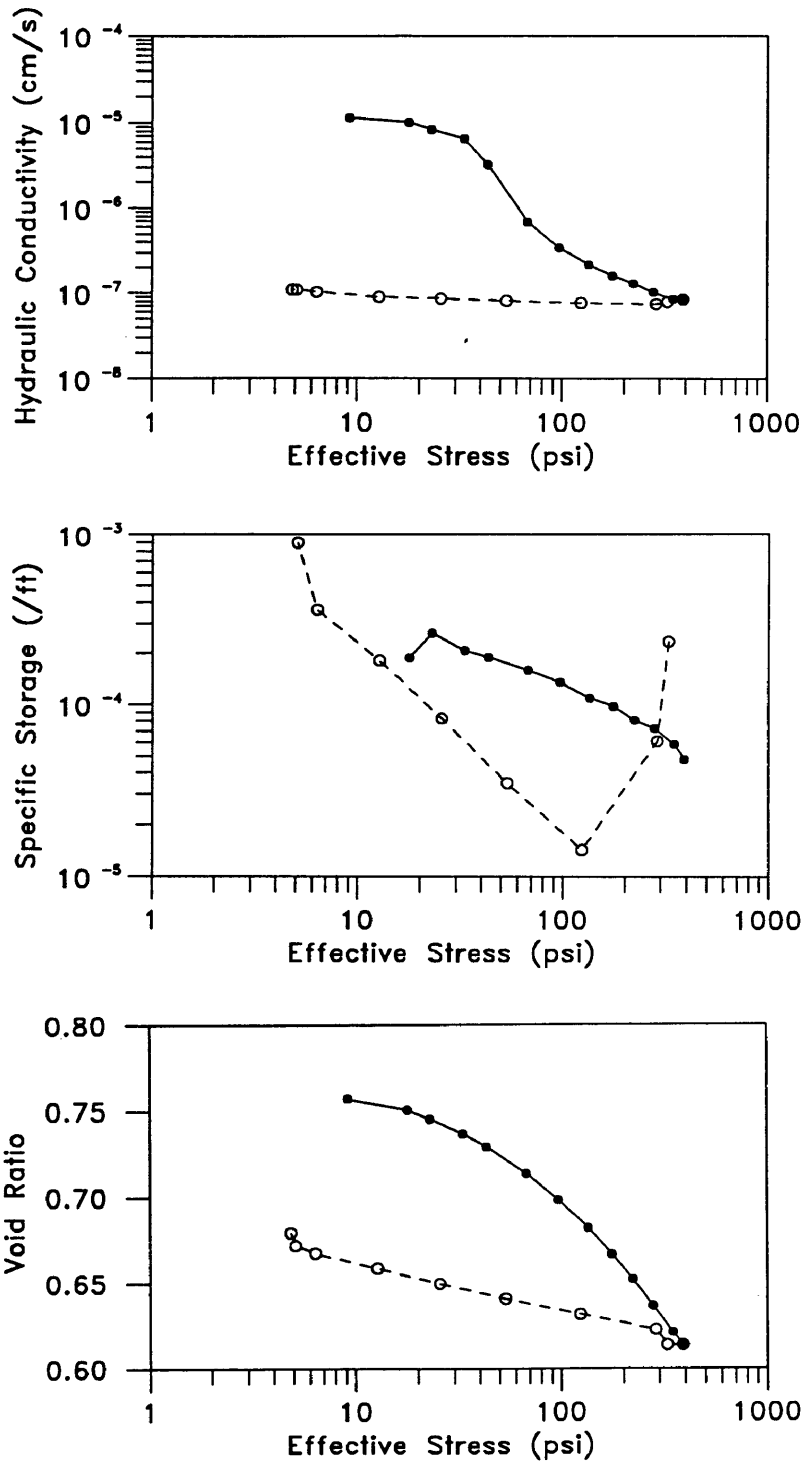

Figure A.2.3 k-σ', S_s-σ', and e-σ' Plots, Undisturbed Specimen, w_o = 25.2%

Table A.2 Geotechnical Properties, Undisturbed Specimen, w_o = 25.2%

σ' (psi)	u_b (psi)	Flowrate (cm^3/s)	k (cm/s)	Void Ratio e
9.18	0.008	1.5106E-04	1.1E-05	0.7571
17.85	0.009	1.5106E-04	1.0E-05	0.7506
22.95	0.011	1.5106E-04	8.3E-06	0.7452
33.15	0.014	1.5106E-04	6.5E-06	0.7367
43.35	0.028	1.5106E-04	3.3E-06	0.7290
67.83	0.066	7.5531E-05	6.9E-07	0.7136
96.90	0.133	7.5531E-05	3.4E-07	0.6982
135.15	0.106	3.7766E-05	2.1E-07	0.6820
175.95	0.142	3.7766E-05	1.6E-07	0.6666
223.12	0.175	3.7766E-05	1.3E-07	0.6520
279.22	0.220	3.7766E-05	1.0E-07	0.6366
349.34	0.134	1.8883E-05	8.5E-08	0.6212
390.14	0.134	1.8883E-05	8.5E-08	0.6139
326.65	0.144	1.8883E-05	7.9E-08	0.6139
288.14	0.152	1.8883E-05	7.5E-08	0.6228
123.67	0.148	1.8883E-05	7.7E-08	0.6316
53.55	0.140	1.8883E-05	8.1E-08	0.6409
25.50	0.132	1.8883E-05	8.6E-08	0.6497
12.75	0.126	1.8883E-05	9.0E-08	0.6586
6.37	0.110	1.8883E-05	1.0E-07	0.6675
5.10	0.104	1.8883E-05	1.1E-07	0.6719
4.84	0.104	1.8883E-05	1.1E-07	0.6794

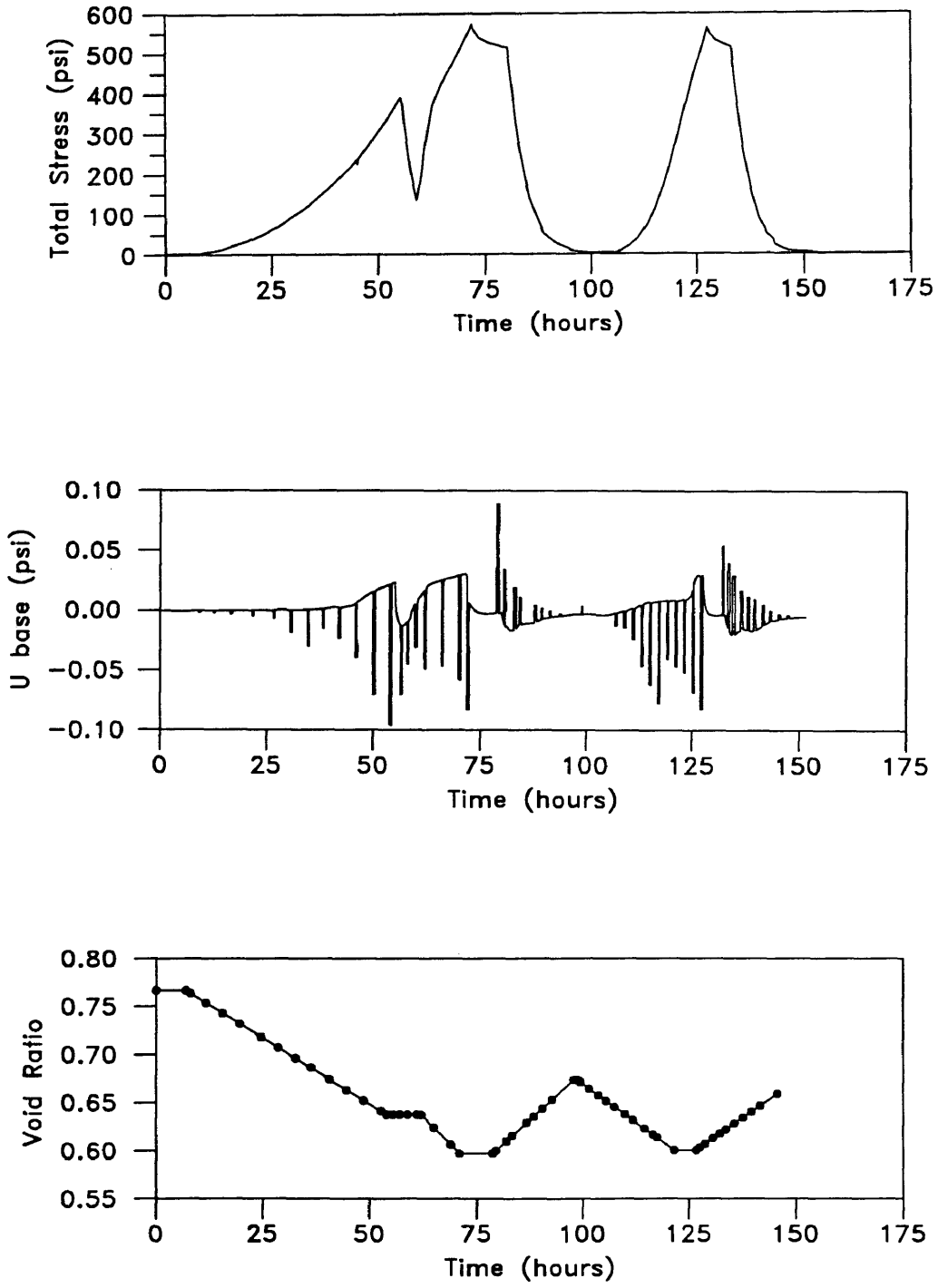

Figure A.3.1 Time History Plots, Undisturbed Specimen, w_o = 10.6%

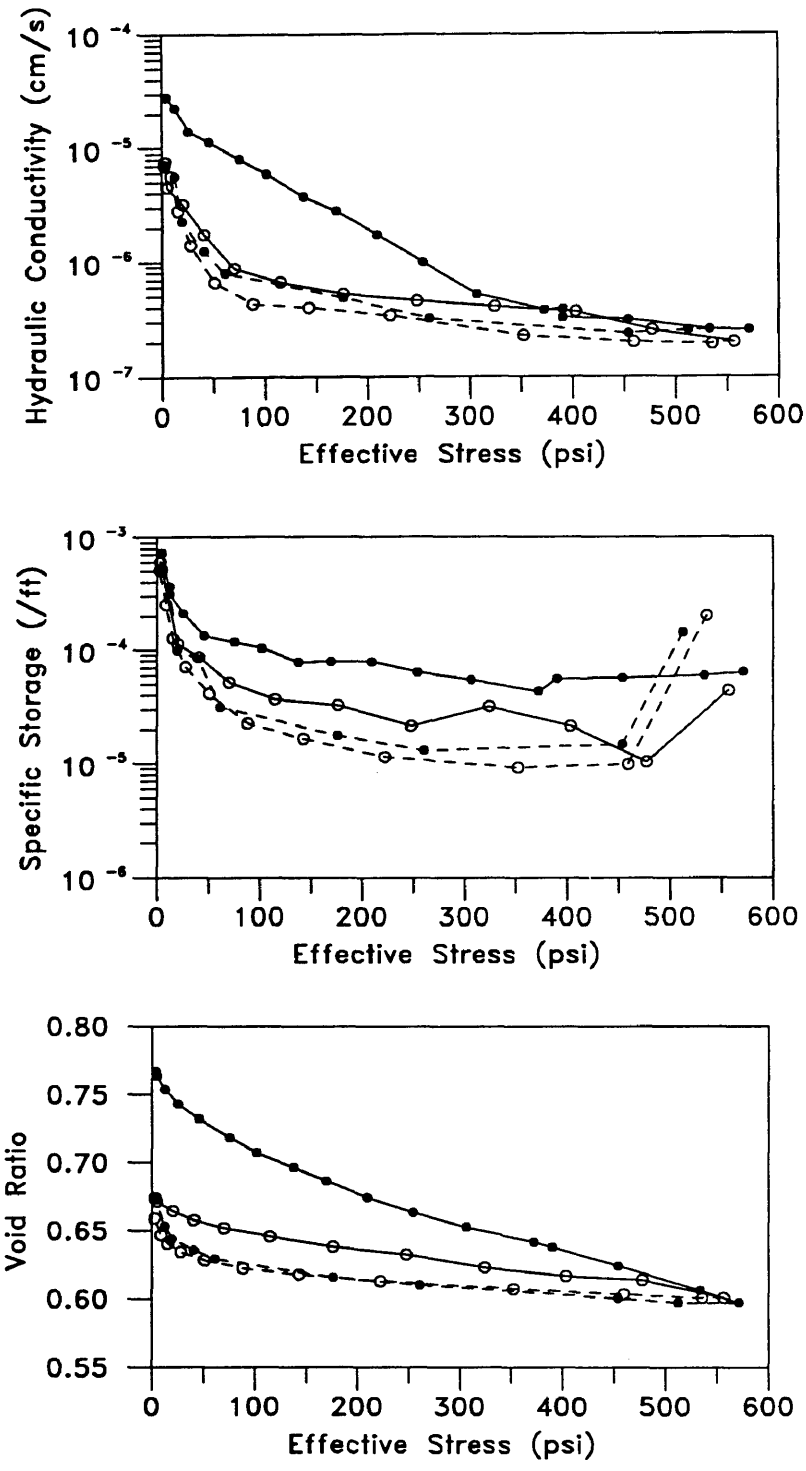

Figure A.3.2 k-σ', S_s-σ', and e-σ' Plots, Undisturbed Specimen, w_o = 10.6%

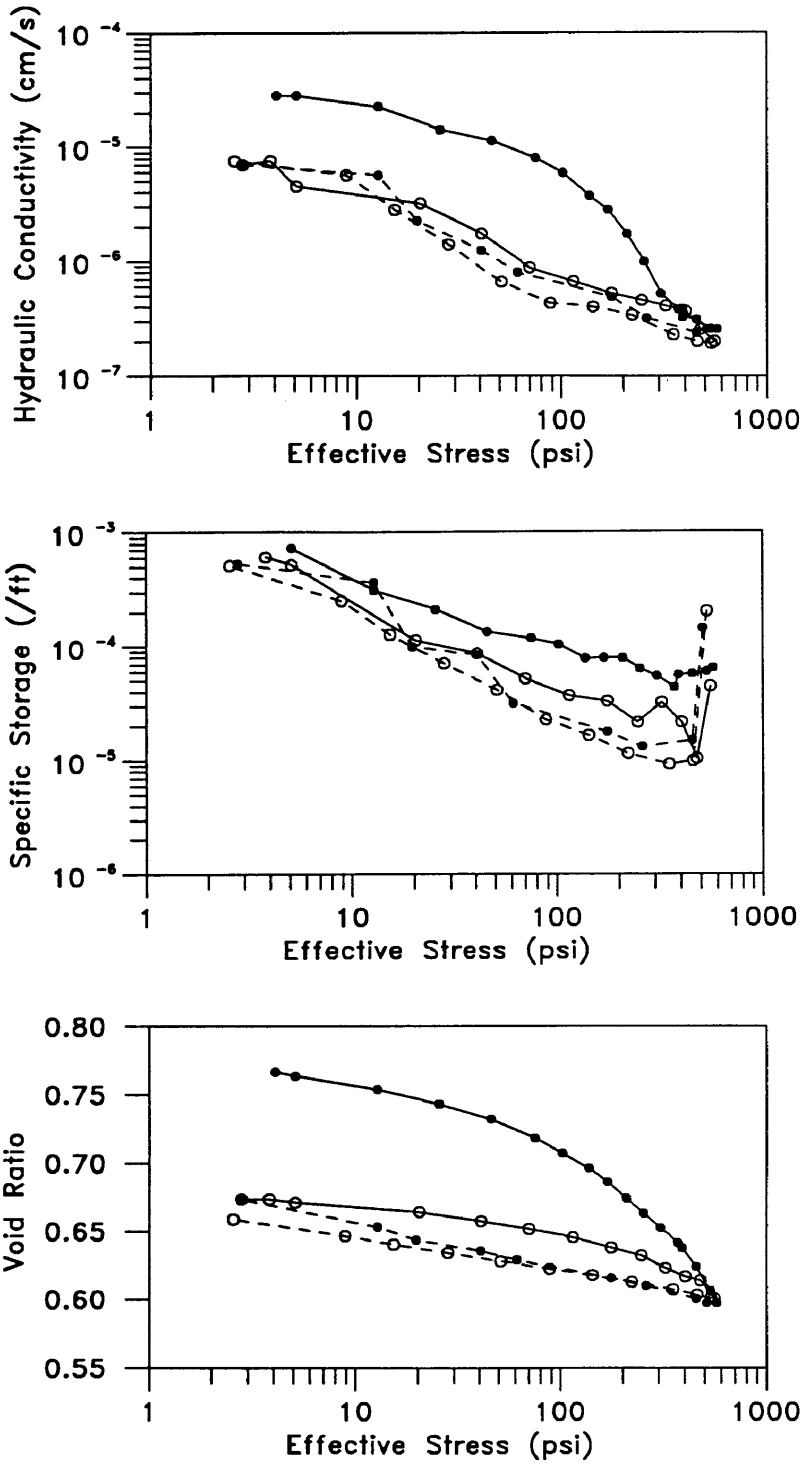

Figure A.3.3 k-σ', S_s-σ', and e-σ' Plots, Undisturbed Specimen, w_o = 10.6%

Table A.3 Geotechnical Properties, Undisturbed Specimen, w_o = 10.6%

σ′ (psi)	u_b (psi)	Flowrate (cm^3/s)	k (cm/s)	Void Ratio e
4.08	0.004	1.8883E-04	2.8E-05	0.7667
5.10	0.004	1.8883E-04	2.8E-05	0.7637
12.75	0.005	1.8883E-04	2.2E-05	0.7539
25.50	0.008	1.8883E-04	1.4E-05	0.7431
45.90	0.010	1.8883E-04	1.1E-05	0.7321
75.22	0.014	1.8883E-04	8.0E-06	0.7184
102.00	0.019	1.8883E-04	5.9E-06	0.7074
137.70	0.030	1.8883E-04	3.7E-06	0.6964
169.57	0.016	7.5531E-05	2.8E-06	0.6866
209.09	0.026	7.5531E-05	1.7E-06	0.6745
253.72	0.045	7.5531E-05	1.0E-06	0.6635
305.99	0.086	7.5531E-05	5.2E-07	0.6526
372.29	0.118	7.5531E-05	3.8E-07	0.6416
285.59	0.057	3.7766E-05	3.9E-07	0.6378
175.95	0.035	3.7766E-05	6.4E-07	0.6378
203.99	0.037	3.7766E-05	6.1E-07	0.6378
346.79	0.066	3.7766E-05	3.4E-07	0.6378
453.89	0.072	3.7766E-05	3.1E-07	0.6242
532.94	0.087	3.7766E-05	2.6E-07	0.6065
571.18	0.088	3.7766E-05	2.6E-07	0.5974
512.03	0.088	3.7766E-05	2.6E-07	0.5974
453.89	0.047	1.8883E-05	2.4E-07	0.6006
260.09	0.035	1.8883E-05	3.2E-07	0.6101
175.95	0.023	1.8883E-05	4.9E-07	0.6157
61.20	0.014	1.8883E-05	8.0E-07	0.6293
40.80	0.009	1.8883E-05	1.2E-06	0.6358
19.63	0.005	1.8883E-05	2.2E-06	0.6438
12.75	0.002	1.8883E-05	5.6E-06	0.6534
2.80	0.007	7.5533E-05	6.9E-06	0.6738
3.82	0.006	7.5533E-05	7.5E-06	0.6738
5.10	0.010	7.5533E-05	4.5E-06	0.6713
20.40	0.014	7.5533E-05	3.2E-06	0.6646
40.80	0.026	7.5533E-05	1.7E-06	0.6579
70.12	0.051	7.5533E-05	8.8E-07	0.6520
114.75	0.067	7.5533E-05	6.7E-07	0.6457
175.95	0.085	7.5533E-05	5.3E-07	0.6381
247.34	0.049	3.7766E-05	4.6E-07	0.6323
323.84	0.055	3.7766E-05	4.1E-07	0.6231
402.89	0.061	3.7766E-05	3.7E-07	0.6167
476.84	0.088	3.7766E-05	2.6E-07	0.6138
556.39	0.112	3.7766E-05	2.0E-07	0.6008
535.49	0.058	1.8883E-05	1.9E-07	0.6008

Table A.3 (continued)

σ' (psi)	u_b (psi)	Flowrate (cm^3/s)	k (cm/s)	Void Ratio e
458.99	0.056	1.8883E-05	2.0E-07	0.6036
351.89	0.049	1.8883E-05	2.3E-07	0.6073
221.84	0.033	1.8883E-05	3.4E-07	0.6129
142.80	0.028	1.8883E-05	4.0E-07	0.6178
88.48	0.026	1.8883E-05	4.3E-07	0.6224
51.00	0.017	1.8883E-05	6.6E-07	0.6283
28.05	0.008	1.8883E-05	1.4E-06	0.6344
15.30	0.004	1.8883E-05	2.8E-06	0.6405
8.92	0.002	1.8883E-05	5.6E-06	0.6467
2.55	0.006	7.5531E-05	7.5E-06	0.6592

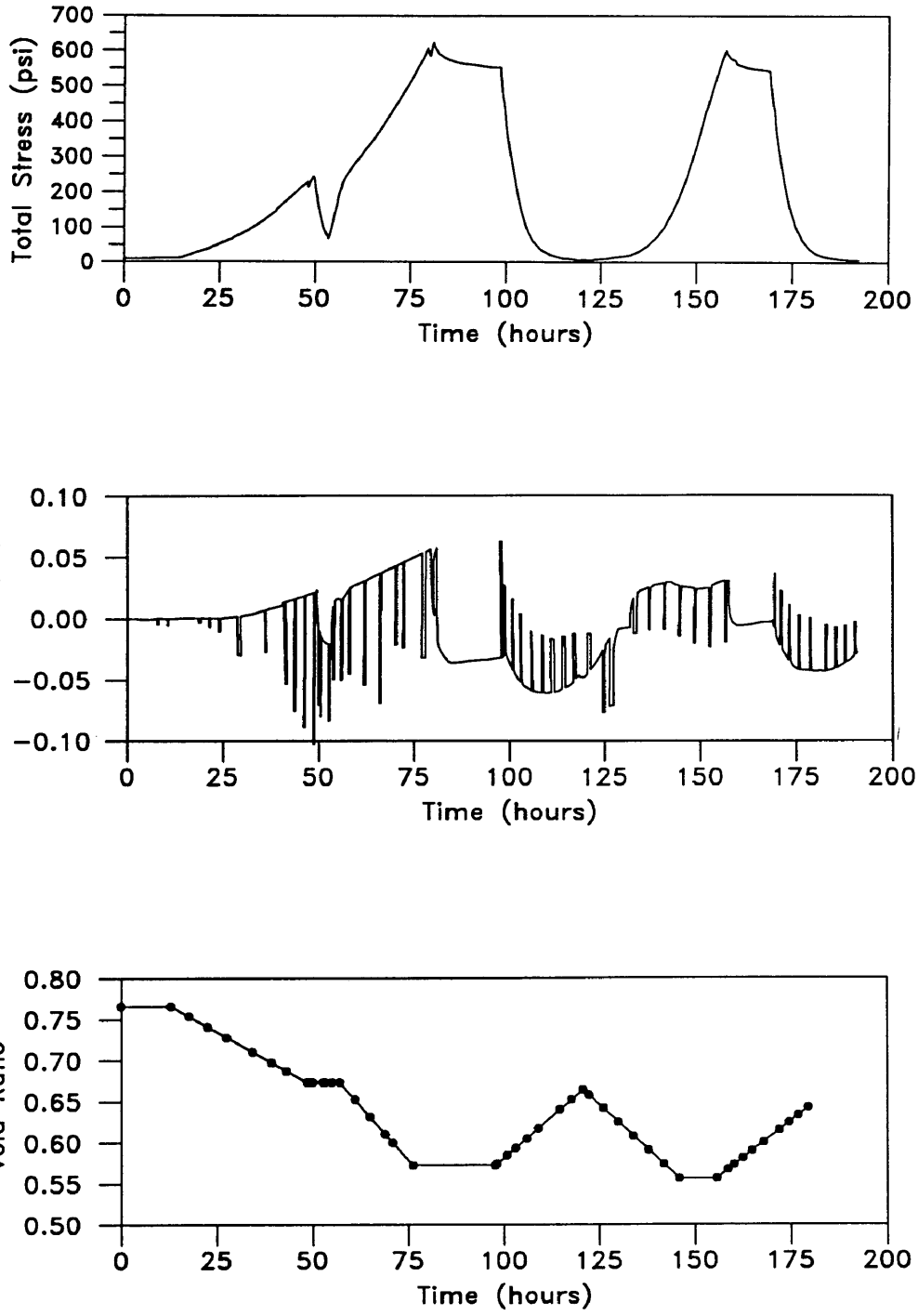

Figure A.4.1 Time History Plots, Undisturbed Specimen, w_o = 7.2%

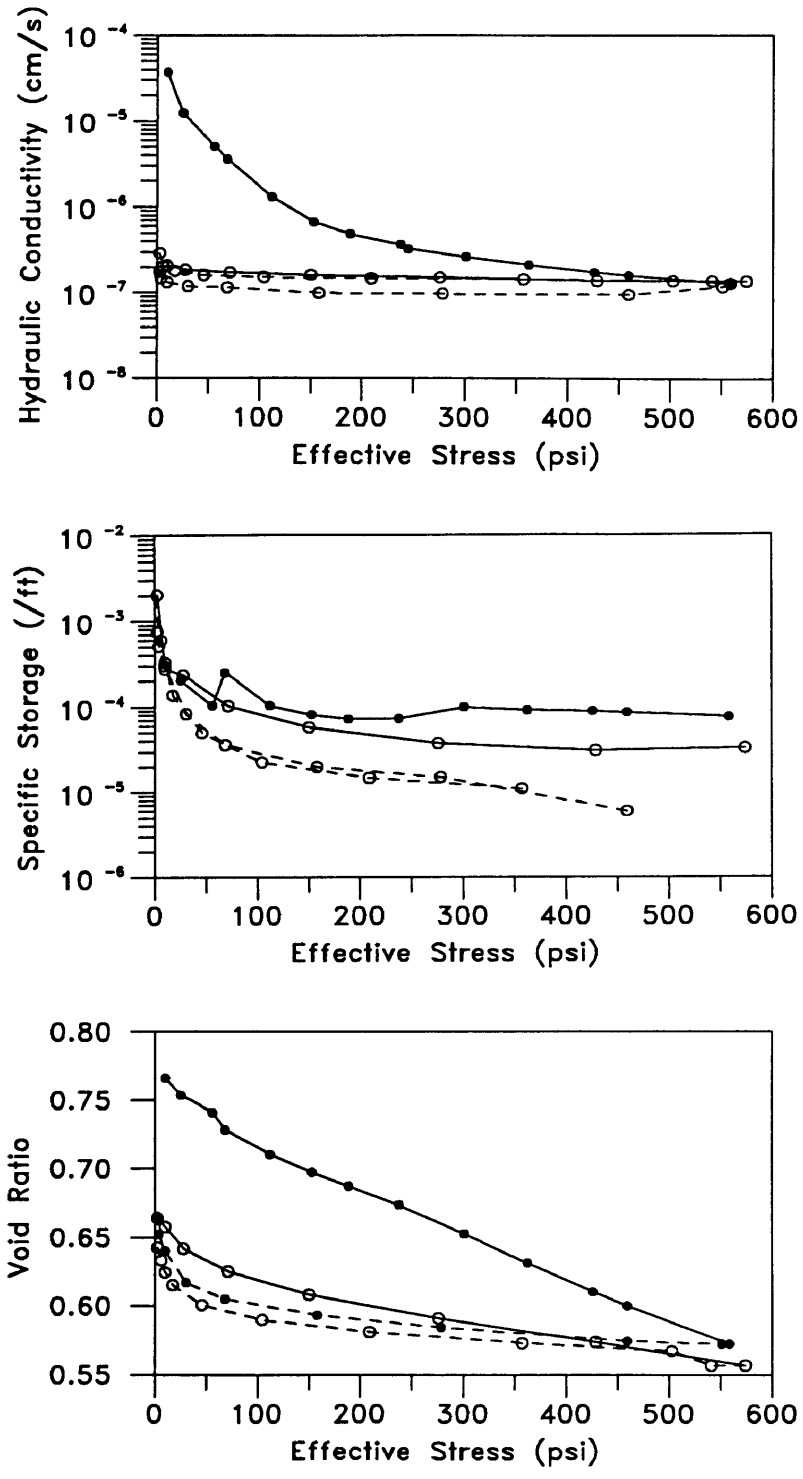

Figure A.4.2 k-σ', S_s-σ', and e-σ' Plots, Undisturbed Specimen, w_o = 7.2%

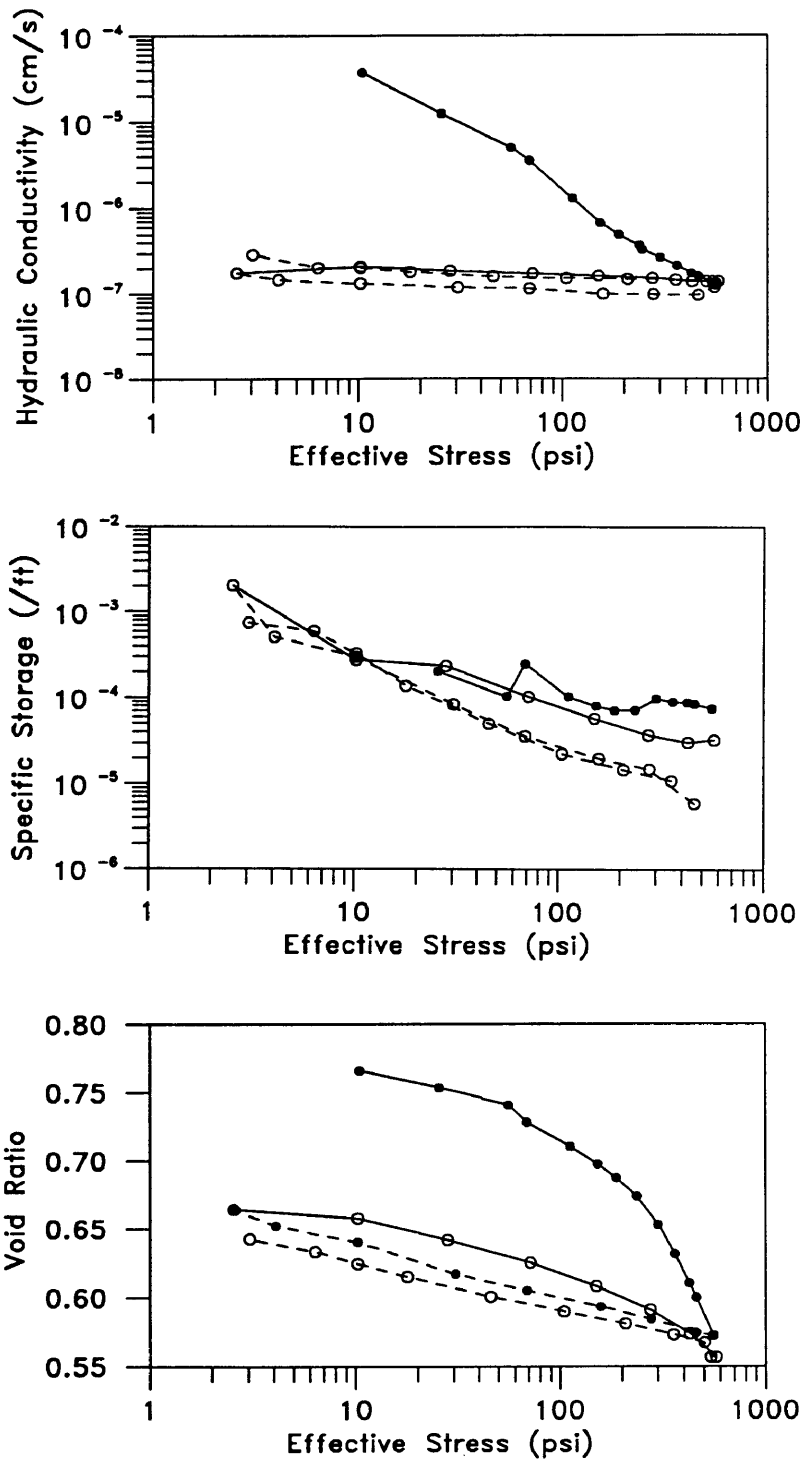

Figure A.4.3 k-σ', S_s-σ', and e-σ' Plots, Undisturbed Specimen, w_o = 7.2%

Table A.4 Geotechnical Properties, Undisturbed Specimen, w_o = 7.2%

σ′ (psi)	u_b (psi)	Flowrate (cm^3/s)	k (cm/s)	Void Ratio e
10.45	0.003	1.8883E-04	3.7E-05	0.7661
25.50	0.009	1.8883E-04	1.2E-05	0.7537
56.10	0.022	1.8883E-04	5.1E-06	0.7409
68.85	0.031	1.8883E-04	3.6E-06	0.7281
112.20	0.034	7.5531E-05	1.3E-06	0.7104
153.00	0.066	7.5531E-05	6.8E-07	0.6973
188.69	0.091	7.5531E-05	4.9E-07	0.6873
237.14	0.121	7.5531E-05	3.7E-07	0.6736
221.84	0.062	3.7766E-05	3.6E-07	0.6736
173.40	0.065	3.7766E-05	3.5E-07	0.6736
81.60	0.062	3.7766E-05	3.6E-07	0.6736
91.80	0.062	3.7766E-05	3.6E-07	0.6736
183.59	0.065	3.7766E-05	3.5E-07	0.6736
244.79	0.068	3.7766E-05	3.3E-07	0.6736
300.89	0.084	3.7766E-05	2.7E-07	0.6526
362.09	0.105	3.7766E-05	2.1E-07	0.6315
425.84	0.064	1.8883E-05	1.8E-07	0.6105
458.99	0.069	1.8883E-05	1.6E-07	0.6000
558.43	0.085	1.8883E-05	1.3E-07	0.5725
550.78	0.094	1.8883E-05	1.2E-07	0.5725
458.99	0.058	9.4415E-06	9.7E-08	0.5745
277.94	0.057	9.4415E-06	9.8E-08	0.5845
158.10	0.056	9.4415E-06	1.0E-07	0.5933
68.85	0.048	9.4415E-06	1.2E-07	0.6052
30.60	0.047	9.4415E-06	1.2E-07	0.6172
10.20	0.042	9.4415E-06	1.3E-07	0.6403
4.08	0.038	9.4415E-06	1.5E-07	0.6522
2.55	0.032	9.4415E-06	1.8E-07	0.6642
10.20	0.032	1.1330E-05	2.1E-07	0.6578
28.05	0.036	1.1330E-05	1.9E-07	0.6419
71.40	0.039	1.1330E-05	1.7E-07	0.6252
150.45	0.041	1.1330E-05	1.6E-07	0.6081
275.39	0.044	1.1330E-05	1.5E-07	0.5910
428.39	0.048	1.1330E-05	1.4E-07	0.5738
573.73	0.048	1.1330E-05	1.4E-07	0.5567
540.59	0.048	1.1330E-05	1.4E-07	0.5567
502.34	0.048	1.1330E-05	1.4E-07	0.5674
356.99	0.046	1.1330E-05	1.5E-07	0.5732
209.09	0.045	1.1330E-05	1.5E-07	0.5812
104.55	0.044	1.1330E-05	1.5E-07	0.5899
45.90	0.042	1.1330E-05	1.6E-07	0.6000
17.85	0.037	1.1330E-05	1.8E-07	0.6152

Table A.4 (continued)

σ' (psi)	u_b (psi)	Flowrate (cm^3/s)	k (cm/s)	Void Ratio e
10.20	0.033	1.1330E-05	2.0E-07	0.6246
6.37	0.033	1.1330E-05	2.0E-07	0.6333
3.06	0.023	1.1330E-05	2.9E-07	0.6427

Appendix B:

Geotechnical Properties of Reconstituted Specimens

The results of five reconstituted natural clay specimens are presented in this appendix. The undesiccated reconstituted specimen had an initial water content of 33.5%. Four the specimens were allowed to air dry from an average initial water content of 30% to similar water contents of the undisturbed materials. The desiccated water contents of these specimens were 21.0%, 17.9%, 9.4%, and 6.4%, respectively. The reconstituted specimens were then subjected to the same testing regime as the undisturbed samples. The time history plots illustrate the total stress, base pore pressure, and void ratio measured throughout the entire testing program. Like the undisturbed specimens, each reconstituted sample was fully loaded to over 500 psi and unloaded in less than 125 hours. Hydraulic conductivity, specific storage, and void ratio relationships with effective stress are plotted in both the linear and logarithmic format. Each specimen was tested in a single compression-rebound cycle. The undesiccated specimen at a water content of 33.5%, was retested in a second compression-rebound cycle. The following legend identifies the testing cycles represented by each of the plots:

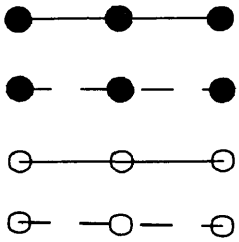

Data tables of the specimen geotechnical properties are included with each of the plots. All plots were developed with data of the final soil phase relationships, total sample deformation, and rate of deformation. These data were incorporated with the l.v.d.t. calibration curve to calculate the void ratio-time relationship with stresses applied during the test.

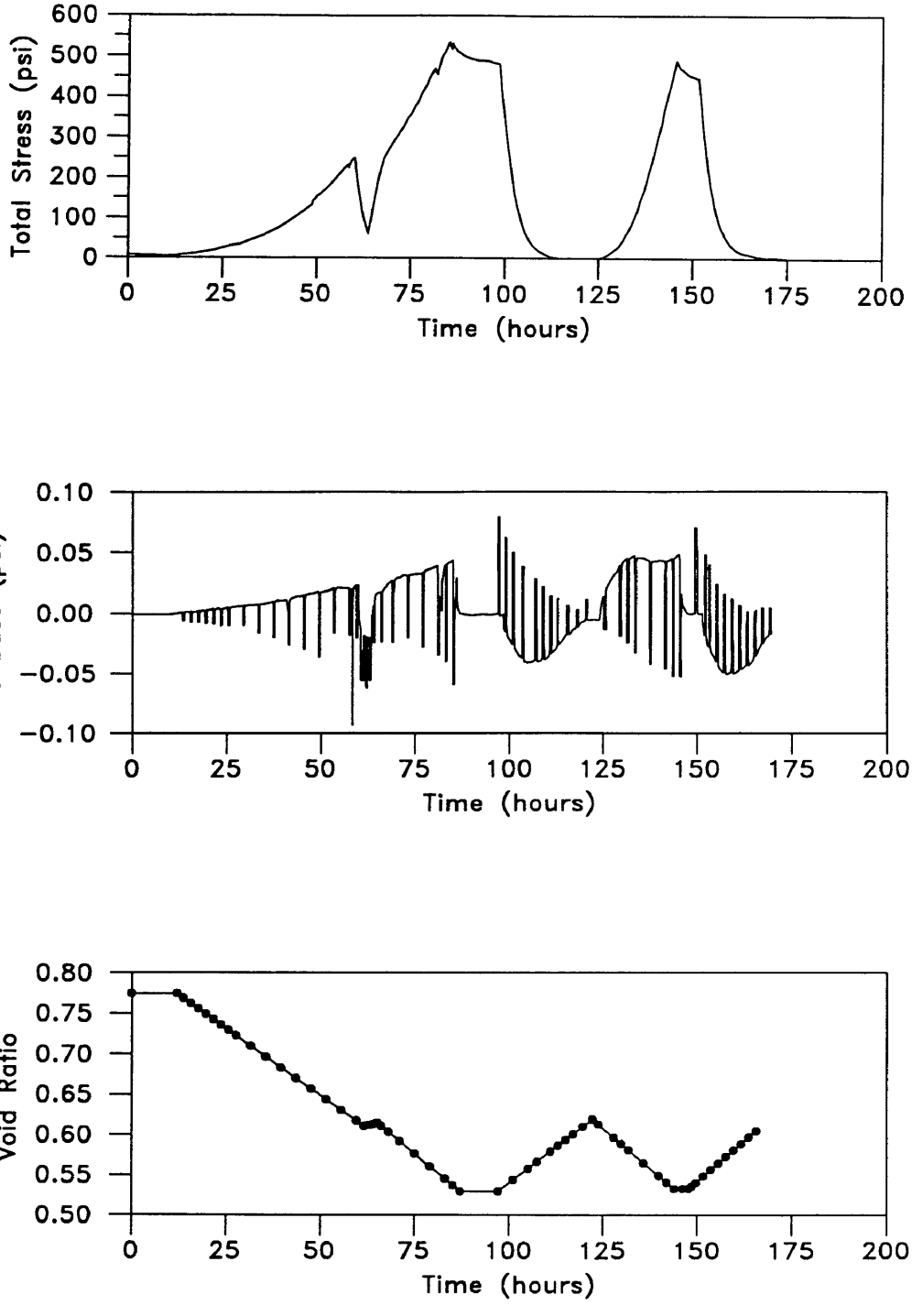

Figure B.1.1 Time History Plots, Reconstituted Specimen, w_o = 33.5%

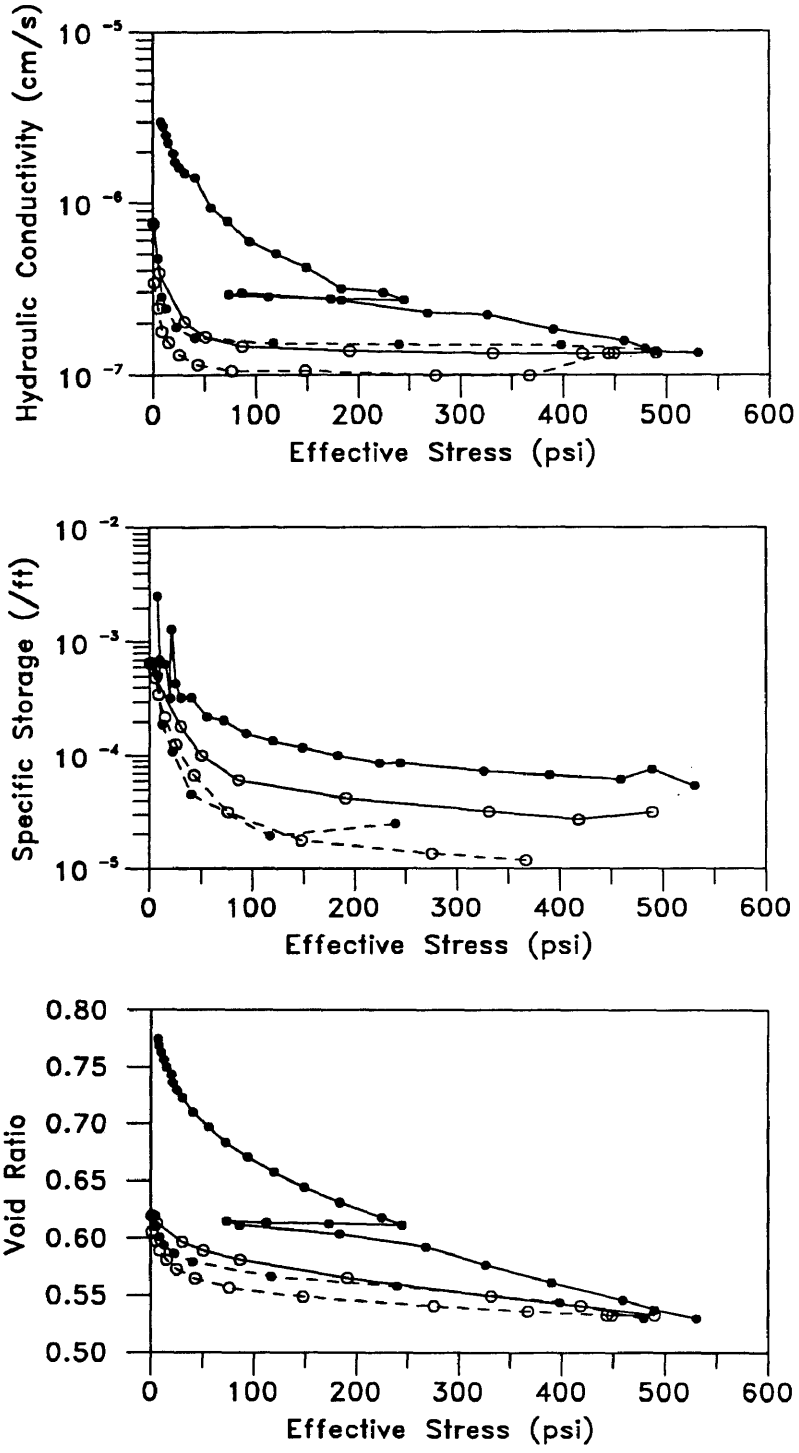

Figure B.1.2 k-σ', S_s-σ', and e-σ' Plots, Reconstituted Specimen, w_o = 33.51%

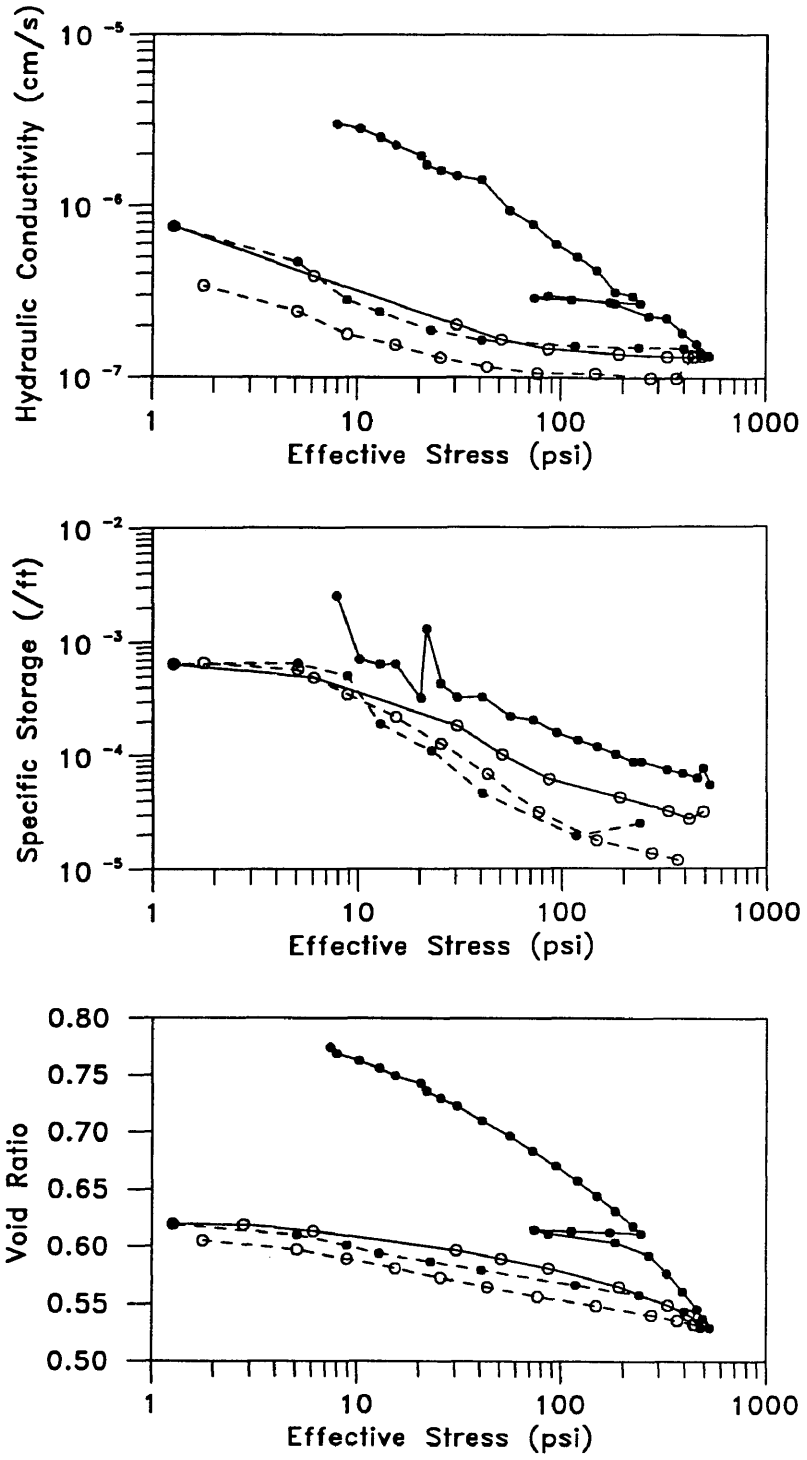

Figure B.1.3 k-σ', S_s-σ', and e-σ' Plots, Reconstituted Specimen, w_o = 33.5%

Table B.1 Geotechnical Properties, Reconstituted Specimen, w_o = 33.5%

σ′ (psi)	u_b (psi)	Flowrate (cm^3/s)	k (cm/s)	Void Ratio e
7.39	0.049	7.5531E-05	9.4E-07	0.7745
7.90	0.024	3.7766E-05	9.4E-07	0.7692
10.20	0.008	3.7766E-05	2.8E-06	0.7626
12.75	0.009	3.7766E-05	2.5E-06	0.7561
15.30	0.010	3.7766E-05	2.2E-06	0.7495
20.40	0.012	3.7766E-05	2.0E-06	0.7429
21.67	0.013	3.7766E-05	1.7E-06	0.7363
25.50	0.014	3.7766E-05	1.6E-06	0.7297
30.60	0.015	3.7766E-05	1.5E-06	0.7231
40.80	0.016	3.7766E-05	1.4E-06	0.7100
56.10	0.024	3.7766E-05	9.4E-07	0.6968
72.67	0.029	3.7766E-05	7.7E-07	0.6836
94.35	0.038	3.7766E-05	5.9E-07	0.6705
119.85	0.045	3.7766E-05	5.0E-07	0.6573
149.17	0.054	3.7766E-05	4.2E-07	0.6442
183.59	0.036	1.8883E-05	3.1E-07	0.6310
224.39	0.038	1.8883E-05	3.0E-07	0.6178
244.79	0.042	1.8883E-05	2.7E-07	0.6112
173.40	0.041	1.8883E-05	2.7E-07	0.6124
112.20	0.040	1.8883E-05	2.8E-07	0.6135
73.95	0.039	1.8883E-05	2.9E-07	0.6147
86.70	0.038	1.8883E-05	3.0E-07	0.6112
183.59	0.042	1.8883E-05	2.7E-07	0.6038
267.74	0.050	1.8883E-05	2.2E-07	0.5924
326.39	0.051	1.8883E-05	2.2E-07	0.5767
390.14	0.062	1.8883E-05	1.8E-07	0.5610
458.99	0.072	1.8883E-05	1.6E-07	0.5457
489.59	0.083	1.8883E-05	1.4E-07	0.5375
530.39	0.084	1.8883E-05	1.3E-07	0.5296
479.39	0.080	1.8883E-05	1.4E-07	0.5296
397.79	0.076	1.8883E-05	1.5E-07	0.5439
239.69	0.075	1.8883E-05	1.5E-07	0.5581
117.30	0.074	1.8883E-05	1.5E-07	0.5666
40.80	0.069	1.8883E-05	1.6E-07	0.5794
22.95	0.060	1.8883E-05	1.9E-07	0.5866
12.75	0.047	1.8883E-05	2.4E-07	0.5937
8.92	0.040	1.8883E-05	2.8E-07	0.6008
5.10	0.024	1.8883E-05	4.7E-07	0.6100
1.27	0.015	1.8883E-05	7.5E-07	0.6193
2.80	0.023	1.8883E-05	5.0E-07	0.6190
6.12	0.029	1.8883E-05	3.9E-07	0.6130
30.60	0.056	1.8883E-05	2.0E-07	0.5966

Table B.1 continued

σ' (psi)	u_b (psi)	Flowrate (cm^3/s)	k (cm/s)	Void Ratio e
51.00	0.068	1.8883E-05	1.7E-07	0.5891
86.70	0.077	1.8883E-05	1.5E-07	0.5811
191.24	0.082	1.8883E-05	1.4E-07	0.5651
331.49	0.085	1.8883E-05	1.3E-07	0.5491
418.19	0.085	1.8883E-05	1.3E-07	0.5408
489.59	0.084	1.8883E-05	1.3E-07	0.5328
448.79	0.085	1.8883E-05	1.3E-07	0.5328
443.69	0.085	1.8883E-05	1.3E-07	0.5328
367.19	0.068	1.1330E-05	9.9E-08	0.5360
275.39	0.068	1.1330E-05	9.9E-08	0.5405
147.90	0.064	1.1330E-05	1.1E-07	0.5486
76.50	0.064	1.1330E-05	1.1E-07	0.5566
43.35	0.059	1.1330E-05	1.1E-07	0.5647
25.50	0.052	1.1330E-05	1.3E-07	0.5728
15.30	0.044	1.1330E-05	1.5E-07	0.5809
8.92	0.038	1.1330E-05	1.8E-07	0.5890
5.10	0.028	1.1330E-05	2.4E-07	0.5971
1.78	0.020	1.1330E-05	3.4E-07	0.6052

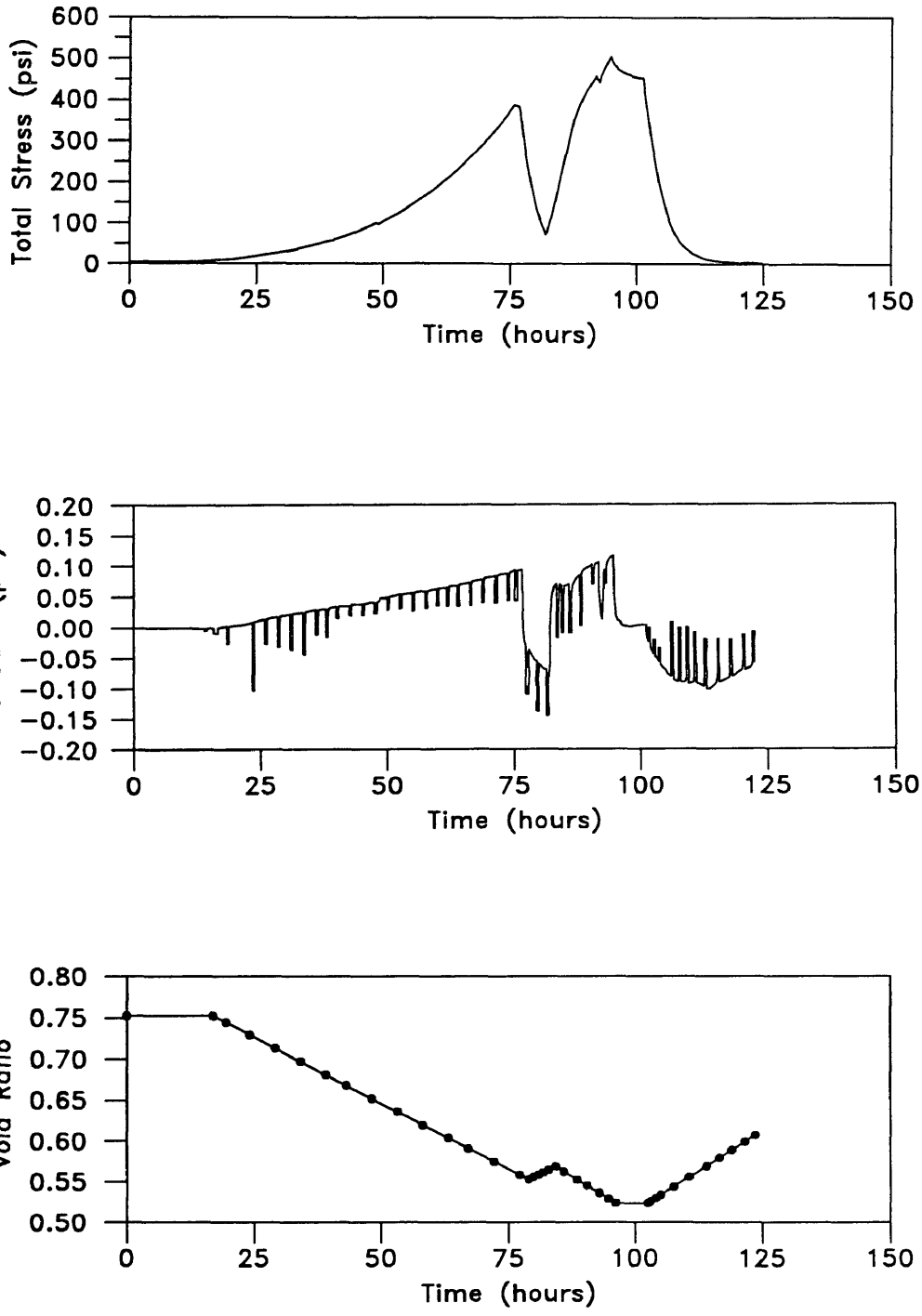

Figure B.2.1 Time History Plots, Reconstituted Specimen, w_o = 21.0%

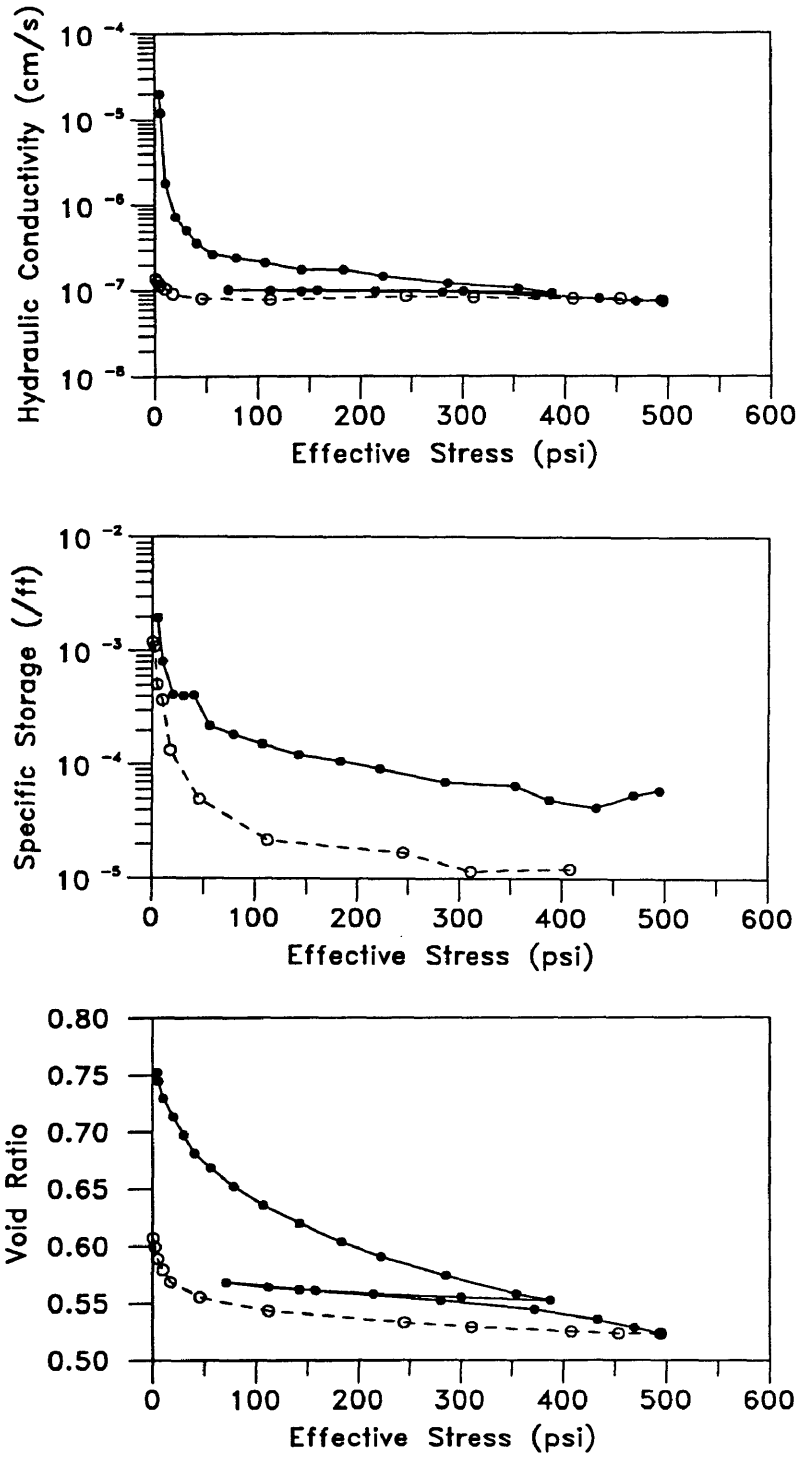

Figure B.2.2 k-σ', S_s-σ', and e-σ' Plots, Reconstituted Specimen, w_o = 21.0%

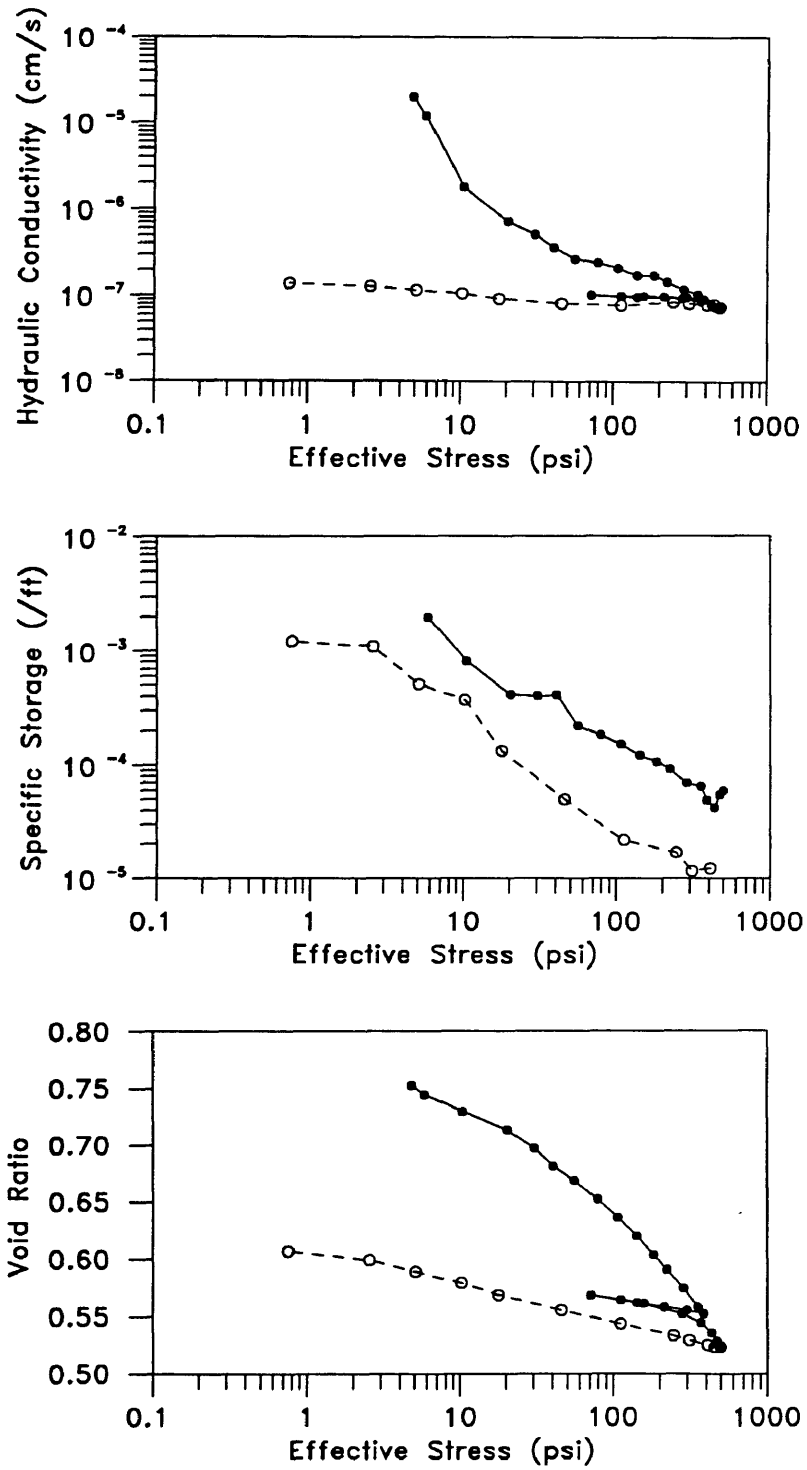

Figure B.2.3 k-σ', S_s-σ', and e-σ' Plots, Reconstituted Specimen, w_o = 21.0%

Table B.2 Geotechnical Properties, Reconstituted Specimen, w_0 = 21.0%

σ' (psi)	u_b (psi)	Flowrate (cm^3/s)	k (cm/s)	Void Ratio e
4.84	0.006	1.8883E-04	2.0E-05	0.7525
5.86	0.010	1.8883E-04	1.2E-05	0.7445
10.45	0.067	1.8883E-04	1.8E-06	0.7296
20.40	0.040	4.5319E-05	7.2E-07	0.7135
30.60	0.056	4.5319E-05	5.1E-07	0.6973
40.80	0.040	2.2660E-05	3.6E-07	0.6812
56.10	0.018	7.5532E-06	2.6E-07	0.6683
79.05	0.020	7.5532E-06	2.4E-07	0.6521
107.10	0.023	7.5532E-06	2.1E-07	0.6360
142.80	0.028	7.5532E-06	1.7E-07	0.6198
183.59	0.028	7.5532E-06	1.7E-07	0.6037
221.84	0.033	7.5532E-06	1.4E-07	0.5908
285.59	0.040	7.5532E-06	1.2E-07	0.5746
354.44	0.046	7.5532E-06	1.0E-07	0.5585
387.59	0.052	7.5532E-06	9.2E-08	0.5527
300.89	0.074	1.1330E-05	9.7E-08	0.5556
214.19	0.073	1.1330E-05	9.8E-08	0.5585
158.10	0.072	1.1330E-05	9.9E-08	0.5614
112.20	0.072	1.1330E-05	9.9E-08	0.5643
71.40	0.070	1.1330E-05	1.0E-07	0.5684
142.80	0.074	1.1330E-05	9.7E-08	0.5623
280.49	0.076	1.1330E-05	9.4E-08	0.5524
372.29	0.082	1.1330E-05	8.7E-08	0.5448
433.49	0.030	3.7766E-06	7.9E-08	0.5356
469.19	0.032	3.7766E-06	7.5E-08	0.5287
494.69	0.032	3.7766E-06	7.5E-08	0.5234
453.89	0.030	3.7766E-06	7.9E-08	0.5234
407.99	0.030	3.7766E-06	7.9E-08	0.5254
311.09	0.029	3.7766E-06	8.2E-08	0.5294
244.79	0.028	3.7766E-06	8.5E-08	0.5333
112.20	0.092	1.1330E-05	7.8E-08	0.5436
45.90	0.088	1.1330E-05	8.1E-08	0.5555
17.85	0.078	1.1330E-05	9.2E-08	0.5690
10.20	0.068	1.1330E-05	1.1E-07	0.5793
5.10	0.062	1.1330E-05	1.2E-07	0.5889
2.55	0.056	1.1330E-05	1.3E-07	0.5992
0.76	0.052	1.1330E-05	1.4E-07	0.6071

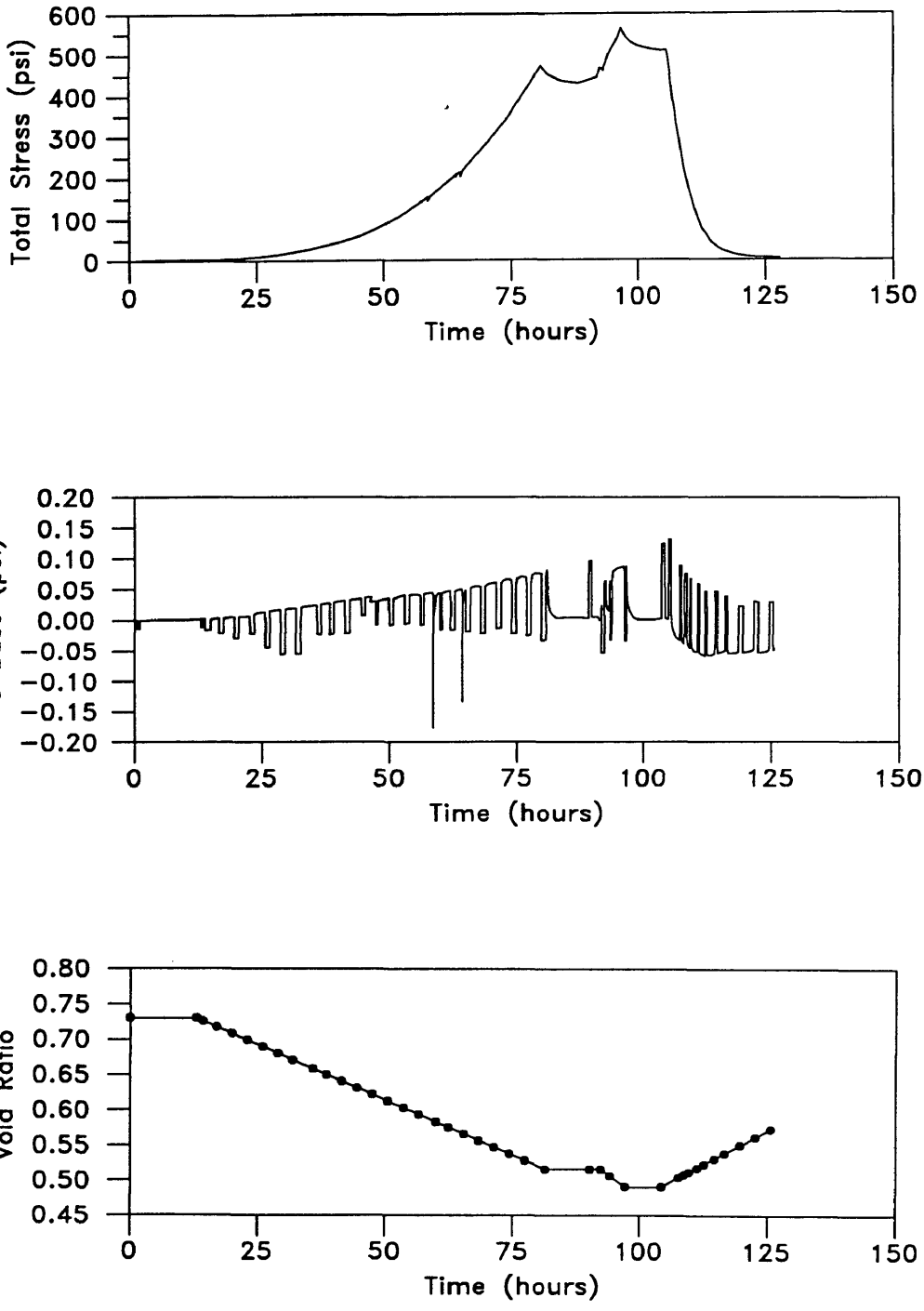

Figure B.3.1 Time History Plots, Reconstituted Specimen, w_o = 17.9%

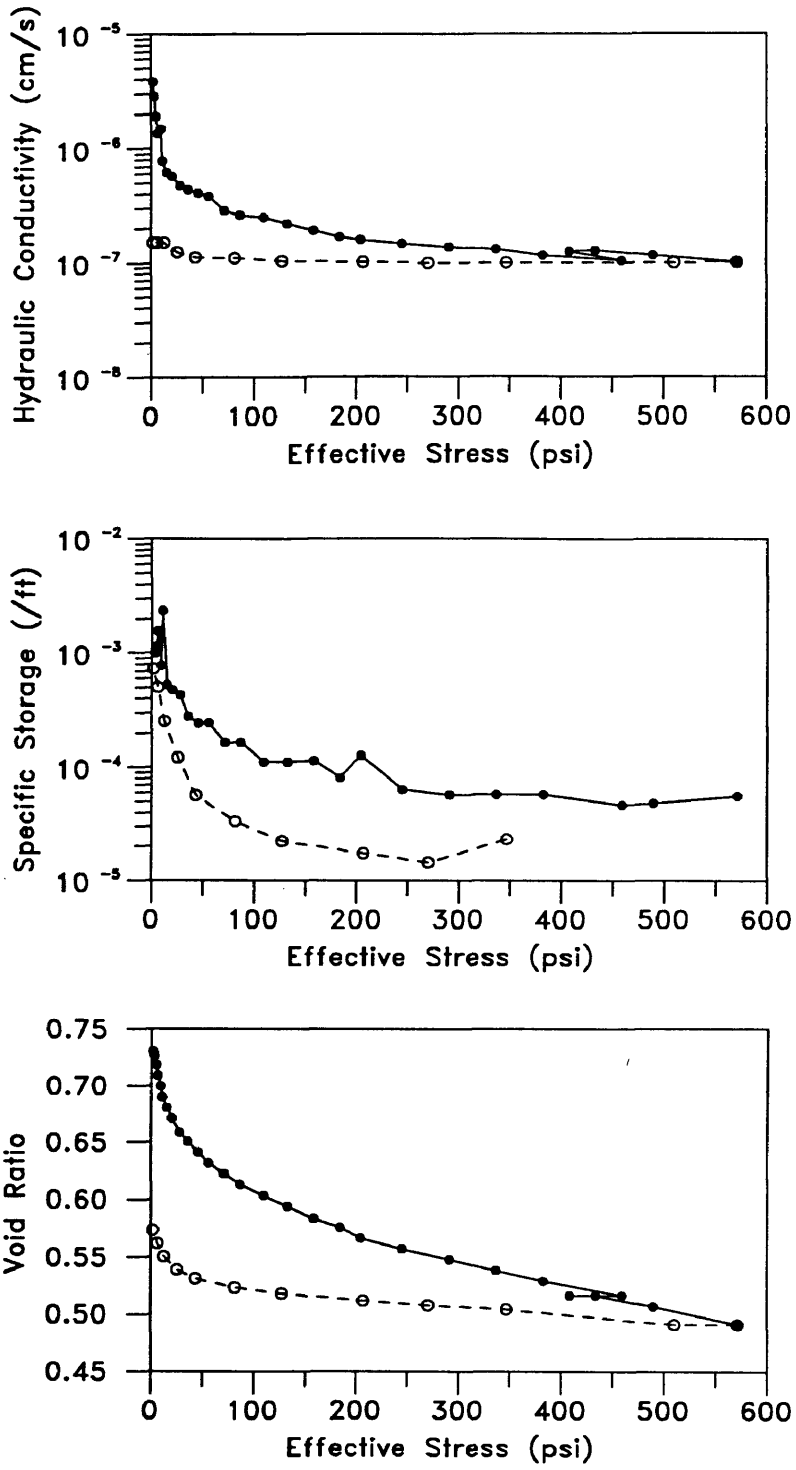

Figure B.3.2 k-σ', S_s-σ', and e-σ' Plots, Reconstituted Specimen, w_o = 17.9%

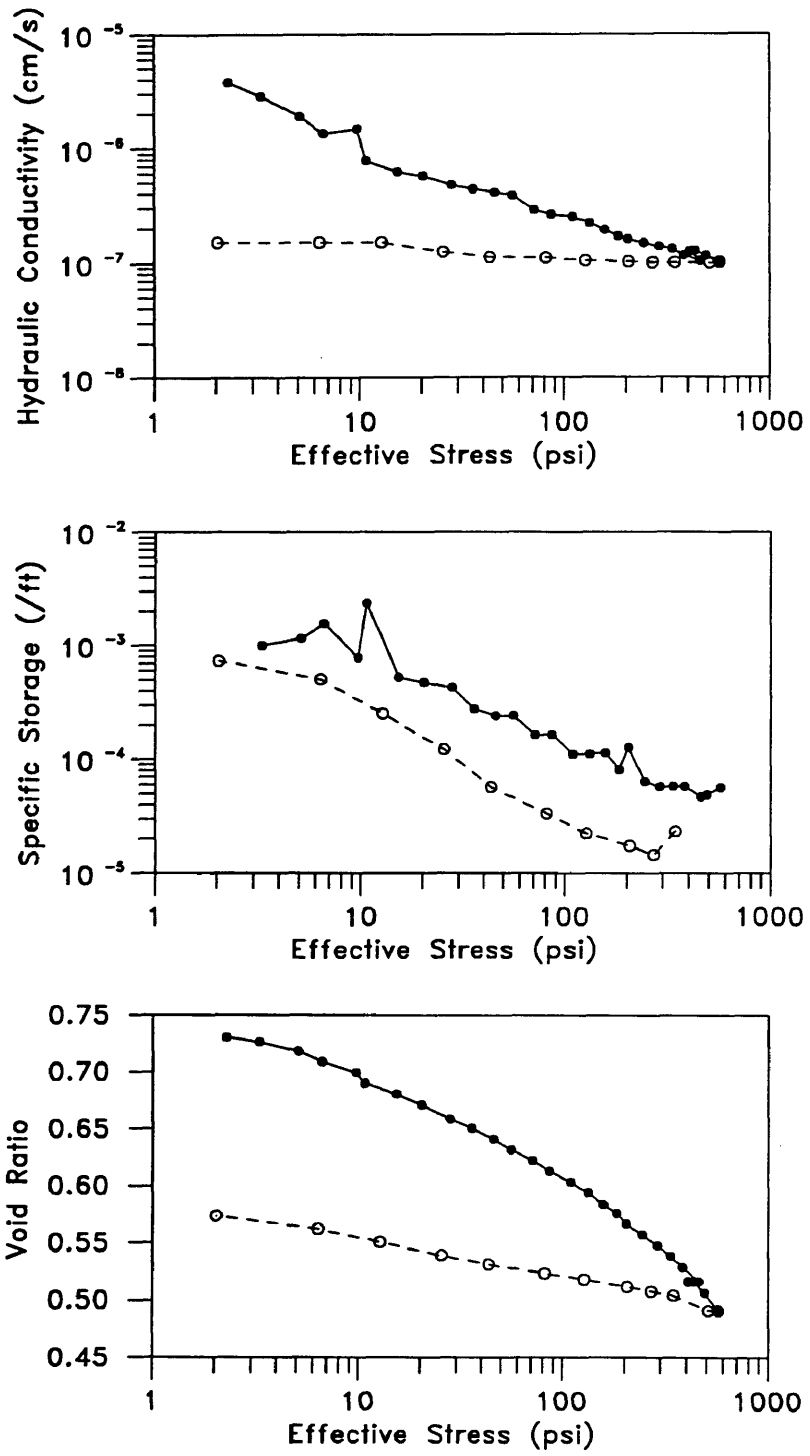

Figure B.3.3 k-σ', S_s-σ', and e-σ' Plots, Reconstituted Specimen, w_o = 17.9%

Table B.3 Geotechnical Properties, Reconstituted Specimen, w_o = 17.9%

σ′ (psi)	u_b (psi)	Flowrate (cm^3/s)	k (cm/s)	Void Ratio e
2.29	0.012	7.5531E-05	3.8E-06	0.7554
3.31	0.016	7.5531E-05	2.9E-06	0.7263
5.10	0.024	7.5531E-05	1.9E-06	0.7182
6.63	0.034	7.5531E-05	1.3E-06	0.7088
9.69	0.031	7.5531E-05	1.5E-06	0.6994
10.71	0.059	7.5531E-05	7.7E-07	0.6900
15.30	0.074	7.5531E-05	6.2E-07	0.6806
20.40	0.080	7.5531E-05	5.7E-07	0.6712
28.05	0.048	3.7766E-05	4.8E-07	0.6586
35.70	0.052	3.7766E-05	4.4E-07	0.6505
45.90	0.056	3.7766E-05	4.1E-07	0.6411
56.10	0.030	1.8883E-05	3.8E-07	0.6317
71.40	0.040	1.8883E-05	2.9E-07	0.6223
86.70	0.044	1.8883E-05	2.6E-07	0.6129
109.65	0.046	1.8883E-05	2.5E-07	0.6035
132.60	0.052	1.8883E-05	2.2E-07	0.5941
158.10	0.060	1.8883E-05	1.9E-07	0.5834
183.59	0.068	1.8883E-05	1.7E-07	0.5759
203.99	0.072	1.8883E-05	1.6E-07	0.5665
244.79	0.078	1.8883E-05	1.5E-07	0.5571
290.69	0.084	1.8883E-05	1.4E-07	0.5477
336.59	0.088	1.8883E-05	1.3E-07	0.5383
382.49	0.100	1.8883E-05	1.1E-07	0.5289
458.99	0.112	1.8883E-05	1.0E-07	0.5163
407.99	0.092	1.8883E-05	1.2E-07	0.5163
433.49	0.090	1.8883E-05	1.3E-07	0.5163
489.59	0.100	1.8883E-05	1.1E-07	0.5068
571.18	0.114	1.8883E-05	1.0E-07	0.4909
509.99	0.115	1.8883E-05	9.9E-08	0.4909
346.79	0.115	1.8883E-05	9.9E-08	0.5041
270.29	0.115	1.8883E-05	9.9E-08	0.5080
206.54	0.112	1.8883E-05	1.0E-07	0.5118
127.50	0.110	1.8883E-05	1.0E-07	0.5180
81.60	0.104	1.8883E-05	1.1E-07	0.5234
43.35	0.102	1.8883E-05	1.1E-07	0.5312
25.50	0.092	1.8883E-05	1.2E-07	0.5389
12.75	0.076	1.8883E-05	1.5E-07	0.5505
6.37	0.076	1.8883E-05	1.5E-07	0.5621
2.04	0.076	1.8883E-05	1.5E-07	0.5737

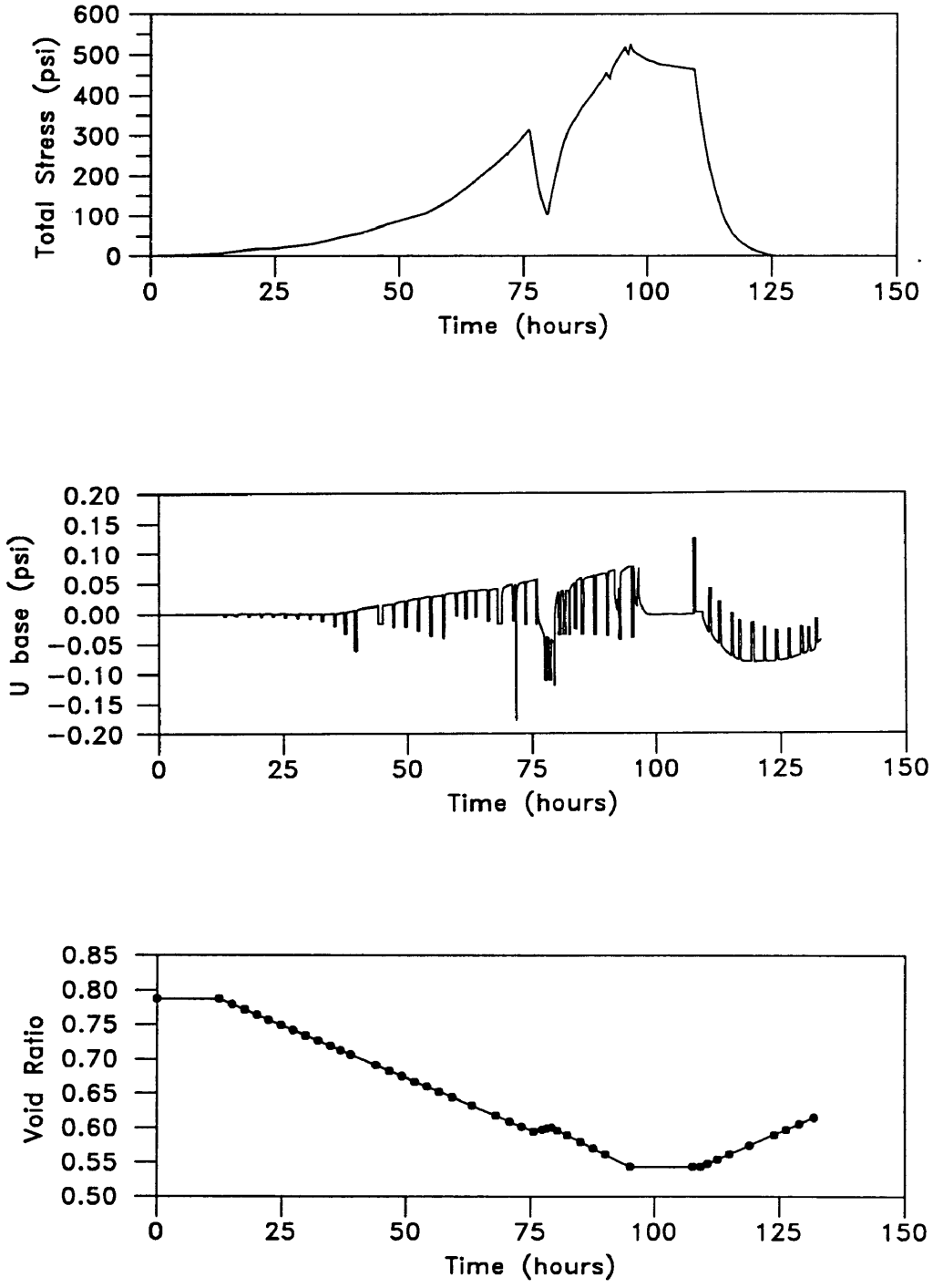

Figure B.4.1 Time History Plots, Reconstituted Specimen, w_o = 9.4%

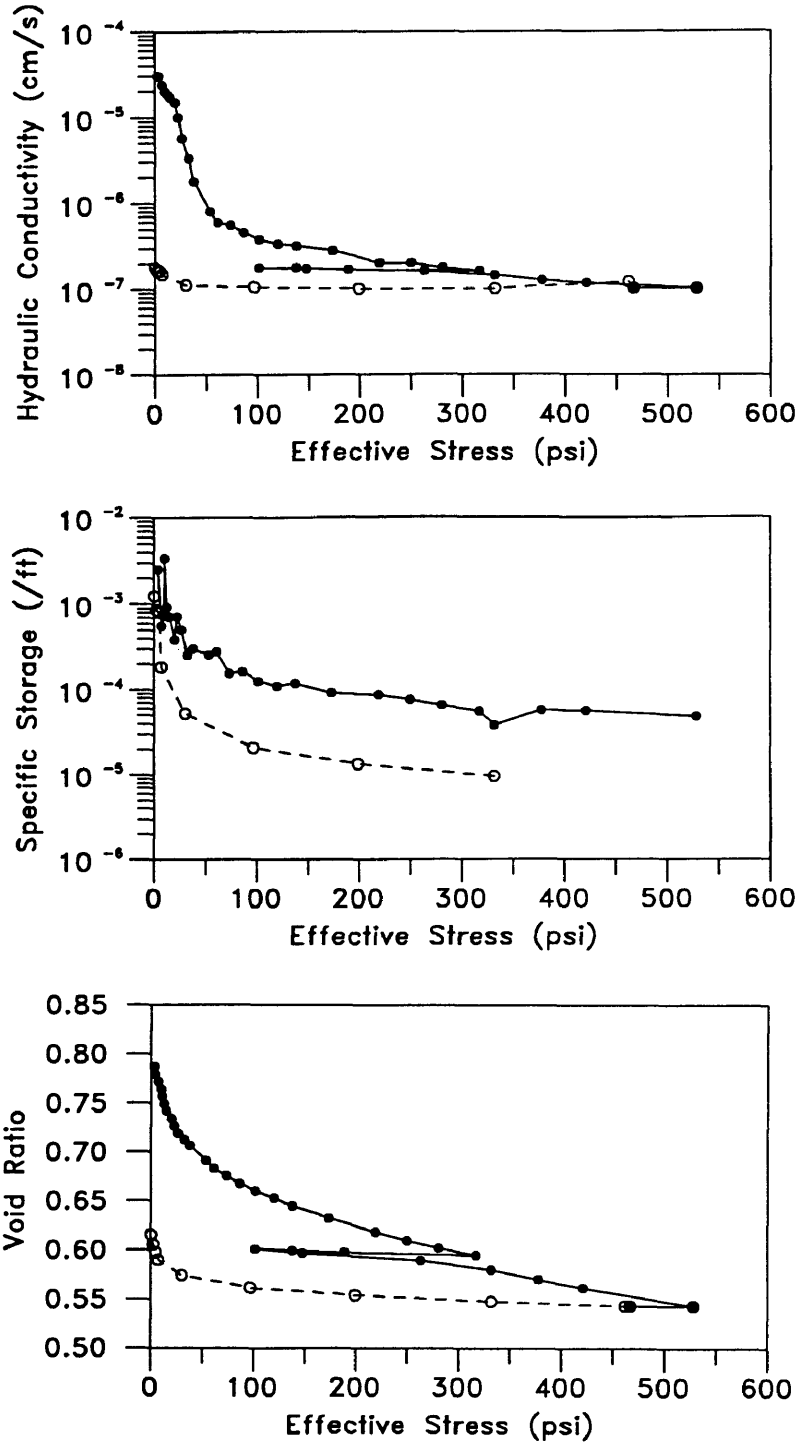

Figure B.4.2 k-σ', S_s-σ', and e-σ' Plots, Reconstituted Specimen, w_o = 9.4%

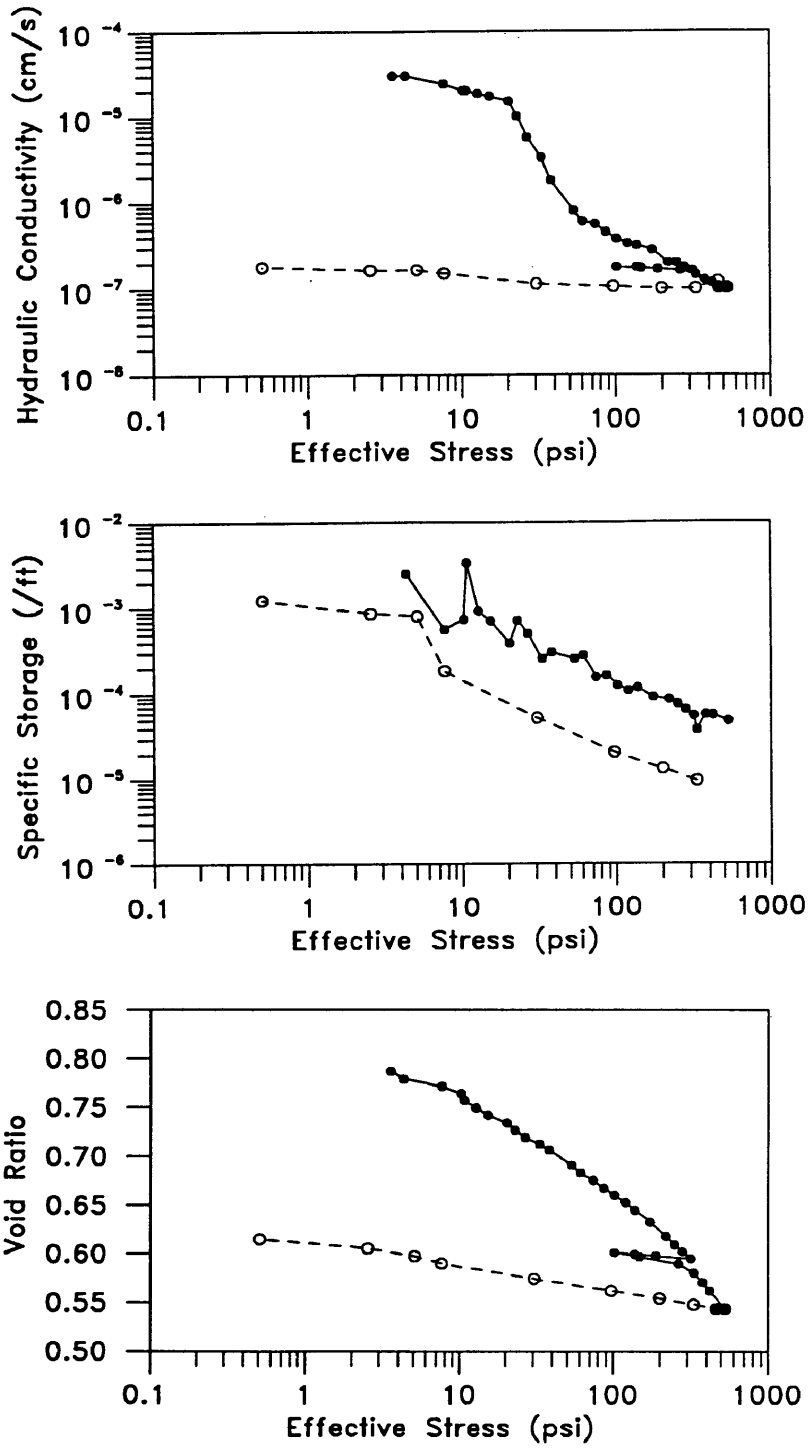

Figure B.4.3 k-σ', S_s-σ', and e-σ' Plots, Reconstituted Specimen, w_o = 9.4%

Table B.4 Geotechnical Properties, Reconstituted Specimen, w_o = 9.4%

σ′ (psi)	u_b (psi)	Flowrate (cm^3/s)	k (cm/s)	Void Ratio e
3.57	0.004	1.8883E-04	2.9E-05	0.7873
4.33	0.004	1.8883E-04	3.0E-05	0.7793
7.65	0.005	1.8883E-04	2.4E-05	0.7717
10.71	0.006	1.8883E-04	2.0E-05	0.7570
12.75	0.007	1.8883E-04	1.9E-05	0.7494
15.30	0.007	1.8883E-04	1.7E-05	0.7421
20.40	0.008	1.8883E-04	1.5E-05	0.7341
22.95	0.012	1.8883E-04	1.0E-05	0.7268
26.77	0.021	1.8883E-04	5.7E-06	0.7191
33.15	0.036	1.8883E-04	3.4E-06	0.7127
38.25	0.067	1.8883E-04	1.8E-06	0.7066
53.55	0.030	3.7766E-05	8.0E-07	0.6913
61.20	0.040	3.7766E-05	6.0E-07	0.6831
73.95	0.043	3.7766E-05	5.6E-07	0.6754
86.70	0.053	3.7766E-05	4.6E-07	0.6675
102.00	0.064	3.7766E-05	3.8E-07	0.6602
119.85	0.072	3.7766E-05	3.4E-07	0.6528
137.70	0.038	1.8883E-05	3.2E-07	0.6449
173.40	0.043	1.8883E-05	2.8E-07	0.6327
219.29	0.060	1.8883E-05	2.0E-07	0.6180
249.89	0.060	1.8883E-05	2.0E-07	0.6094
280.49	0.068	1.8883E-05	1.8E-07	0.6021
316.70	0.074	1.8883E-05	1.6E-07	0.5948
188.69	0.072	1.8883E-05	1.7E-07	0.5977
137.70	0.068	1.8883E-05	1.8E-07	0.5995
102.00	0.068	1.8883E-05	1.8E-07	0.6012
147.90	0.070	1.8883E-05	1.7E-07	0.5968
262.64	0.074	1.8883E-05	1.6E-07	0.5895
331.49	0.084	1.8883E-05	1.4E-07	0.5800
377.39	0.096	1.8883E-05	1.3E-07	0.5705
420.74	0.102	1.8883E-05	1.2E-07	0.5617
527.84	0.118	1.8883E-05	1.0E-07	0.5435
466.64	0.118	1.8883E-05	1.0E-07	0.5435
461.54	0.020	3.7766E-06	1.2E-07	0.5435
331.49	0.072	1.1330E-05	1.0E-07	0.5479
198.89	0.072	1.1330E-05	1.0E-07	0.5542
96.90	0.068	1.1330E-05	1.1E-07	0.5618
30.60	0.064	1.1330E-05	1.1E-07	0.5744
7.65	0.048	1.1330E-05	1.5E-07	0.5898
5.10	0.044	1.1330E-05	1.6E-07	0.6974

Table B.4 continued

σ' (psi)	u_b (psi)	Flowrate (cm^3/s)	k (cm/s)	Void Ratio e
2.55	0.044	1.1330E-05	1.7E-07	0.6056
0.51	0.040	1.1330E-05	1.8E-07	0.6151

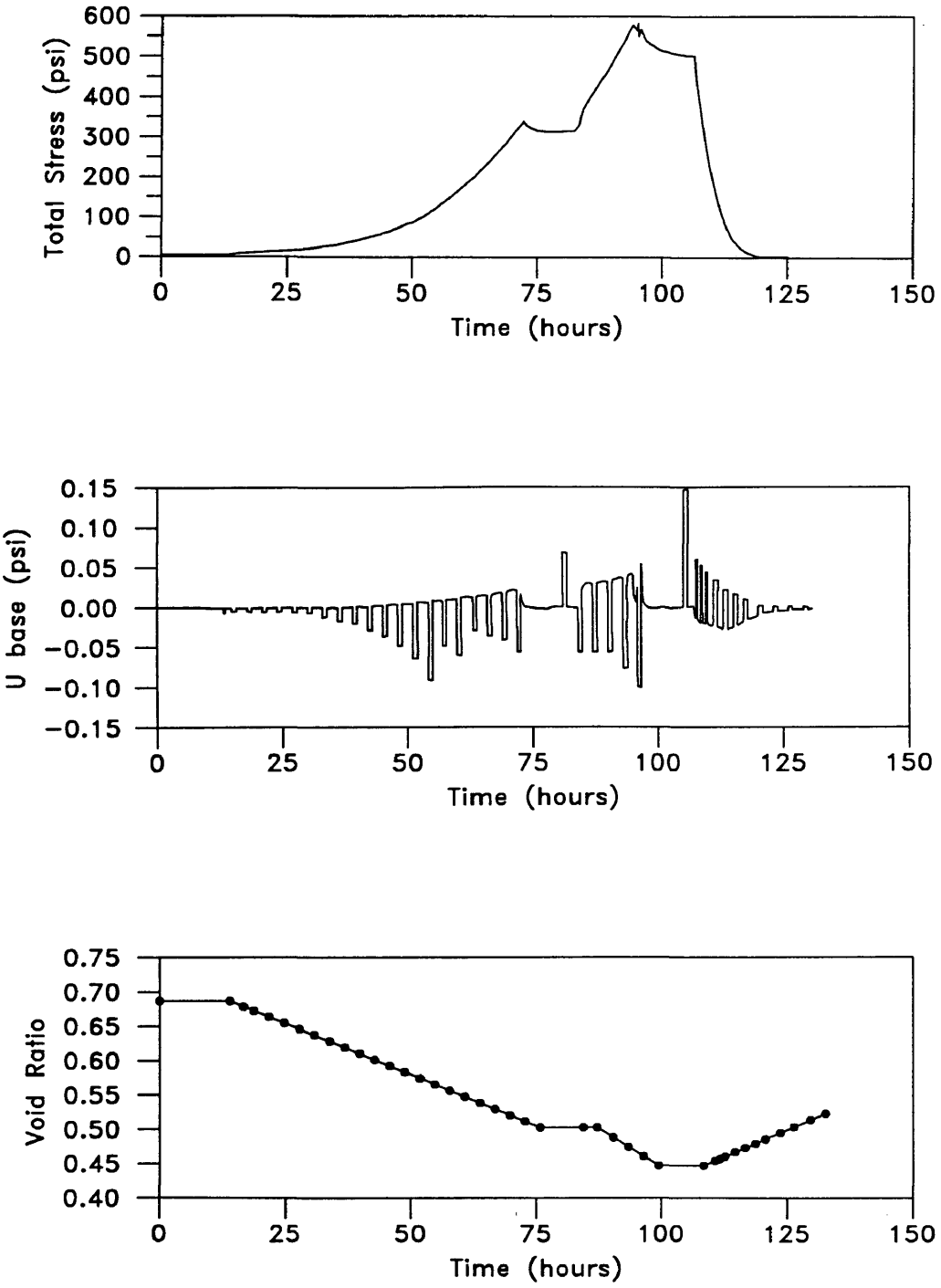

Figure B.5.1 Time History Plots, Reconstituted Specimen, w_o = 6.4%

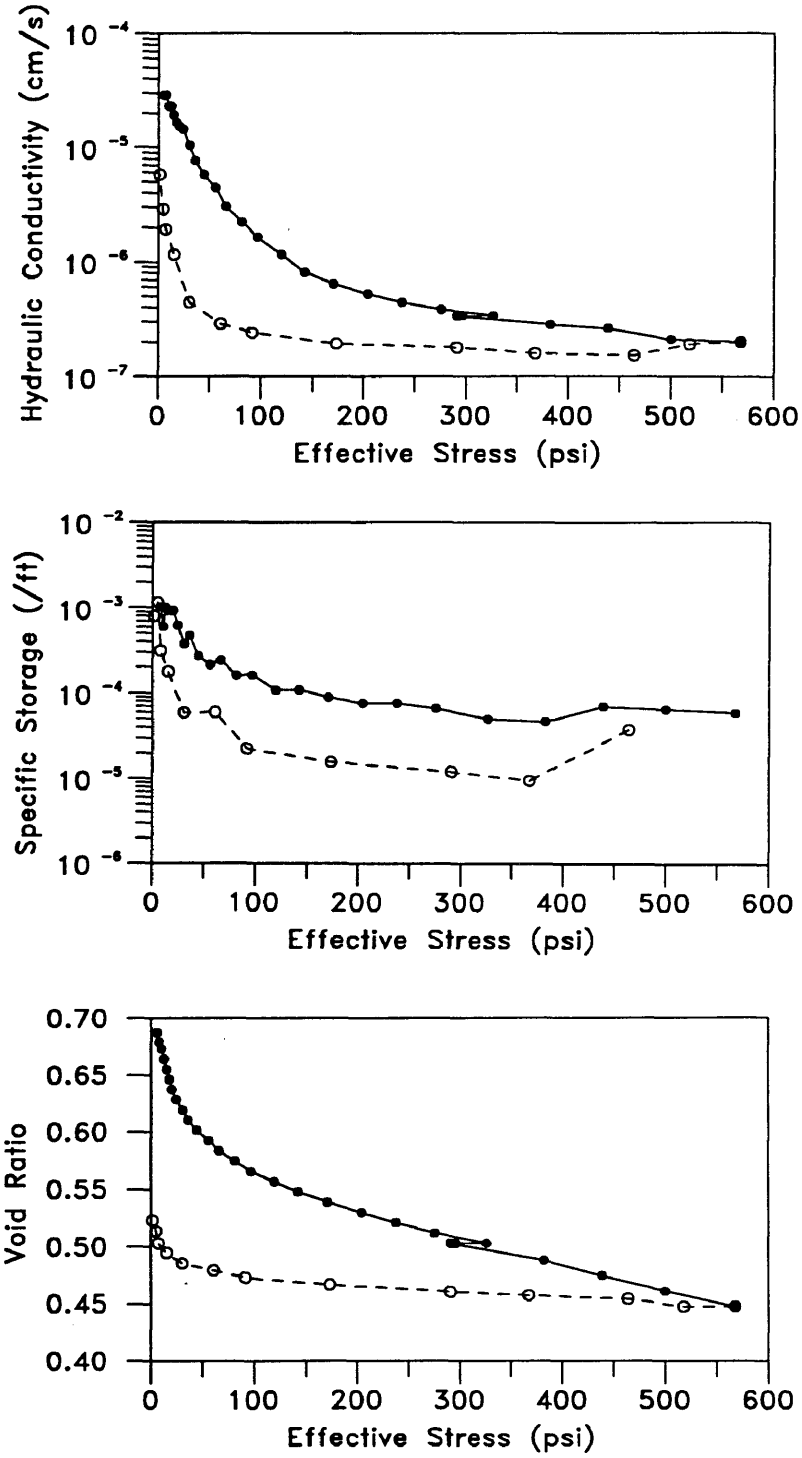

Figure B.5.2 k-σ', S_s-σ', and e-σ' Plots, Reconstituted Specimen, w_o = 6.4%

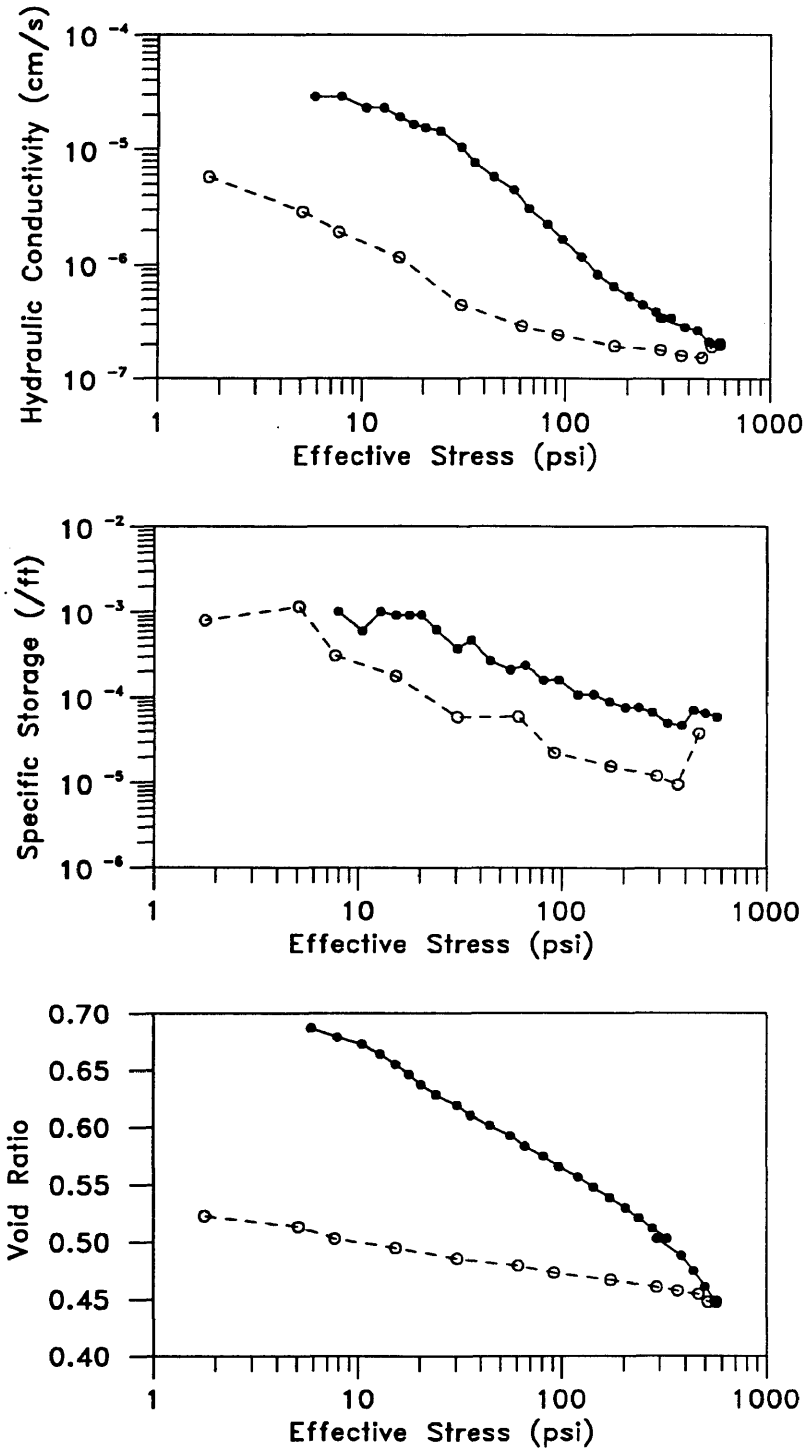

Figure B.5.3 k-σ', S_s-σ', and e-σ' Plots, Reconstituted Specimen, w_o = 6.4%

Table B.5 Geotechnical Properties, Reconstituted Specimen, w_o = 6.4%

σ' (psi)	u_b (psi)	Flowrate (cm^3/s)	k (cm/s)	Void Ratio e
5.86	0.004	1.8883E-04	3.1E-05	0.7508
5.86	0.004	1.8883E-04	2.9E-05	0.6871
7.90	0.004	1.8883E-04	2.9E-05	0.6790
10.45	0.005	1.8883E-04	2.3E-05	0.6730
12.75	0.005	1.8883E-04	2.3E-05	0.6641
15.30	0.006	1.8883E-04	1.9E-05	0.6551
17.85	0.007	1.8883E-04	1.7E-05	0.6462
20.40	0.008	1.8883E-04	1.5E-05	0.6372
24.22	0.008	1.8883E-04	1.4E-05	0.6283
30.60	0.011	1.8883E-04	1.1E-05	0.6193
35.70	0.015	1.8883E-04	7.7E-06	0.6104
44.62	0.020	1.8883E-04	5.8E-06	0.6014
56.10	0.026	1.8883E-04	4.4E-06	0.5925
66.30	0.038	1.8883E-04	3.0E-06	0.5835
81.60	0.052	1.8883E-04	2.2E-06	0.5746
96.90	0.070	1.8883E-04	1.7E-06	0.5656
119.85	0.100	1.8883E-04	1.2E-06	0.5567
142.80	0.057	7.5531E-05	8.1E-07	0.5477
170.85	0.072	7.5531E-05	6.4E-07	0.5387
203.99	0.044	3.7766E-05	5.3E-07	0.5298
237.14	0.052	3.7766E-05	4.4E-07	0.5208
275.39	0.060	3.7766E-05	3.9E-07	0.5119
326.39	0.068	3.7766E-05	3.4E-07	0.5029
295.79	0.068	3.7766E-05	3.4E-07	0.5029
290.69	0.068	3.7766E-05	3.4E-07	0.5029
382.49	0.082	3.7766E-05	2.8E-07	0.4881
438.59	0.088	3.7766E-05	2.6E-07	0.4745
499.79	0.110	3.7766E-05	2.1E-07	0.4610
567.36	0.115	3.7766E-05	2.0E-07	0.4475
517.64	0.120	3.7766E-05	1.9E-07	0.4475
464.09	0.075	1.8883E-05	1.5E-07	0.4543
367.19	0.072	1.8883E-05	1.6E-07	0.4574
290.69	0.064	1.8883E-05	1.8E-07	0.4606
173.40	0.060	1.8883E-05	1.9E-07	0.4668
91.80	0.048	1.8883E-05	2.4E-07	0.4730
61.20	0.040	1.8883E-05	2.9E-07	0.4793
30.60	0.026	1.8883E-05	4.4E-07	0.4855
15.30	0.010	1.8883E-05	1.2E-06	0.4948
7.65	0.006	1.8883E-05	1.9E-06	0.5032
5.10	0.004	1.8883E-05	2.9E-06	0.5135
1.78	0.002	1.8883E-05	5.8E-06	0.5229